Twist sense control in terminally functionalized *ortho*-phenylenes

Supporting Information

*Gopi Nath Vemuri, Rathiesh R. Pandian, Brian J. Spinello, Erika B. Stopler, Zacharias J. Kinney, and C. Scott Hartley**

Department of Chemistry & Biochemistry, Miami University, Oxford, OH 45056, USA

Table of Contents

List of Figures

List of Schemes

List of Tables

Synthesis

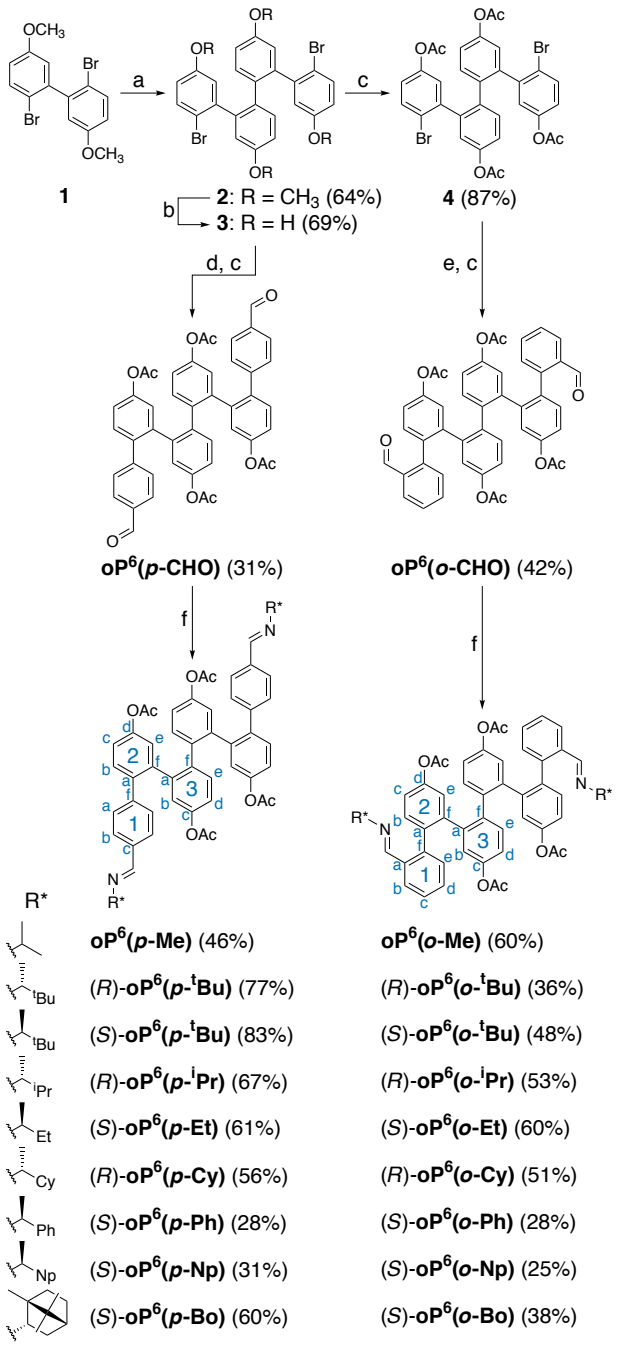

Scheme S1. Synthesis of imine-functionalized *o*-phenylene hexamers. Reagents and conditions: (a) (i) *n*-BuLi, THF, −78 °C, (ii) CuCN, rt, (iii) duroquinone, rt; (b) BBr_3, CH_2Cl_2, −78 °C to rt; (c) Ac_2O, NEt_3, $CHCl_3$, 40 °C; (d) 4-formylphenylboronic acid, $Pd(PPh_3)_4$, Na_2CO_3(aq), THF/EtOH, 90 °C; (e) 2-formylphenylboronic acid, $Pd(PPh_3)_4$, Na_2CO_3(aq), THF/EtOH, 90 °C; (f) amine, TFA, $CHCl_3$, 3 Å MS, rt.

The chosen synthetic approach, shown in Scheme S1, was similar to that used by Fukushima and Aida for other *o*-phenylene oligomers.[1] Briefly, 2,2′-dibromo-5,5′-dimethoxybiphenyl **1** was homocoupled through oxidation of the corresponding cyanocuprate[2] to give tetramer **2**. The methoxy groups were then deprotected with BBr_3, yielding **3**. For the para-substituted series, compound **3** was subjected to Suzuki coupling followed by acetylation to give dialdehyde **oP^6(*p*-CHO)** in modest, but useful, yield over two steps. For the ortho-substituted series, better results were obtained if the oligomer was acetylated first, giving **4**, followed by Suzuki coupling and re-acetylation to give

dialdehyde **oP^6(*o*-CHO)**. The series of *p*- and *o*-imines were then prepared under standard conditions for imine condensation and purified by gel permeation chromatography.

UV–vis spectra of *p*-imines

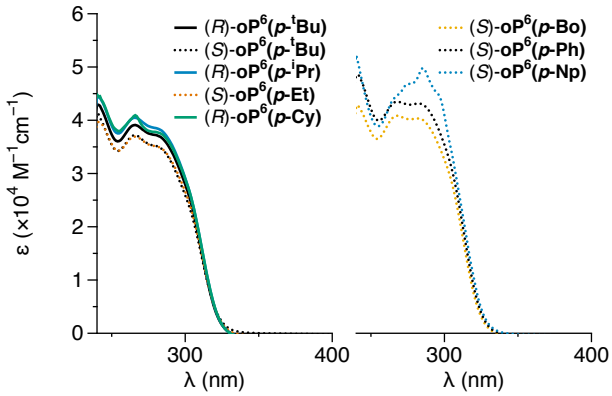

Figure S1. UV–vis spectra of the *p*-imine series dissolved in chloroform (10 μM).

TD-DFT CD predictions of Fukushima and Aida's *o*-phenylene octamer

The *o*-phenylene octamer **S1** was reported by Fukushima and Aida, who showed that it could be resolved by mechanical separation as it crystallizes as a conglomerate.[1] For this compound, the orientation of the NO_2 group does not need to accounted for as the experimental CD spectrum was recorded for a solid sample. The geometry was optimized at the PCM($CHCl_3$)/B97-D/TZV(2d,2p) level, followed by calculation of the CD spectrum at the PCM($CHCl_3$)/TD/CAM-B3LYP/6-31G(d,p) level. Cartesian coordinates of the optimized geometry are included in a separate text file. Note that the dispersion correction, while critically important for determining relative conformational energies, is not needed for the calculation of excitation energies in these systems.[3]

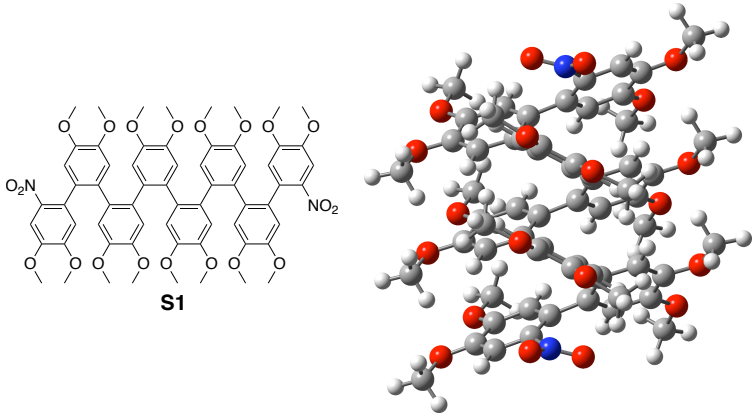

Figure S2. Optimized geometry of (*M*)-**S1** (PCM($CHCl_3$)/B97-D/TZV(2d,2p)).

	Energy (E_h)	ZPC (E_h)	Total Energy (E_h)	IF
S1	−4089.785304	1.162832	−4088.622472	0

Table S1. Geometry optimization data for (*M*)-**S1** (PCM($CHCl_3$)/B97-D/TZV(2d,2p)). ZPC = zero-point correction, IF = number of imaginary frequencies.

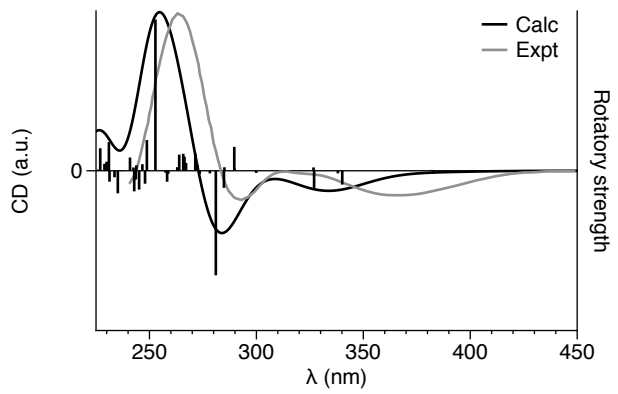

Figure S3. Calculated rotary strengths (vertical lines) and CD spectrum for (*M*)-**S1**. The spectrum was estimated by assuming a half-width at half-height of 0.2 eV. The experimental spectrum was extracted from reference [1].

Computational studes of *p*-imines

TD-DFT CD predictions of ***oP^6(p-H)***

Cartesian coordinates of the optimized geometries are included in a separate text file. The acetoxy groups were not expected to significantly impact properties of interest; thus, they were oriented by first generating a library of possible orientations in Tinker,[4] followed by PM7 optimization with MOPAC.[5] The most stable twofold-symmetric orientation was then used for ab initio geometry optimizations. As the stabilities of *o*-phenylenes are highly sensitive to dispersion interactions, DFT optimizations were done at the dispersion-corrected PCM($CHCl_3$)/B97-D/TZV(2d,2p) level,[6] which is commonly used in studies of arene–arene stacking[7,8] and is known to give good results for *o*-phenylenes.[9]

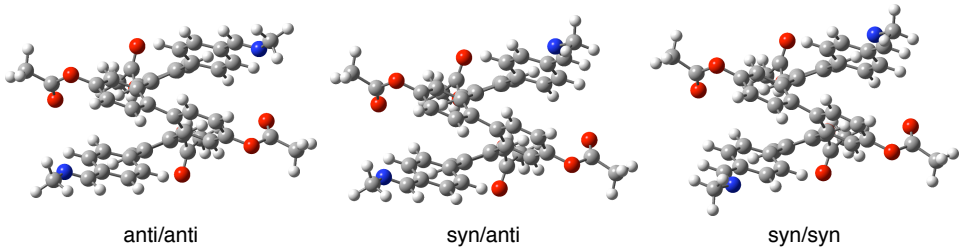

Figure S4. Optimized geometries of (*M*)-**oP^6(*p*-H)** (PCM($CHCl_3$)/B97-D/TZV(2d,2p)).

Conformer	Energy (E_h)	ZPC (E_h)	Total Energy (E_h)	IF
anti/anti (C_2)	−2563.679152	0.747449	−2562.931703	0
syn/anti (C_1)	−2563.678936	0.747219	−2562.931717	0
syn/syn (C_2)	−2563.678828	0.747012	−2562.931816	0

Table S2. Geometry optimization data for (*M*)-**oP^6(*p*-H)** (PCM($CHCl_3$)/B97-D/TZV(2d,2p)). ZPC = zero-point correction, IF = number of imaginary frequencies.

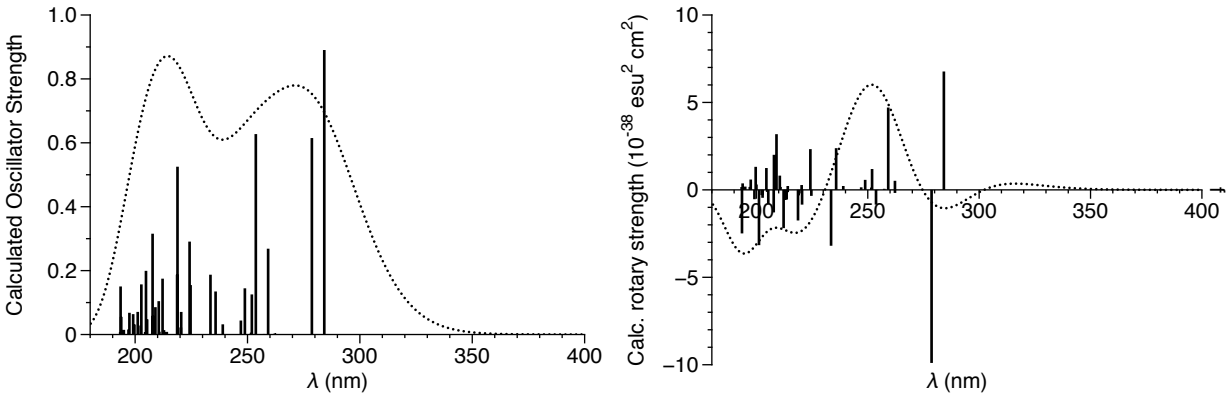

Figure S5. Calculated UV (left) and CD (right) spectra of (*M*)-**oP^6(*p*-H)**, anti/anti conformer (PCM($CHCl_3$)/TD/CAM-B3LYP/6-31G(d,p)//PCM($CHCl_3$)/B97-D/TZV(2d,2p)). 48 excitations were calculated, spectra were estimated by assuming a 0.333 eV half-width at half-height.

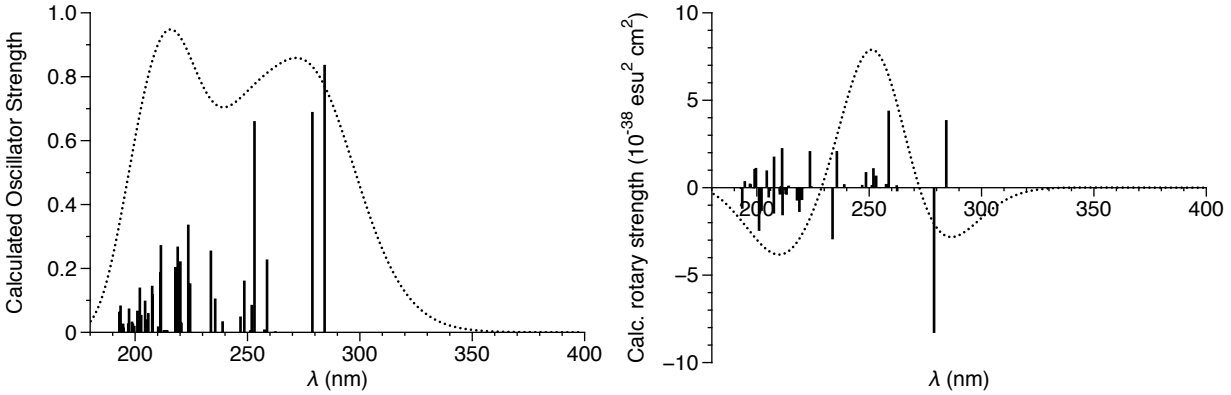

Figure S6. Calculated UV (left) and CD (right) spectra of (*M*)-**oP^6(*p*-H)**, syn/anti conformer (PCM($CHCl_3$)/TD/CAM-B3LYP/6-31G(d,p)//PCM($CHCl_3$)/B97-D/TZV(2d,2p)). 48 excitations were calculated, spectra were estimated by assuming a 0.333 eV half-width at half-height.

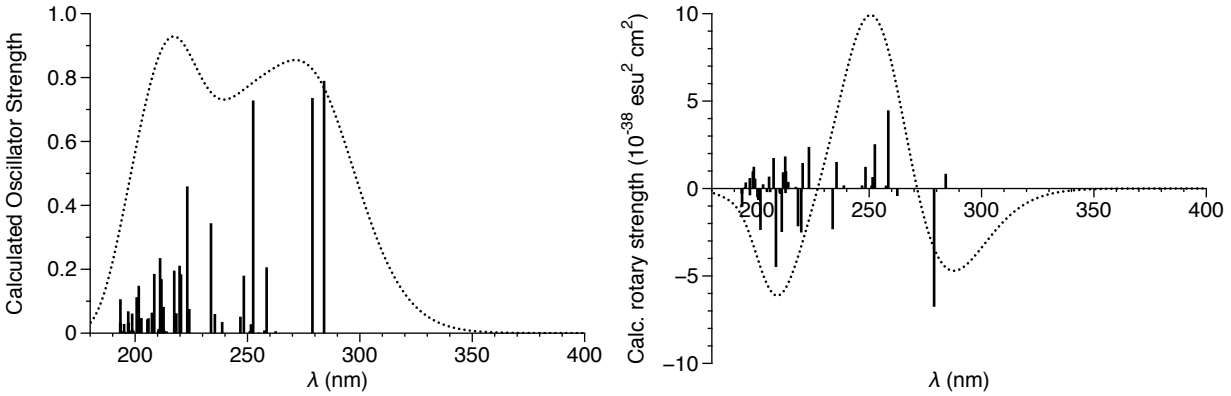

Figure S7. Calculated UV (left) and CD (right) spectra of (*M*)-**oP^6(*p*-H)**, syn/syn conformer (PCM($CHCl_3$)/TD/CAM-B3LYP/6-31G(d,p)//PCM($CHCl_3$)/B97-D/TZV(2d,2p)). 48 excitations were calculated, spectra were estimated by assuming a 0.333 eV half-width at half-height.

The two lowest-energy transitions for each conformer, which correspond to the Cotton effect at 300 nm, are principally associated with HOMO → LUMO and HOMO → LUMO+1 transitions. As shown in Figure S8 for the

anti/anti conformer, these transitions involve orbitals with significant contributions from the oligomer termini. In contrast, the Cotton effect at 260 nm derives primarily from the HOMO–1 ⟶ LUMO+2 transition, which is centered on the *o*-phenylene backbone.

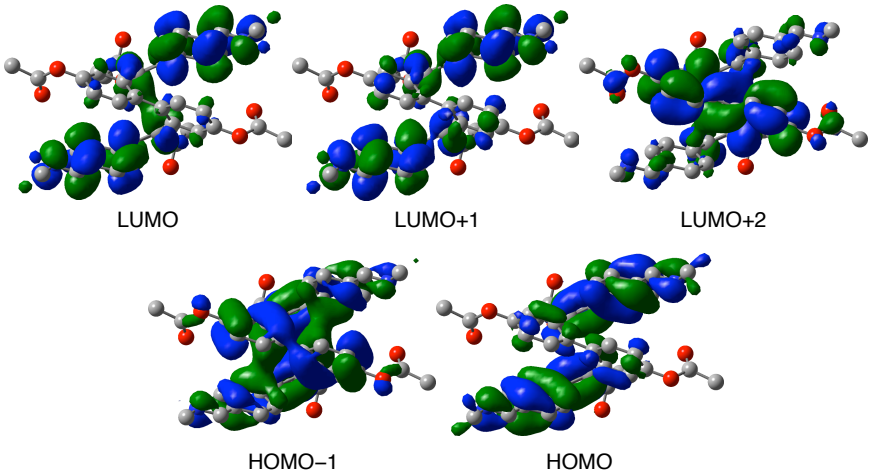

Figure S8. Frontier MOs for (*M*)-**oP^6(*p*-H)**, anti/anti conformer.

oP^4(p-^{t}Bu) geometry optimization

To identify global conformational energy minima, PES scans for rotation about the C*–N bond of (*R*)-**oP^4(*p*-^{t}Bu)** were carried out at the B97-D/cc-pVDZ level for four configurations differing in the handedness of the helix and the syn/anti orientation of the imine N atom. The lowest energy conformers were then chosen for full geometry optimizations at the PCM($CHCl_3$)/B97-D/TZV(2d,2p) level. Cartesian coordinates of the optimized geometries are included in a separate text file.

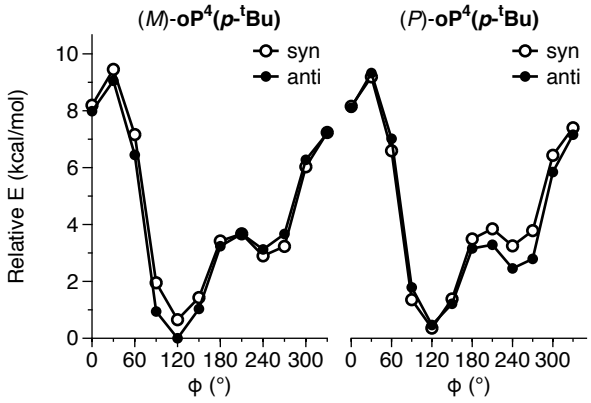

Figure S9. PES scans for (*R*)-**oP^4(*p*-^{t}Bu)** (B97-D/cc-pVDZ).

Conformer	Energy (E_h)	ZPC (E_h)	Total Energy (E_h)	IF
anti-(*M*)-(*R*)-**oP^4(*p*-^{t}Bu)**	−1254.237800	0.519638	−1253.718162	0
syn-(*P*)-(*R*)-**oP^4(*p*-^{t}Bu)**	−1254.237509	0.519516	−1253.717993	0

Table S3. Geometry optimization data for (*R*)-**oP^4(*p*-^{t}Bu)** (PCM($CHCl_3$)/B97-D/TZV(2d,2p)). ZPC = zero-point correction, IF = number of imaginary frequencies.

Single-point calculations were also carried out at the B98 level to test for the significance of dispersion interactions to the relative conformer stability.

Conformer	Energy (E_h)
anti-(*M*)-(*R*)-**oP^4(*p*-^{t}Bu)**	−1254.645382
syn-(*P*)-(*R*)-**oP^4(*p*-^{t}Bu)**	−1254.645741

Table S4. Single-point energy calculations of (*R*)-**oP^4(*p*-^{t}Bu)** at the PCM($CHCl_3$)/B98/TZV(2d,2p)//-PCM($CHCl_3$)/B97-D/TZV(2d,2p) level.

UV–vis spectra of *o*-imines

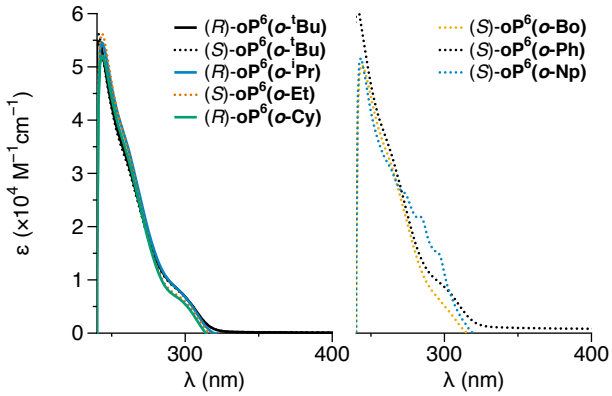

Figure S10. UV–vis spectra of the *o*-imine series dissolved in chloroform (10 μM).

Correlation of mean ii/oo *de*'s with io *de*'s for *o*-imine series

The plots in Figure S11 were generated by assuming that the ii and oo conformers exhibit either the opposite or same twist sense of chiral induction.

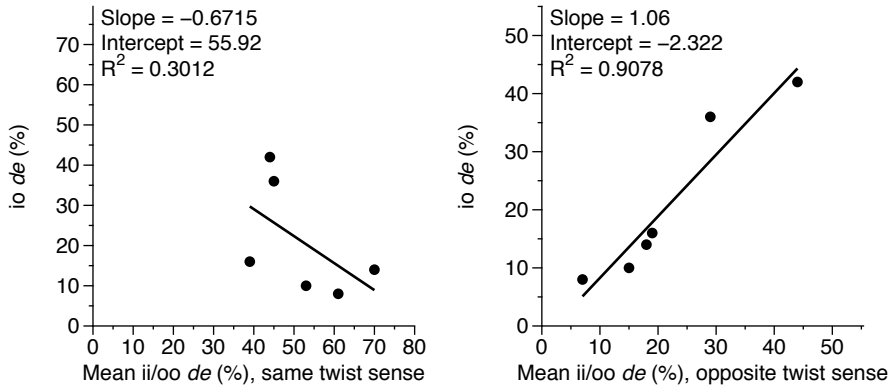

Figure S11. Correlation between io *de*'s and mean ii/oo *de*'s for the *o*-imine series, assuming the same twist sense for the ii/oo conformers (left) or the opposite twist sense (right).

Computational studes of *o*-imines

Geometry optimization of ***oP^6(o-H)***

Cartesian coordinates of the optimized geometries are included in a separate text file. As for **oP^6(*p*-H)**, the acetoxy groups were oriented by first generating a library of possible orientations in Tinker, followed by PM7 optimization with MOPAC. The most stable twofold-symmetric orientation was then used for ab initio geometry optimizations. DFT optimizations were done at the dispersion-corrected PCM($CHCl_3$)/B97-D/TZV(2d,2p) level.

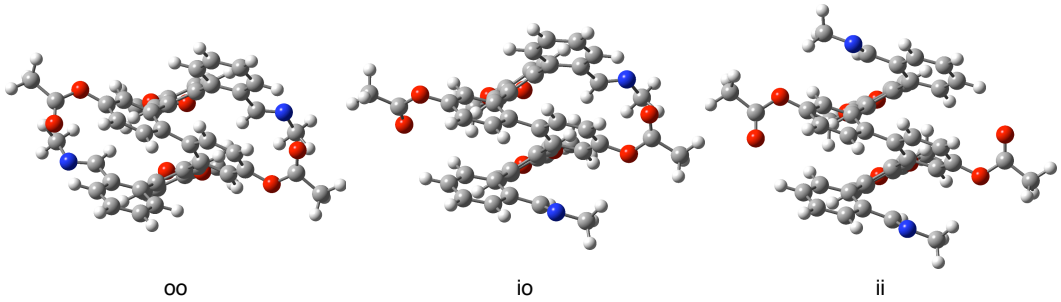

Figure S12. Optimized geometries of (*M*)-**oP^6(*o*-H)** (PCM($CHCl_3$)/B97-D/TZV(2d,2p)).

Conformer	Energy (E_h)	ZPC (E_h)	Total Energy (E_h)	IF
oo (C_2)	−2563.672841	0.749333	−2562.923508	0
io (C_1)	−2563.674943	0.748792	−2562.926151	0
ii (C_2)	−2563.673945	0.748235	−2562.925710	0

Table S5. Geometry optimization data for (*M*)-**oP^6(*p*-H)** (PCM($CHCl_3$)/B97-D/TZV(2d,2p)). ZPC = zero-point correction, IF = number of imaginary frequencies.

*(R)-**oP^4(o-^{t}Bu)** and (S)-**oP^4(o-Bo)** geometry optimizations*

To identify global conformational energy minima, PES scans for rotation about the C*–N bond of (*R*)-**oP^4(*o*-^{t}Bu)** and (*S*)-**oP^4(*o*-Bo)** were carried out at the B97-D/cc-pVDZ level for four configurations differing in the handedness of the helix and inward or outward orientations of the imines. Both syn/anti orientations of the imine N atom were considered in all cases; one specific orientation was favored in all cases, so just the minimum energy conformers are included in the plots. The lowest-energy conformations were chosen for full geometry optimizations. Cartesian coordinates of the optimized geometries are included in a separate text file.

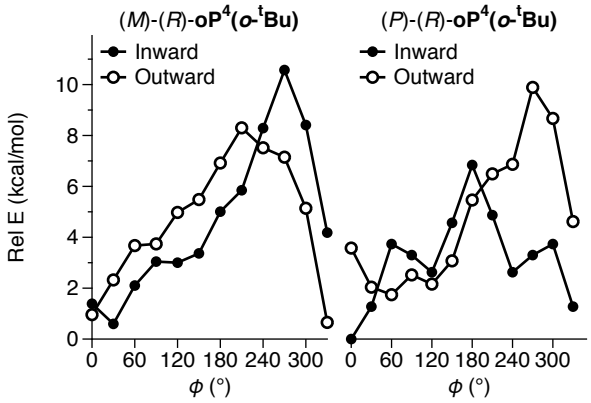

Figure S13. PES scans for (*R*)-**oP^4(*o*-^{t}Bu)** (B97-D/cc-pVDZ).

Conformer	Energy (E_h)	ZPC (E_h)	Total Energy (E_h)	IF
(*M*,*i*)-(*R*)-**oP^4(*p*-^{t}Bu)**	−1254.235361	0.519847	−1253.715514	0
(*M*,*o*)-(*R*)-**oP^4(*p*-^{t}Bu)**	−1254.238284	0.520001	−1253.718283	0
(*P*,*i*)-(*R*)-**oP^4(*p*-^{t}Bu)**	−1254.236939	0.519962	−1253.716977	0
(*P*,*o*)-(*R*)-**oP^4(*p*-^{t}Bu)**	−1254.236849	0.519735	−1253.717114	0

Table S6. Geometry optimization data for (*R*)-**oP^4(*o*-^{t}Bu)** (PCM($CHCl_3$)/B97-D/TZV(2d,2p)). ZPC = zero-point correction, IF = number of imaginary frequencies.

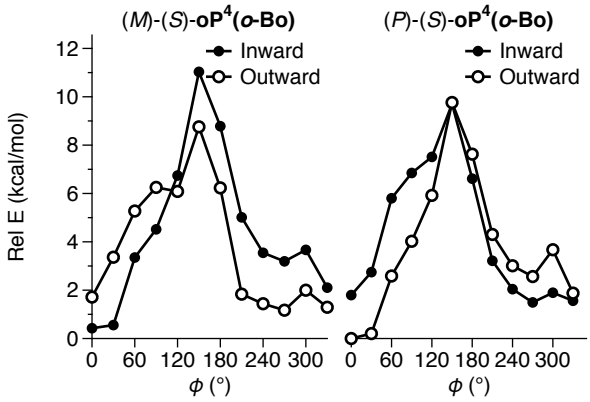

Figure S14. PES scans for (*S*)-**oP^4(*o*-Bo)** (B97-D/cc-pVDZ).

Conformer	Energy (E_h)	ZPC (E_h)	Total Energy (E_h)	IF
(*M*,*i*)-(*S*)-**oP^4(*o*-Bo)**	−1408.998404	0.590532	−1408.407872	0
(*M*,*o*)-(*S*)-**oP^4(*o*-Bo)**	−1408.997145	0.590231	−1408.406914	0
(*P*,*i*)-(*S*)-**oP^4(*o*-Bo)**	−1408.996476	0.590477	−1408.405999	0
(*P*,*o*)-(*S*)-**oP^4(*o*-Bo)**	−1408.999228	0.590285	−1408.408943	0

Table S7. Geometry optimization data for (*S*)-**oP^4(*o*-Bo)** (PCM($CHCl_3$)/B97-D/TZV(2d,2p)). ZPC = zero-point correction, IF = number of imaginary frequencies.

NMR assignments

NMR assignments for the aromatic ^{1}H and ^{13}C nuclei are given below. Assignments were made from the one- and two-dimensional spectra, with chemical shifts extracted from the 1D spectra where possible. In many cases, it was more straightforward to obtain ^{13}C chemical shifts indirectly via the HSQC and HMBC spectra.

p-Substituted oligomers

Position	^{1}H δ (ppm)	^{13}C δ (ppm)
1a	6.61	129.20
1b	7.48	129.57
1c		134.01
1f		146.55
2a		136.03
2b	7.05	130.89
2c	7.16	120.41
2d		150.77
2e	6.15	124.80
2f		139.68
3a		139.40
3b	6.92	124.18
3c		149.87
3d	6.48	121.64
3e	5.66	132.34
3f		136.69
ald.	9.90	192.19

Table S8. NMR assignments for **oP^6(*p*-CHO)**.

Position	^{1}H δ (ppm)	^{13}C δ (ppm)
1a	6.48	129.0
1b	7.31	127.9
1c		134.3
1f		142.6
2a		137.0
2b	7.03	130.9
2c	7.09	120.2
2d		150.3
2e	6.09	123.9
2f		139.9
3a		139.8
3b	6.87	123.9
3c		149.8
3d	6.47	121.2
3e	5.73	132.8
3f		137.0
imine	8.20	158.4

Table S9. NMR assignments for **oP^{6}(*p*-Me)**.

Position	^{1}H δ (ppm)		^{13}C δ (ppm)
	Major	Minor	
1a	6.48	6.49	128.7
1b	7.33	7.32	127.6
1c			133.9
1f			142.1
2a			137.0
2b	7.03	7.05	130.7
2c	7.09	7.09	120.1
2d			150.0
2e	6.10	6.10	123.7
2f			139.6
3a			138.8
3b	6.87	6.88	123.6
3c			149.5
3d	6.45	6.48	121.0
3e	5.74	5.69	132.6
3f			137.2
imine	8.12	8.11	158.4

Table S10. NMR assignments for (*R*)-**oP^{6}(*p*-^{t}Bu)**.

Position	^{1}H δ (ppm)		^{13}C δ (ppm)
	Major	Minor	
1a	6.49	6.49	128.8
1b	7.32	7.31	127.8
1c			134.1
1f			142.2
2a			136.8
2b	7.05	7.04	130.8
2c	7.10	7.10	120.1
2d			150.0
2e	6.10	6.10	123.7
2f			140.0
3a			139.1
3b	6.88	6.88	123.8
3c			149.7
3d	6.46	6.47	121.1
3e	5.73	5.70	132.5
3f			136.7
imine	8.13	8.12	158.6

Table S11. NMR assignments for (*R*)-**oP^{6}(*p*-^{i}Pr)**.

Position	^{1}H δ (ppm)		^{13}C δ (ppm)
	Major	Minor	
1a	6.48	6.48	128.9
1b	7.30	7.32	127.8
1c			133.9
1f			142.5
2a			136.9
2b	7.04	7.02	130.8
2c	7.09	7.09	120.2
2d			150.2
2e	6.09	6.09	123.8
2f			139.8
3a			139.6
3b	6.87	6.87	123.8
3c			149.6
3d	6.47	6.47	121.2
3e	5.73	5.71	132.7
3f			136.8
imine	8.15	8.15	159.0

Table S12. NMR assignments for (*S*)-**oP^{6}(*p*-Et)**.

Position	^{1}H δ (ppm)		^{13}C δ (ppm)
	Major	Minor	
1a	6.48	6.48	128.9
1b	7.31	7.30	127.9
1c			134.0
1f			142.4
2a			136.9
2b	7.03	7.04	130.8
2c	7.09	7.09	120.2
2d			150.1
2e	6.10	6.10	123.8
2f			139.8
3a			139.6
3b	6.88	6.87	123.8
3c			149.6
3d	6.48	6.46	121.2
3e	5.73	5.71	132.8
3f			136.9
imine	8.09	8.08	158.8

Table S13. NMR assignments for (*R*)-**oP^{6}(*p*-Cy)**.

Position	^{1}H δ (ppm)		^{13}C δ (ppm)
	Major	Minor	
1a	6.48	6.49	128.9
1b	7.36	7.34	128.0
1c			134.5
1f			142.3
2a			137.0
2b	7.03	7.05	130.8
2c	7.10	7.10	120.2
2d			150.2
2e	6.11	6.11	123.9
2f			139.8
3a			137.1
3b	6.88	6.89	123.9
3c			149.7
3d	6.47	6.52	121.2
3e	5.74	5.71	132.8
3f			139.8
imine	8.10	8.10	158.9

Table S14. NMR assignments for (*S*)-**oP^{6}(*p*-Bo)**.

Position	^{1}H δ (ppm)		^{13}C δ (ppm)
	Major	Minor	
1a	6.52	6.52	128.7
1b	7.40	7.40	127.9
1c			133.8
1f			142.5
2a			136.7
2b	7.06	7.06	130.7
2c	7.13	7.13	120.1
2d			149.8
2e	6.13	6.13	123.7
2f			139.4
3a			139.5
3b	6.91	6.91	123.7
3c			149.4
3d	6.52–6.49	6.52–6.49	121.1
3e	5.76	5.72	132.6
3f			136.7
imine	8.31	8.30	159.5

Table S15. NMR assignments for (*S*)-**oP^{6}(*p*-Ph)**.

Position	^{1}H δ (ppm)		^{13}C δ (ppm)
	Major	Minor	
1a	6.50	6.50	128.9
1b	7.40	7.38	128.7
1c			133.8
1f			142.6
2a			136.7
2b	7.03	7.03	130.8
2c	7.10	7.10	120.1
2d			150.0
2e	6.11	6.11	123.8
2f			139.4
3a			139.4
3b	6.88	6.88	123.9
3c			149.4
3d	6.44	6.43	121.1
3e	5.72	5.66	132.6
3f			136.7
imine	8.33	8.32	159.7

Table S16. NMR assignments for (*S*)-**oP^{6}(*p*-Np)**.

o-Substituted oligomers

For the *o*-substituted oligomers, full assignments were made for the achiral **oP^{6}(*o*-CHO)** and **oP^{6}(*o*-Me)**. Because of the complexity of the spectra for the chiral oligomers, only protons H_{3e} were fully assigned to the eight distinct environments (both diastereomers of the ii, oo, and io conformers).

Position	^{1}H δ (ppm)				^{13}C δ (ppm)
	oo	ii	io		
1a					134.6
1b	7.70	7.51	7.65	7.45	127.7
1c	7.13–7.02	7.13–7.02	7.13–7.02	7.13–7.02	132.2
1d	7.25–7.16	7.25–7.16	7.25–7.16	7.25–7.16	127.2
1e	6.46	6.47	6.51	6.32	131.4
1f					143.3
2a					132.6
2b	6.86	6.82	6.82	6.86	134.3
2c	7.32–7.16	7.32–7.16	7.32–7.16	7.32–7.16	120.2
2d					150.6
2e	6.24	6.21	6.213	6.18	124.6
2f					140.4
3a					139.2
3b	6.95	6.89	6.90	6.95	124.6
3c					150.1
3d	6.60	6.54	6.56	6.61	121.1
3e	5.60	5.75	5.72	5.63	132.7
3f					136.2
ald.	9.07	9.16	9.08	9.23	191.0

Table S17. NMR assignments for **oP^{6}(*o*-CHO)**.

Position	^{1}H δ (ppm)				^{13}C δ (ppm)
	oo	ii	io		
1a					135.7
1b	7.66	7.64	7.63	7.56	127.4
1c	7.13–7.09	7.13–7.09	7.07–7.04	7.07–7.04	126.9
1d	6.92–6.90	6.92–6.90	6.79–6.76	6.79–6.76	128.5
1e	6.38	6.34	6.35	6.33	130.8
1f					139.5
2a					134.7
2b	6.83	7.03	7.09	6.78	133.4
2c	7.11–7.09	7.18–7.16	7.27–7.24	7.06–7.04	119.4
2d					149.7
2e	6.25	6.13	6.23	6.15	124.1
2f					140.6
3a					140.4
3b	6.92	6.76	6.88	6.96	124.1
3c					149.5
3d	6.57	6.51	6.57	6.68	120.7
3e	5.54	5.87	5.82	5.64	132.8
3f					136.9
8	7.02	7.40	7.51	7.13	158.1

Table S18. NMR assignments for **oP^{6}(*o*-Me)**.

Experimental

Synthesis

General

Unless otherwise noted, all starting materials, reagents, and solvents were purchased from commercial sources and used without further purification. Melting points were determined using an Electrothermal 9100 digital melting point apparatus at a heating rate of 10 ℃/min. NMR spectra were measured for $CDCl_3$ solutions using Bruker Avance 500 or 850 MHz NMR spectrometers. Semi-preparative gel permeation chromatography was performed using a Waters Breeze 2 HPLC equipped with a 19×300 mm Ultrastyragel 500 Å GPC column with toluene as the eluent. 2,2′-Dibromo-5,5′-dimethoxybiphenyl (**1**) was synthesized following literature procedures.[10]

***o*-Phenylene tetramer 2**

To a stirred solution of **1** (10.0 g, 27.0 mmol) in anhydrous THF (500 mL) at −78 ℃ under argon was added *n*-butyl lithium (15.2 mL, 24.3 mmol, 1.6 M in hexane) dropwise over 10 min and the reaction was stirred for 40 min. CuCN (1.2 gm, 14 mmol) was added in one portion and the dry ice bath was removed. The resulting suspension was stirred for 2 h at rt (until all the CuCN had dissolved). Duroquinone (6.6 g, 41 mmol) was then added in one portion and the dark-colored reaction was stirred for 2 h at rt. The reaction was quenched by adding NH_3(aq) (80 mL) to the reaction and stirring for 10 min. Both layers were separated, and the aqueous layer was extracted with EtOAc (3 × 100 mL). The combined organic extracts were washed with sat. NH_4Cl(aq) (50 mL), water (50 mL), and brine (50 mL), dried over $MgSO_4$, filtered, and concentrated. Purification by flash chromatography (1:9 EtOAc:hexanes) gave **2** (5.1 g, 64%) as a pale yellow solid: mp 132.1–133.9 ℃; ^{1}H NMR (500 MHz, $CDCl_3$, Figure S15) δ 7.46–7.17 (m, 4H), 7.09–6.25 (m, 8H), 3.82–3.39 (m, 12H); ^{13}C NMR (125 MHz, $CDCl_3$, Figure S16) δ 158.1, 158.0, 157.7, 157.5, 140.6, 133.2, 132.9, 122.0, 117.0, 115.5, 114.7, 113.4, 55.4; HRMS (ESI) calcd for $C_{28}H_{25}Br_2O_4$ ([M + H$^+$]) 583.0119, found 583.0125.

***o*-Phenylene tetramer 3**

To a stirred solution of **2** (1.0 g, 1.7 mmol) in CH_2Cl_2 (10 mL) at −78 ℃, was added BBr_3 (10.27 mL, 10.27 mmol, 1 M in CH_2Cl_2) dropwise over 10 min. The dry ice bath was then removed and the resulting brown-colored solution was stirred for 16 h at rt. The reaction was then quenched with the slow addition of ice (40 mL) and the mixture extracted with EtOAc (5 × 40 mL). The combined organic extracts were washed with brine (40 mL), dried over $MgSO_4$, filtered, and concentrated. Purification by flash chromatography (3:2 EtOAc:hexanes) gave **1** (0.62 g, 69%) as a light brown solid: mp 291.3–293.1 ℃; ^{1}H NMR (500 MHz, DMSO-d_6, Figure S17) δ 9.62 (m, 4H), 7.44 (d, J = 8.7 Hz, 2H), 7.26 (d, J = 8.5 Hz, 1H), 6.90 (d, J = 8.5 Hz, 1H), 6.75–6.65 (m, 2H), 6.63–6.39 (m, 6H); ^{13}C NMR (125 MHz, DMSO-d_6, Figure S17) δ 156.6, 156.4, 155.6, 155.5, 143.6, 141.0, 133.4, 133.0, 132.1, 129.8, 129.5, 118.6, 117.7, 116.5, 114.8, 114.5, 112.9; HRMS (ESI) calcd for $C_{24}H_{17}Br_2O_4$ ([M + H$^+$]) 526.9493, found 526.9491.

***o*-Phenylene tetramer 4**

To a stirred solution of **3** (1.5 g, 2.84 mmol) in $CHCl_3$ (100 mL) was added acetic anhydride (5.4 mL, 57 mmol) followed by Et_3N (2.9 mL, 23 mmol) and the resulting solution was stirred for 24 h at 40 ℃. The reaction mixture was cooled and treated with water (50 mL). The layers were separated and the aqueous layer extracted with $CHCl_3$ (3 × 50 mL). The combined organic layers were washed with water (20 mL) and brine (20 mL), dried over $MgSO_4$, filtered, and concentrated. Purification by flash chromatography (3:7 EtOAc:hexanes) gave **4** (1.72 gm, 87%) as a pale yellow solid: mp 103.4–105.1 ℃; ^{1}H NMR (500 MHz, $CDCl_3$, Figure S19) δ 7.54–7.31 (m, 4H), 7.20–6.57 (m, 8H), 2.29–2.16 (m, 12H); ^{13}C NMR (125 MHz, $CDCl_3$, Figure S20) δ 169.1, 168.9, 168.9, 168.7, 149.3, 136.2, 133.5, 132.6, 123.9, 122.0, 121.4, 121.2, 120.9, 21.2, 21.1, 21.0; HRMS (ESI) calcd for $C_{32}H_{25}Br_2O_8$ ([M + H$^+$]) 694.9916, found 694.9913.

***o*-Phenylene hexamer oP^6(*p*-CHO)**

A Schlenk vacuum tube was charged with **3** (0.5 g, 0.95 mmol), 4-formylphenylboronic acid (0.57 g, 3.78 mmol), and tetrakis(triphenylphosphine)palladium(0) (110 mg, 0.09 mmol) then evacuated and backfilled with Ar (3×). 2 M Na_2CO_3(aq) (2.4 mL, 4.7 mmol), degassed tetrahydrofuran (8.0 mL), and ethyl alcohol (1.0 mL) were then added. The Schlenk tube was degassed by three freeze-pump-thaw cycles and filled with Ar, then sealed and heated to 90 ℃ for 24 h. The reaction mixture was then cooled and diluted with EtOAc (20 mL), water (20 mL) and 2 M HCl(aq) (20

mL). The layers were separated, the aqueous layer was extracted with EtOAc (4 × 40 mL), and the combined organic layers were washed with brine (50 mL), dried over $MgSO_4$, filtered, and concentrated. The crude product was passed through a plug of silica gel (1:9 MeOH:CH_2Cl_2). The residue (0.45 g, 0.78 mmol) was then dissolved in $CHCl_3$ (20 mL), Et_3N (0.8 mL, 6.2 mmol) was added, and the solution was cooled to 0 ℃. Acetic anhydride (1.47 mL, 15.6 mmol) was added and the resulting solution was then stirred for 20 h at 40 ℃. The reaction mixture was cooled, washed with water (20 mL), and the aqueous layer extracted with CH_2Cl_2 (3 × 40 mL). The combined organic extracts were washed with water (2 × 20 mL) and brine (50 mL), dried over $MgSO_4$, filtered, and concentrated. Purification by flash chromatography (2:3 EtOAc:hexanes) followed by recrystallization from CH_2Cl_2 gave **oP^6(*p*-CHO)** as a white solid (220 mg, 31% over two steps): mp 211.42 ℃ (dec);[a] ^{1}H NMR (500 MHz, $CDCl_3$, Figure S21, Table S8) δ 9.90 (s, 2H), 7.48 (d, J = 8.0 Hz, 4H), 7.16 (dd, J = 2.4, 8.4 Hz, 2H), 7.05 (d, J = 8.5 Hz, 2H), 6.92 (d, J = 2.3 Hz, 2H), 6.61 (d, J = 8.0 Hz, 4H), 6.48 (dd, J = 2.4, 8.4 Hz, 2H), 6.15 (d, J = 2.3 Hz, 2H), 5.66 (d, J = 8.5 Hz, 2H), 2.34 (s, 12H); ^{13}C NMR (125 MHz, $CDCl_3$, S22, Table S8) δ 192.2, 169.4, 169.0, 150.8, 149.9, 146.6, 139.7, 139.4, 136.7, 136.0, 134.0, 132.3, 130.9, 129.6, 129.2, 124.2, 123.8, 121.6, 120.4, 21.4, 21.2; HRMS (ESI) calcd for $C_{46}H_{34}O_{10}Na$ ([M + Na^+]) 769.2050, found 769.2057.

_o_-Phenylene hexamer oP^6(_o_-CHO)

A Schlenk tube was charged with **4** (1.8 g, 2.6 mmol), 2-formylphenylboronic acid (1.56 g, 10.4 mmol), and tetrakis(triphenylphosphine)palladium(0) (299 mg, 0.26 mmol) then evacuated and backfilled with Ar (3×). 2 M Na_2CO_3(aq) (5.2 mL, 10.4 mmol), degassed tetrahydrofuran (16 mL), and ethyl alcohol (2 mL) were then added. The Schlenk tube was degassed by three freeze-pump-thaw cycles and filled with Ar, then sealed and heated to 90 ℃ for 24 h. The reaction mixture was then cooled and diluted with EtOAc (50 mL), water (30 mL) and 2 M HCl(aq) (30 mL). The layers were separated, and the aqueous layer was extracted with EtOAc (4 × 50 mL), and the combined organic layers were washed with brine (50 mL), dried over $MgSO_4$, filtered, and concentrated. The crude product was passed through a plug of silica gel (1:9 MeOH:CH_2Cl_2). The residue (1.3 g, 2.25 mmol) was then dissolved in $CHCl_3$ (50 mL), Et_3N (2.3 mL, 17.9 mmol) was added, and the solution was cooled to 0 ℃. Acetic anhydride (4.24 mL, 44.9 mmol) was added and the resulting solution was then stirred for 20 h at 40 ℃. The reaction mixture was cooled, washed with water (50 mL), and the aqueous layer extracted with CH_2Cl_2 (3 × 50 mL). The combined organic extracts were washed with water (2 × 20 mL) and brine (50 mL), dried over $MgSO_4$, and concentrated. Purification by flash chromatography (2:3 EtOAc:hexanes) followed by recrystallization from CH_2Cl_2 gave **oP^6(*o*-CHO)** as a white solid (0.82 g, 42% over two steps): mp 237.85 ℃ (dec);[b] NMR spectra complex because of the mixture of conformers, see Table S17, Figures S70–S73; HRMS (ESI) calcd for $C_{46}H_{35}O_{10}$ ([M + H^+]) 747.2230, found 747.2249.

General procedure for imine condensation

In a glass vial, dialdehyde **oP^6(*p*-CHO)** or **oP^6(*o*-CHO)** (1.0 equiv) and the appropriate amine (2.2 equiv) were dissolved in deacidified chloroform to give a final concentration of 0.02 M. TFA (0.2 equiv) was added followed by 3 Å molecular sieves. The reaction mixture was then allowed to stand for 4 d with occasional stirring. The solution was then transferred to another vial with 2 mL of triethylamine, then the quenched solution was concentrated. The residue was then purified by semi-preparative gel permeation chromatography with toluene as the eluent.

_o_-Phenylene hexamer oP^6(_p_-Me)

Following the general procedure with **oP^6(*p*-CHO)** (32.14 mg) and isopropyl amine, **oP^6(*p*-Me)** was obtained as an off-white solid (16.4 mg, 46%): mp 232.1–233.9 ℃; ^{1}H NMR (500 MHz, $CDCl_3$, Figure S26, Table S9) δ 8.20 (s, 2H), 7.31 (d, J = 8.2 Hz, 4H), 7.09 (dd, J = 8.4, 2.4 Hz, 2H), 7.03 (d, J = 8.4 Hz, 2H), 6.87 (d, J = 2.4 Hz, 2H), 6.48 (d, J = 8.2 Hz, 4H), 6.47 (dd, J = 8.4, 2.4 Hz, 2H), 6.09 (d, J = 2.3 Hz, 2H), 5.73 (d, J = 8.4 Hz, 2H), 3.49 (m, 2H), 2.34 (s, 6H), 2.33 (s, 6H), 1.27–1.19 (m, 12H); ^{13}C NMR (125 MHz, $CDCl_3$, Figure S27, Table S9) δ 169.4, 169.2, 158.4, 150.3, 149.8, 142.6, 139.9, 139.8, 137.0, 137.0, 134.3, 132.8, 130.9, 129.0, 127.9, 123.9, 123.9, 121.2, 120.2, 61.8, 24.4, 24.3, 21.5, 21.4; HRMS (ESI) calcd for $C_{52}H_{49}O_8N_2$ ([M + H^+]) 829.3489, found 829.3479.

[a]Measured by differential scanning calorimetry.
[b]Measured by differential scanning calorimetry.

***o*-Phenylene hexamer (*R*)-oP^6(*p*-^{t}Bu)**

Following the general procedure with **oP^6(*p*-CHO)** (51.13 mg) and (*R*)-(−)-3,3-dimethyl-2-butylamine, (*R*)-**oP^6(*p*-^{t}Bu)** was obtained as an off-white solid (48.51 mg, 77%): mp 153.5–157.1 ℃; NMR spectra complex because of the mixture of conformers, see Table S10, Figures S32–S35; HRMS (ESI) calcd for $C_{58}H_{61}O_8N_2$ ([M + H$^+$]) 913.4428, found 913.4428.

***o*-Phenylene hexamer (*S*)-oP^6(*p*-^{t}Bu)**

Following the general procedure with **oP^6(*p*-CHO)** (51.96 mg) and (*S*)-(+)-3,3-dimethyl-2-butylamine, (*S*)-**oP^6(*p*-^{t}Bu)** was obtained as an off-white solid (52.87 mg, 83%): mp 160.9–162.4 ℃; NMR spectra complex because of the mixture of conformers, see Table S10, Figures S36–S40; HRMS (ESI) calcd for $C_{58}H_{61}O_8N_2$ ([M + H$^+$]) 913.4428, found 913.4445.

***o*-Phenylene hexamer (*R*)-oP^6(*p*-^{i}Pr)**

Following the general procedure with **oP^6(*p*-CHO)** (52.01 mg) and (*R*)-(−)-2-amino-3-methylbutane, (*R*)-**oP^6(*p*-^{i}Pr)** was obtained as an off-white solid (41.25 mg, 67%): mp 166.1–167.9 ℃; NMR spectra complex because of the mixture of conformers, see Table S11, Figures S41–S45; HRMS (ESI) calcd for $C_{56}H_{57}O_8N_2$ ([M + H$^+$]) 885.4115, found 885.4113.

***o*-Phenylene hexamer (*S*)-oP^6(*p*-Et)**

Following the general procedure with **oP^6(*p*-CHO)** (52.33 mg) and (*S*)-(+)-sec-butylamine, (*S*)-**oP^6(*p*-Et)** was obtained as an off-white solid (36.83 mg, 61%): mp 170.8–171.3 ℃; NMR spectra complex because of the mixture of conformers, see Table S12, Figures S46–S49; HRMS (ESI) calcd for $C_{54}H_{53}O_8N_2$ ([M + H$^+$]) 857.3802, found 857.3795.

***o*-Phenylene hexamer (*R*)-oP^6(*p*-Cy)**

Following the general procedure with **oP^6(*p*-CHO)** (54.55 mg) and (*R*)-(−)-1-cyclohexylethylamine, (*R*)-**oP^6(*p*-Cy)** was obtained as an off-white solid (39.52 mg, 56%): mp 162.8–164.7 ℃; NMR spectra complex because of the mixture of conformers, see Table S13, Figures S51–S55; HRMS (ESI) calcd for $C_{62}H_{65}O_8N_2$ ([M + H$^+$]) 965.4741, found 965.4738.

***o*-Phenylene hexamer (*S*)-oP^6(*p*-Bo)**

Following the general procedure with **oP^6(*p*-CHO)** (50.55 mg) and (*R*)-(+)-bornylamine, (*S*)-**oP^6(*p*-Bo)** was obtained as an off-white solid (41.47 mg, 60%): mp 178.6–180.4 ℃; NMR spectra complex because of the mixture of conformers, see Table S14, Figures S65–S69; HRMS (ESI) calcd for $C_{66}H_{69}O_8N_2$ ([M + H$^+$]) 1017.5054, found 1017.5048.

***o*-Phenylene hexamer (*S*)-oP^6(*p*-Ph)**

Following the general procedure with **oP^6(*p*-CHO)** (51.49 mg) and (*S*)-(−)-α-methylbenzylamine, (*S*)-**oP^6(*p*-Ph)** was obtained as a pale yellow solid (18.38 mg, 28%): mp 162.7–164.5 ℃; NMR spectra complex because of the mixture of conformers, see Table S15, Figures S56–S60; HRMS (ESI) calcd $C_{62}H_{53}O_8N_2$ ([M + H$^+$]) 953.3802, found 953.3805.

***o*-Phenylene hexamer (*S*)-oP^6(*p*-Np)**

Following the general procedure with **oP^6(*p*-CHO)** (50.49 mg) and (1*S*)-1-(2-naphthyl)ethanamine, (*S*)-**oP^6(*p*-Np)** was obtained as a pale yellow solid (21.97 mg, 31%): mp 168.3–170.5 ℃; NMR spectra complex because of the mixture of conformers, see Table S16, Figures S61–S64; HRMS (ESI) calcd for $C_{70}H_{57}O_8N_2$ ([M + H$^+$]) 1053.4115, found 1053.4124.

***o*-Phenylene hexamer oP^6(*o*-Me)**

Following the general procedure with **oP^6(*o*-CHO)** (31.69 mg) and isopropyl amine, **oP^6(*o*-Me)** was obtained as an off-white solid (21.3 mg, 60%): mp 245.1–246.4 ℃; NMR spectra complex because of the mixture of conformers, see Table S18, Figures S74–S80; HRMS (ESI) calcd for $C_{52}H_{49}O_8N_2$ ([M + H$^+$]) 829.3489, found 829.3493.

***o*-Phenylene hexamer (*R*)-oP^6(*o*-^{t}Bu)**

Following the general procedure with **oP^6(*o*-CHO)** (50.7 mg) and (*R*)-(−)-3,3-dimethyl-2-butylamine, (*R*)-**oP^6(*o*-^{t}Bu)** was obtained as an off-white solid (22.17 mg, 36%): mp 174.1–176.3 ℃; NMR spectra complex because of the mixture of conformers, see Figures S81–S86; HRMS (ESI) calcd for $C_{58}H_{61}O_8N_2$ ([M + H$^+$]) 913.4428, found 913.4444.

o-Phenylene hexamer (*S*)-oP^6(*o*-^{t}Bu)

Following the general procedure with **oP^6(*o*-CHO)** (53.86 mg) and (*S*)-(+)-3,3-dimethyl-2-butylamine, (*S*)-**oP^6(*o*-^{t}Bu)** was obtained as an off-white solid (31.86 mg, 48%): mp 165.1–166.9 ℃; NMR spectra complex because of the mixture of conformers, see Figures S87–S90; HRMS (ESI) calcd for $C_{58}H_{61}O_8N_2$ ([M + H$^+$]) 913.4428, found 913.4450.

o-Phenylene hexamer (*R*)-oP^6(*o*-^{i}Pr)

Following the general procedure with **oP^6(*o*-CHO)** (25.69 mg) and (*R*)-(–)-2-amino-3-methylbutane, (*R*)-**oP^6(*o*-^{i}Pr)** was obtained as an off-white solid (16.3 mg, 53%): mp 178.9–180.2 ℃; NMR spectra complex because of the mixture of conformers, see Figures S91–S96; HRMS (ESI) calcd for $C_{56}H_{57}O_8N_2$ ([M + H$^+$]) 885.4115, found 885.4134.

o-Phenylene hexamer (*S*)-oP^6(*o*-Et)

Following the general procedure with **oP^6(*o*-CHO)** (26.58 mg) and (*S*)-(+)-sec-butylamine, (*S*)-**oP^6(*o*-Et)** was obtained as an off-white solid (18.35 mg, 60%): mp 187.8–189.8 ℃; NMR spectra complex because of the mixture of conformers, see Figures S97–S102; HRMS (ESI) calcd for $C_{54}H_{53}O_8N_2$ ([M + H$^+$]) 857.3802, found 857.3806.

o-Phenylene hexamer (*R*)-oP^6(*o*-Cy)

Following the general procedure with **oP^6(*o*-CHO)** (50.55 mg) and (*R*)-(–)-1-cyclohexylethylamine, (*R*)-**oP^6(*o*-Cy)** was obtained as an off-white solid (33.21 mg, 51%): mp 149.9–151.7 ℃; NMR spectra complex because of the mixture of conformers, see Figures S103–S108; HRMS (ESI) calcd for $C_{62}H_{65}O_8N_2$ ([M + H$^+$]) 965.4741, found 965.4761.

o-Phenylene hexamer (*S*)-oP^6(*o*-Bo)

Following the general procedure with **oP^6(*o*-CHO)** (23.34 mg) and (*R*)-(+)-bornylamine, (*S*)-**oP^6(*o*-Bo)** was obtained as an off-white solid (12.06 mg, 38%): mp 181.9–183.0 ℃; NMR spectra complex because of the mixture of conformers, see Figures S121–S126; HRMS (ESI) calcd for $C_{66}H_{69}O_8N_2$ ([M + H$^+$]) 1017.5054, found 1017.5056.

o-Phenylene hexamer (*S*)-oP^6(*o*-Ph)

Following the general procedure with **oP^6(*o*-CHO)** (53.62 mg) and (*S*)-(–)-α-methylbenzylamine, (*S*)-**oP^6(*o*-Ph)** was obtained as a pale yellow solid (18.95 mg, 28%): mp 163.0–165.1 ℃; NMR spectra complex because of the mixture of conformers, see Figures S109–S114; HRMS (ESI) calcd for $C_{62}H_{53}O_8N_2$ ([M + H$^+$]) 953.3802, found 953.3813.

o-Phenylene hexamer (*S*)-oP^6(*o*-Np)

Following the general procedure with **oP^6(*o*-CHO)** (22.19 mg) and (1S)-1-(2-naphthyl)ethanamine, (*S*)-**oP^6(*o*-Np)** was obtained as a pale yellow solid (7.8 mg, 25%): mp 170.6–171.9 ℃; NMR spectra complex because of the mixture of conformers, see Figures S115–S120; HRMS (ESI) calcd for $C_{70}H_{57}O_8N_2$ ([M + H$^+$]) 1053.4115, found 1053.4154.

Computational chemistry

DFT calculations were performed using Gaussian 09, rev. B.01.[11] All energy minima were verified to have 0 imaginary frequencies by vibrational frequency analysis.

To obtain reasonable orientations of the acetoxy groups in **oP^6(*p*-H)** and **oP^6(*o*-H)**, conformer libraries were first generated using the Tinker 8.2 scan function using the MMFF force field.[4] The conformers were then optimized at the PM7 level using MOPAC 2016,[12] and the lowest-energy twofold symmetric conformer chosen for further consideration.

CD and UV–vis spectroscopy

CD spectroscopy was performed on an Aviv Model 435 Circular Dichroism Spectrometer in a rectangular 0.1 cm quartz cuvette. Data was collected from 370 to 230 nm with an average of 15 scans per sample and 1 nm bandwidth at 25 ℃. Spectra were acquired for solutions in spectroscopy-grade chloroform at 500 μM or 300 μM for the *p*- and *o*-imines, respectively. The CD spectrum for each imine was obtained by subtracting the blank chloroform spectrum from the sample's raw CD spectrum.

UV–vis spectroscopy was performed on a Perkin Elmer Lambda 35 UV–vis spectrometer in a 1.0 cm cuvette. Data was collected from 700 to 200 nm at 25 ℃. Spectra were acquired for solutions in spectroscopy-grade chloroform at 10 μM. The UV–vis spectrum for each imine was obtained by subtracting the blank chloroform spectrum from the sample's raw spectrum.

NMR Spectra

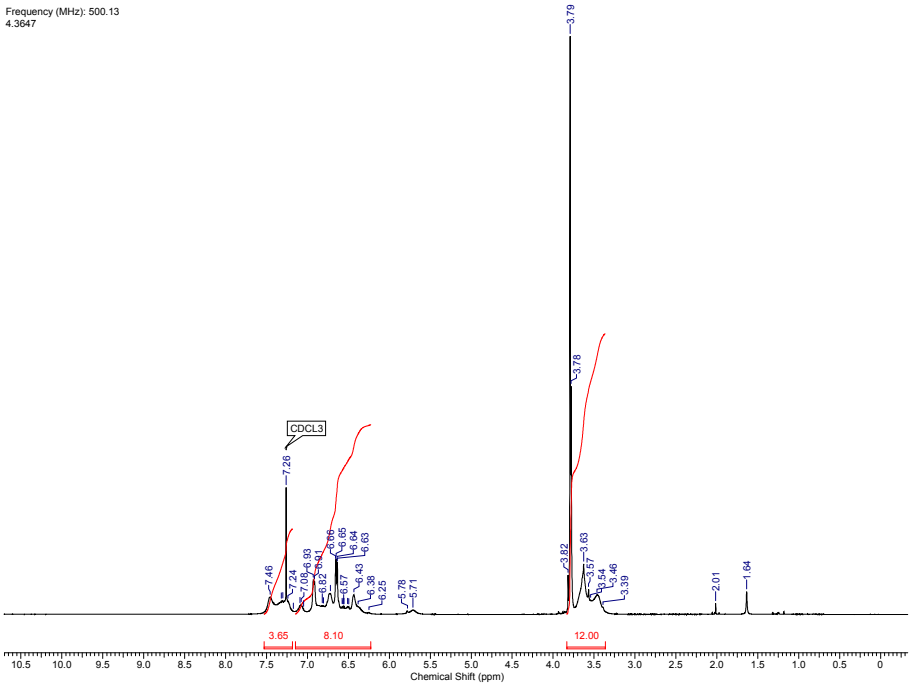

Figure S15. ^{1}H NMR spectrum (500 MHz, $CDCl_3$, rt) of **2**.

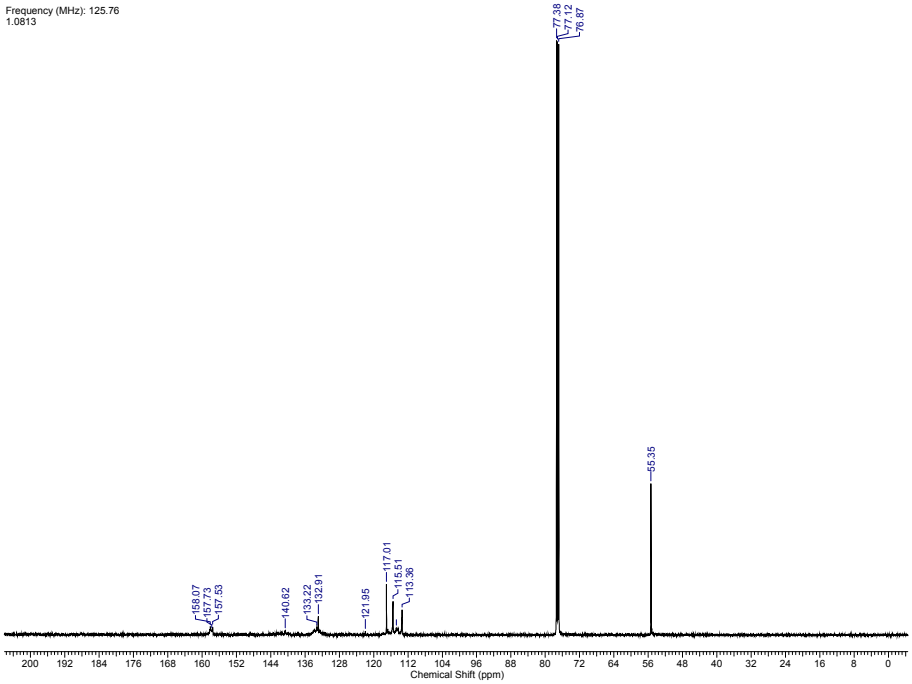

Figure S16. ^{13}C NMR spectrum (125 MHz, $CDCl_3$, rt) of **2**.

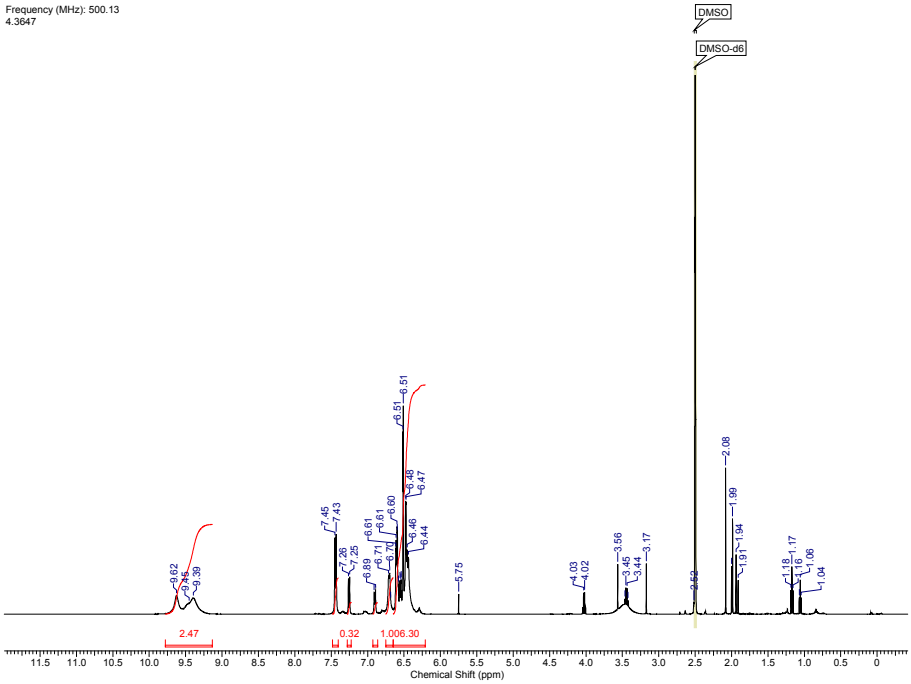

Figure S17. ^{1}H NMR spectrum (500 MHz, $CDCl_3$, rt) of **3**.

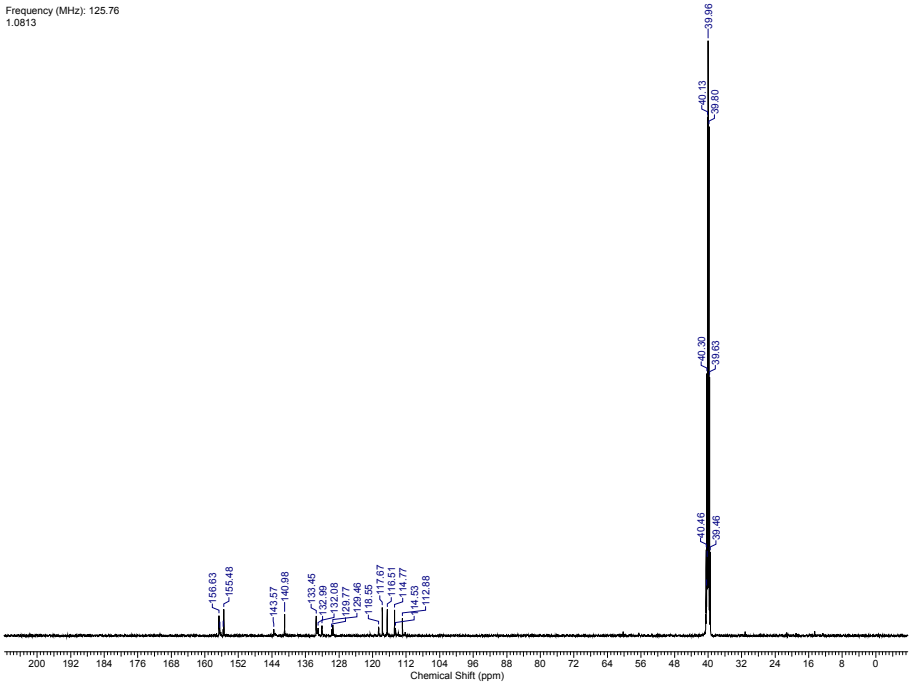

Figure S18. ^{13}C NMR spectrum (125 MHz, $CDCl_3$, rt) of **3**.

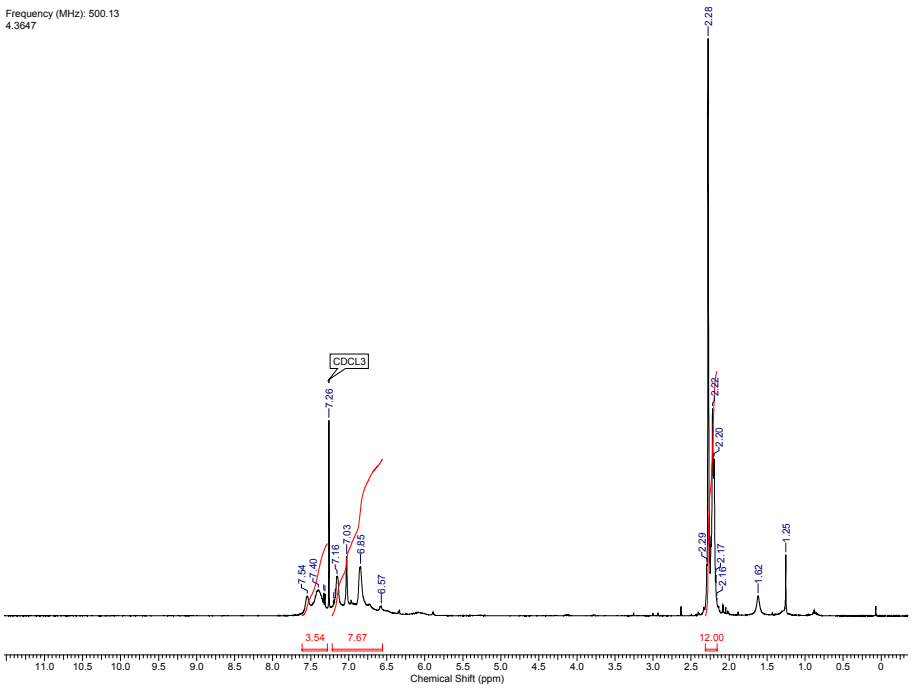

Figure S19. ^{1}H NMR spectrum (500 MHz, $CDCl_3$, rt) of **4**.

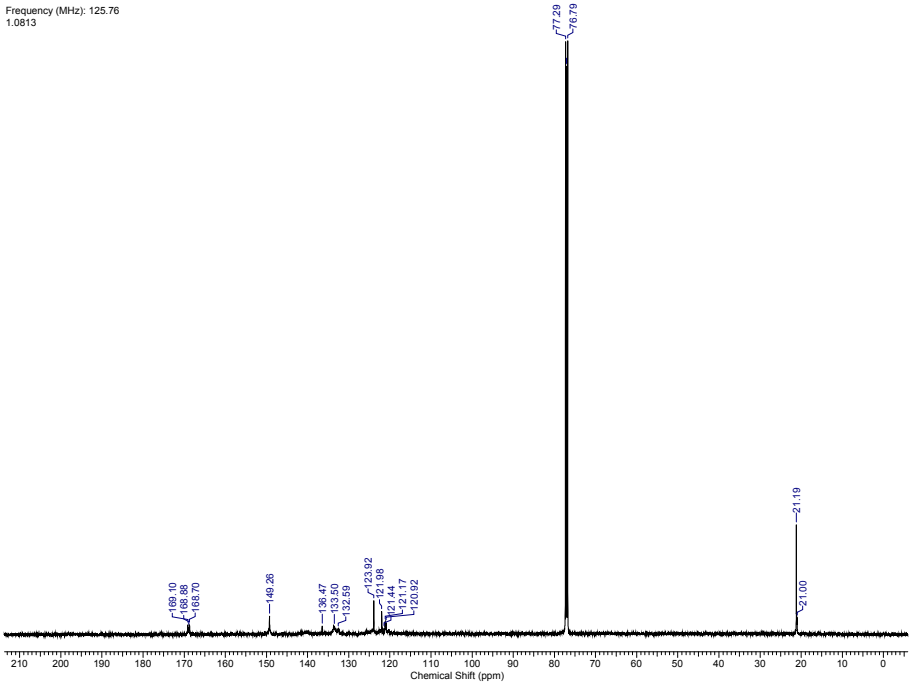

Figure S20. ^{13}C NMR spectrum (125 MHz, $CDCl_3$, rt) of **4**.

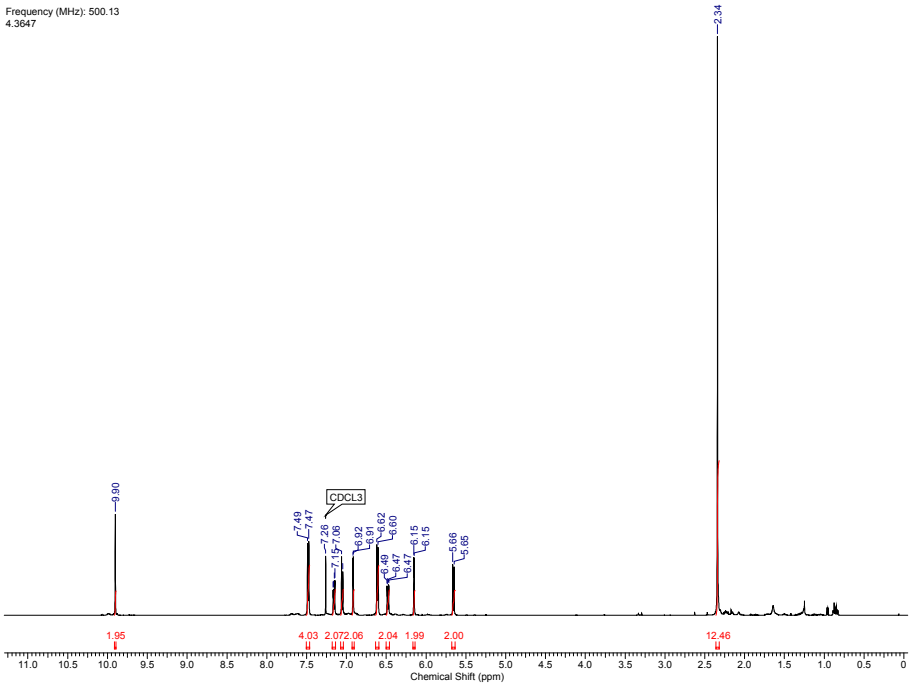

Figure S21. ^{1}H NMR spectrum (500 MHz, $CDCl_3$, rt) of **oP^6(*p*-CHO)**.

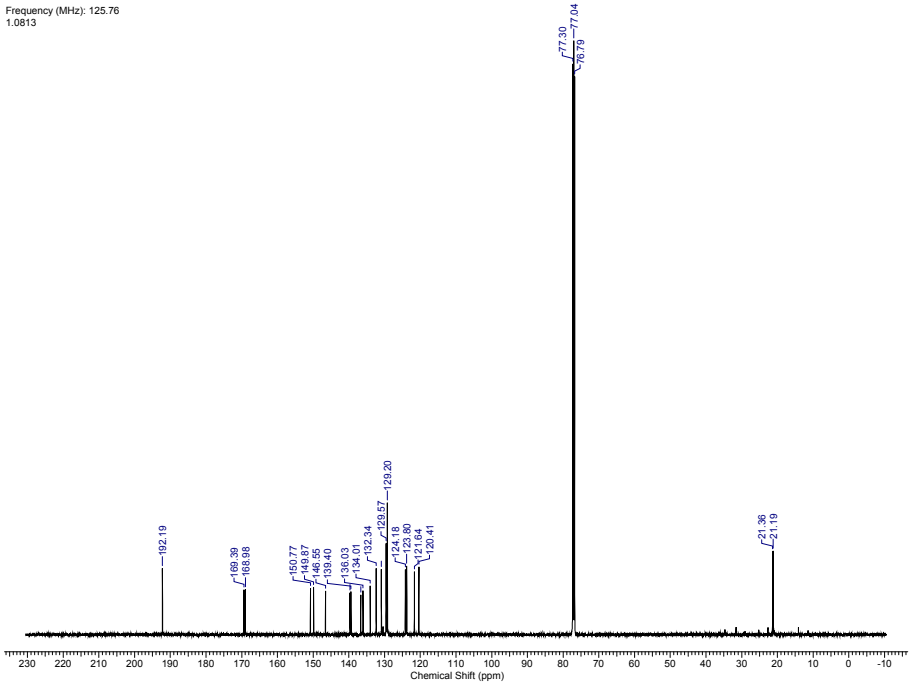

Figure S22. ^{13}C NMR spectrum (125 MHz, $CDCl_3$, rt) of **oP^6(*p*-CHO)**.

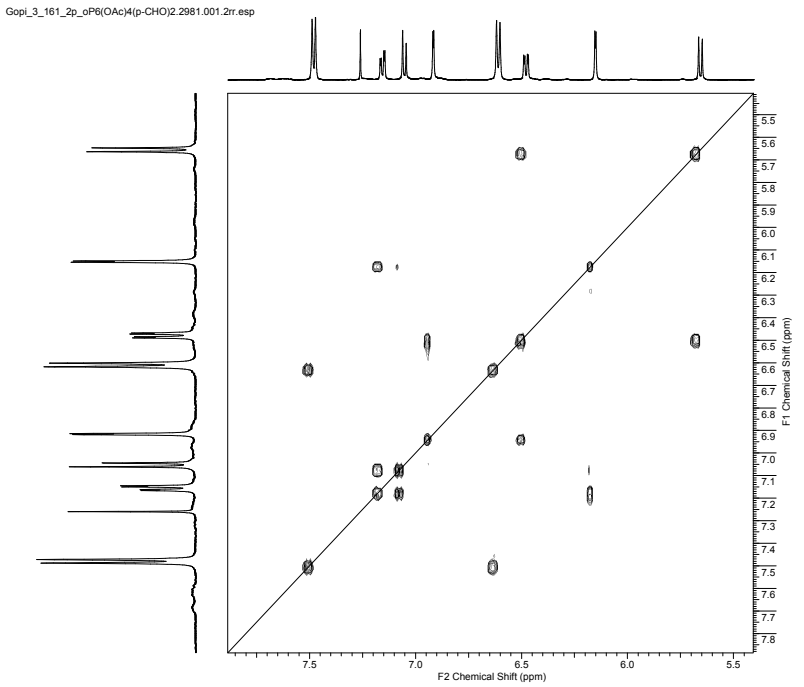

Figure S23. COSY spectrum (500 MHz, $CDCl_3$, rt) of **oP^6(*p*-CHO)**.

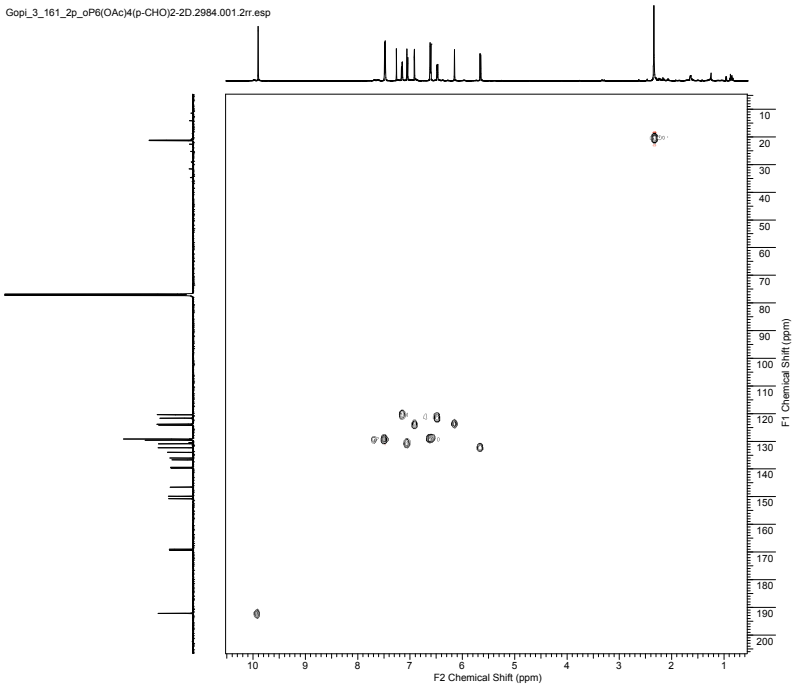

Figure S24. HSQC spectrum (500 MHz, $CDCl_3$, rt) of **oP^6(*p*-CHO)**.

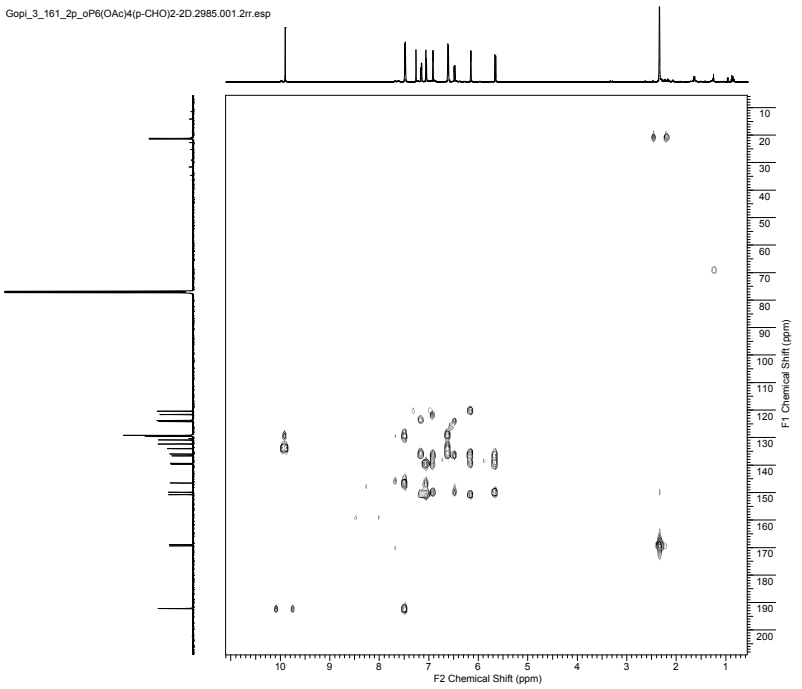

Figure S25. HMBC spectrum (500 MHz, $CDCl_3$, rt) of **oP^6(*p*-CHO)**.

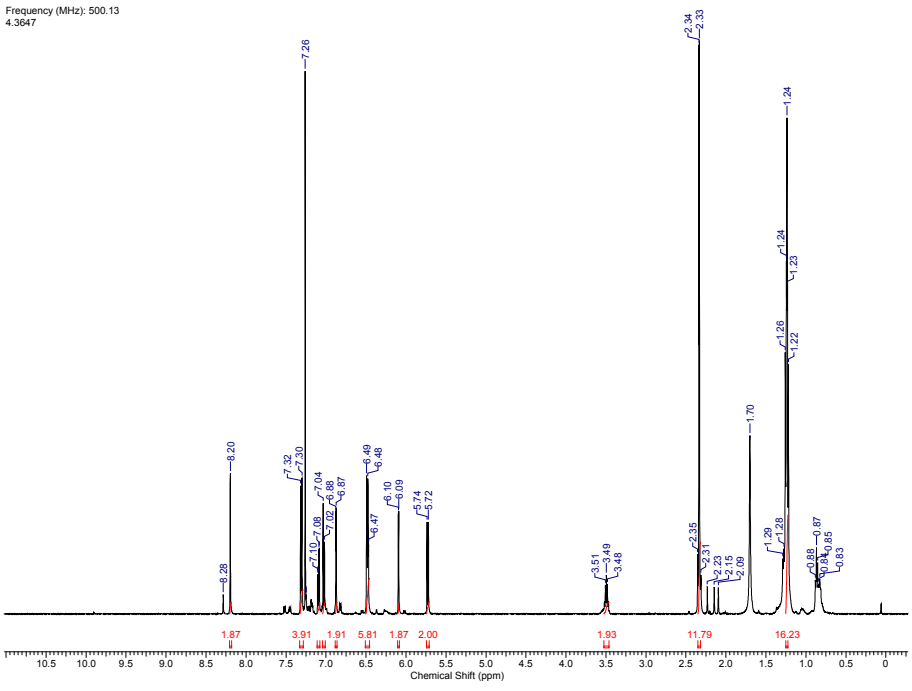

Figure S26. ^{1}H NMR spectrum (500 MHz, $CDCl_3$, 273 K) of **oP^6(*p*-Me)**.

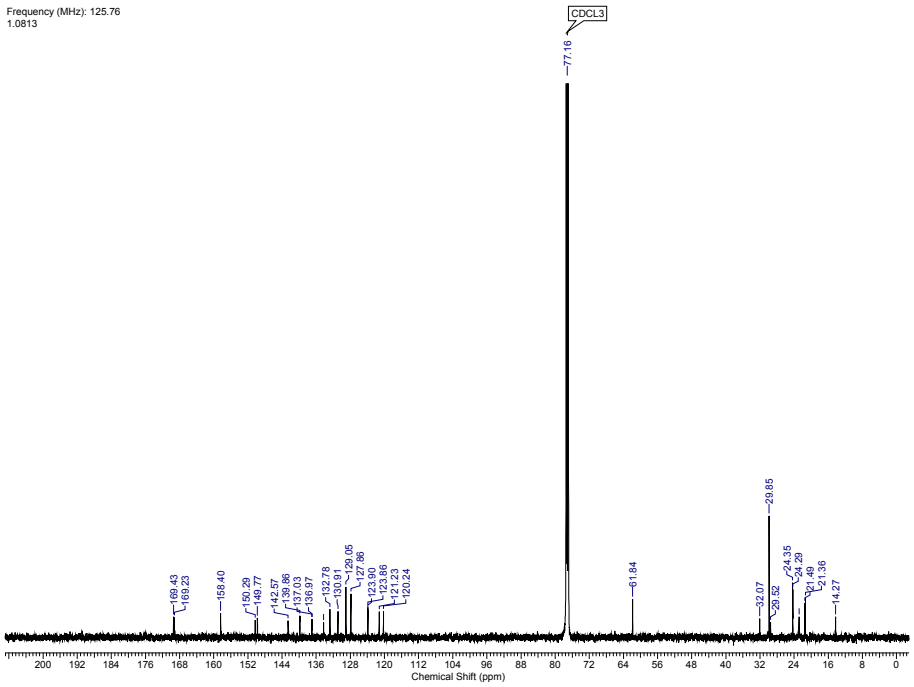

Figure S27. ^{13}C NMR spectrum (125 MHz, $CDCl_3$, 273 K) of **oP^6(*p*-Me)**.

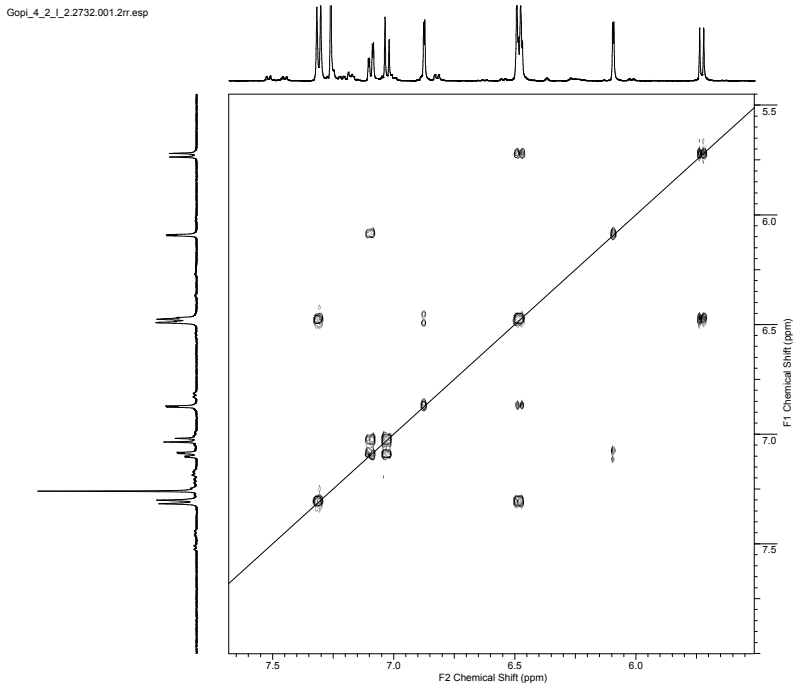

Figure S28. COSY spectrum (500 MHz, $CDCl_3$, 273 K) of **oP^6(*p*-Me)**.

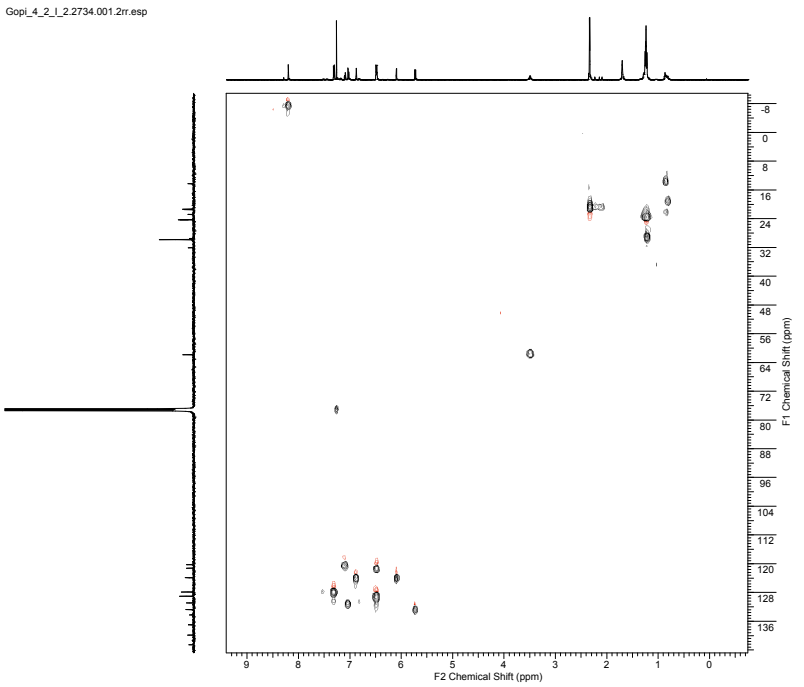

Figure S29. HSQC spectrum (500 MHz, $CDCl_3$, 273 K) of **oP^6(*p*-Me)**.

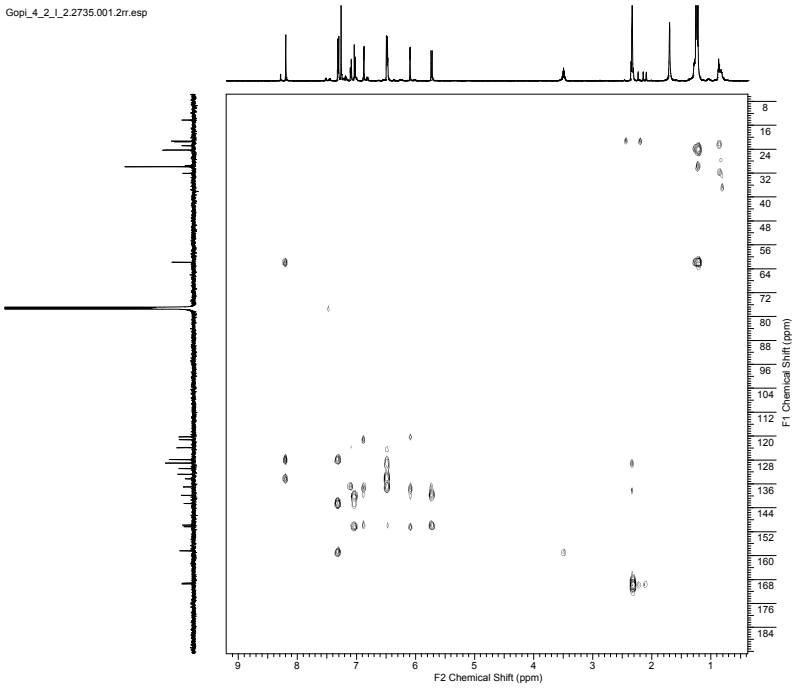

Figure S30. HMBC spectrum (500 MHz, $CDCl_3$, 273 K) of **oP^6(*p*-Me)**.

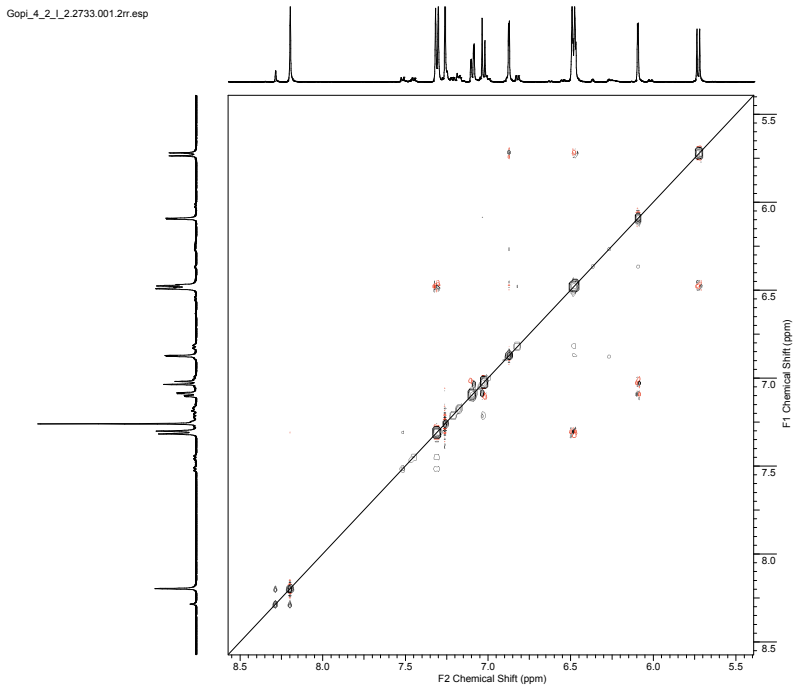

Figure S31. NOESY/EXSY spectrum (500 MHz, $CDCl_3$, 273 K) of **oP^6(*p*-Me)**.

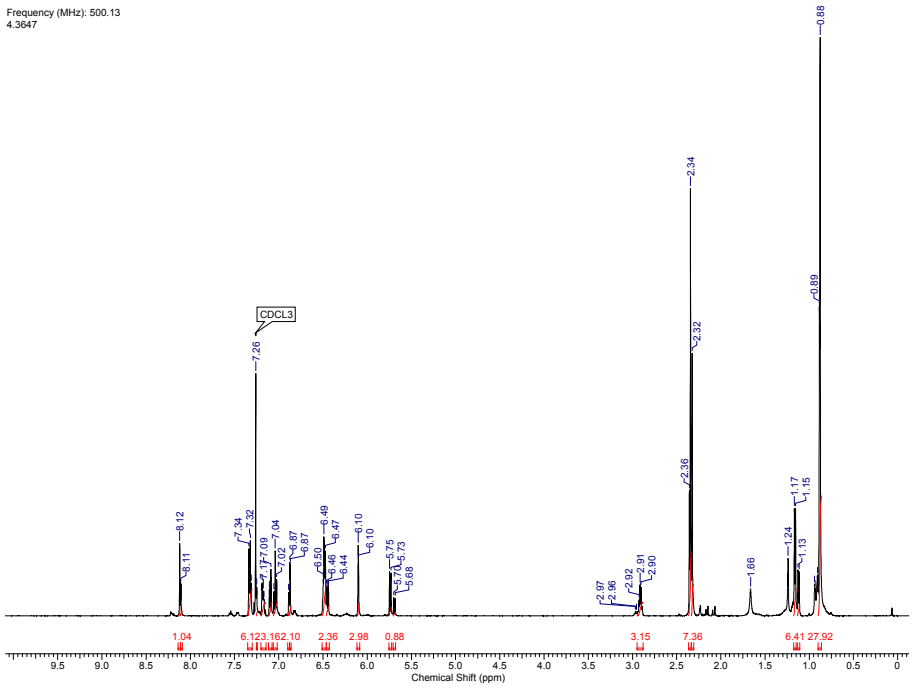

Figure S32. ^{1}H NMR spectrum (500 MHz, $CDCl_3$, 273 K) of (*R*)-**oP^6(*p*-^{t}Bu)**.

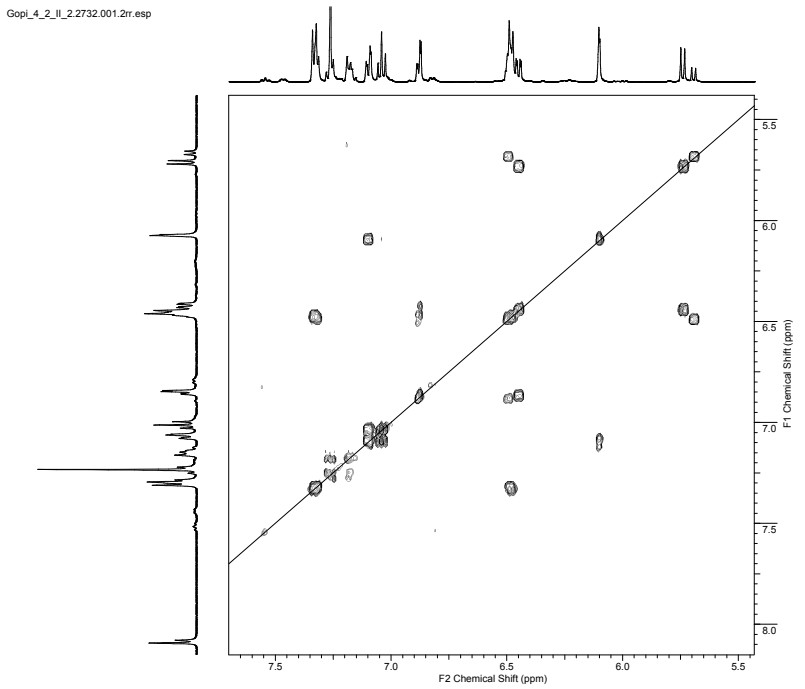

Figure S33. COSY spectrum (500 MHz, $CDCl_3$, 273 K) of (*R*)-**oP^6(*p*-^{t}Bu)**.

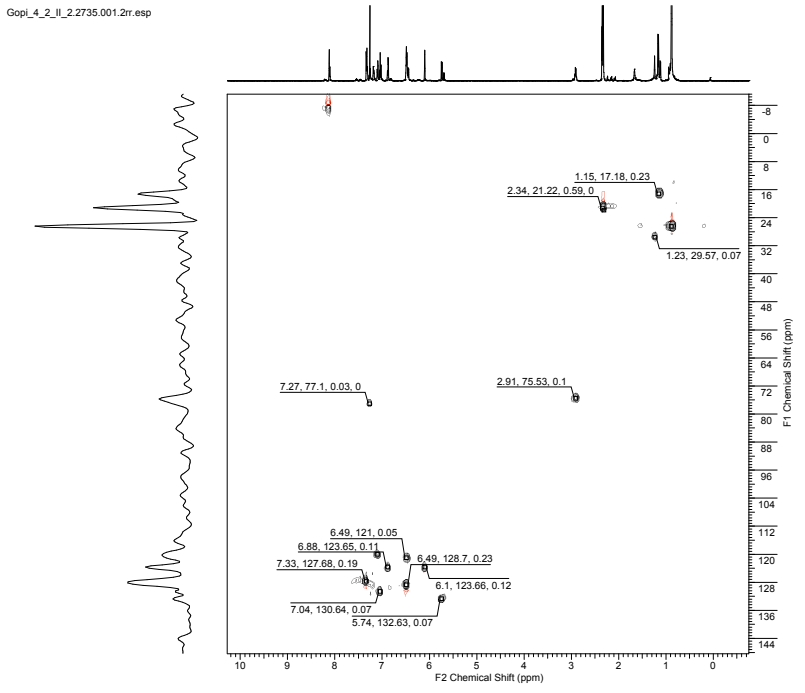

Figure S34. HSQC spectrum (500 MHz, $CDCl_3$, 273 K) of (*R*)-**oP^6(*p*-^{t}Bu)**.

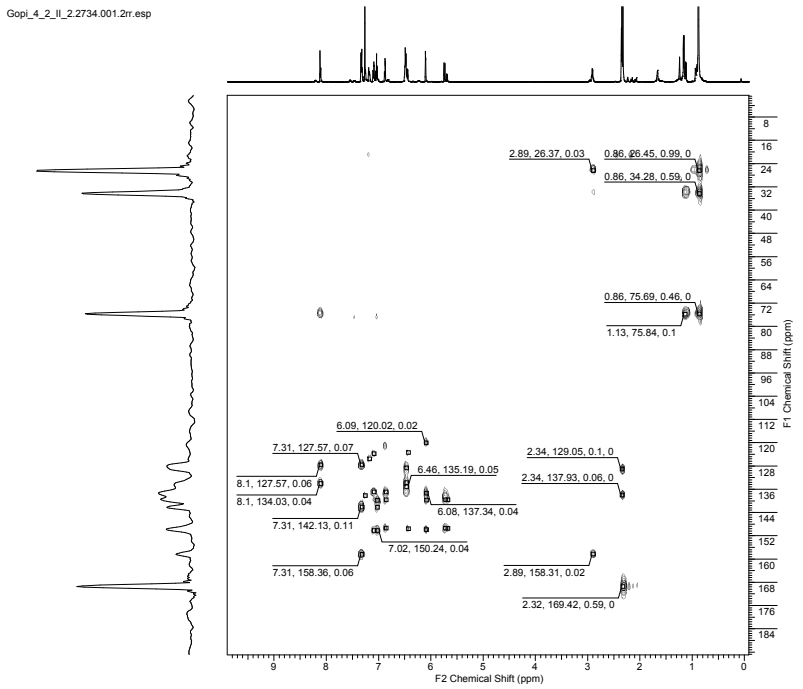

Figure S35. HMBC spectrum (500 MHz, $CDCl_3$, 273 K) of (*R*)-**oP^6(*p*-^{t}Bu)**.

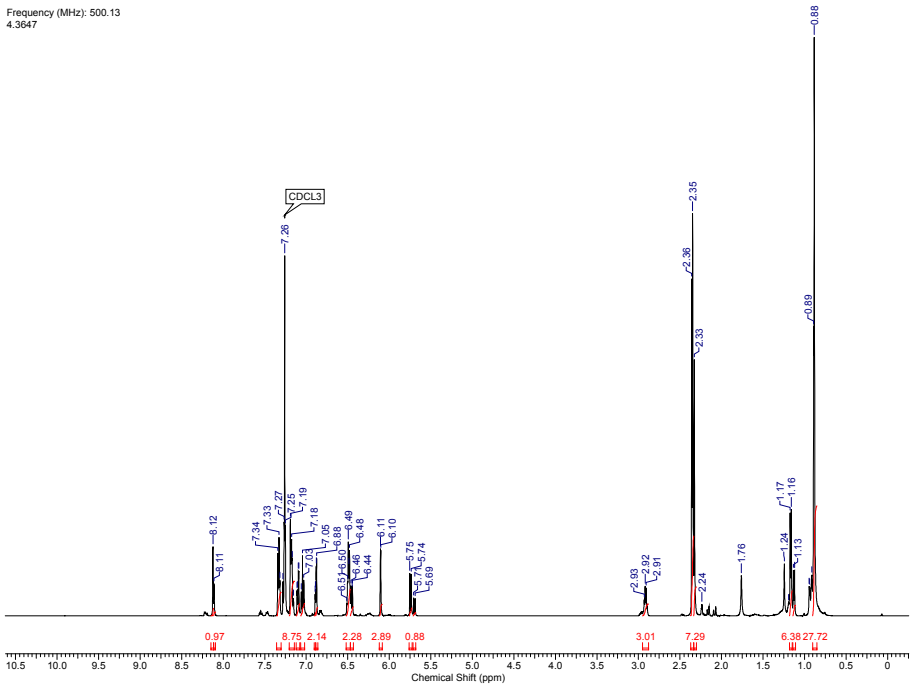

Figure S36. ^{1}H NMR spectrum (500 MHz, $CDCl_3$, 273 K) of (*S*)-**oP^6(*p*-^{t}Bu)**.

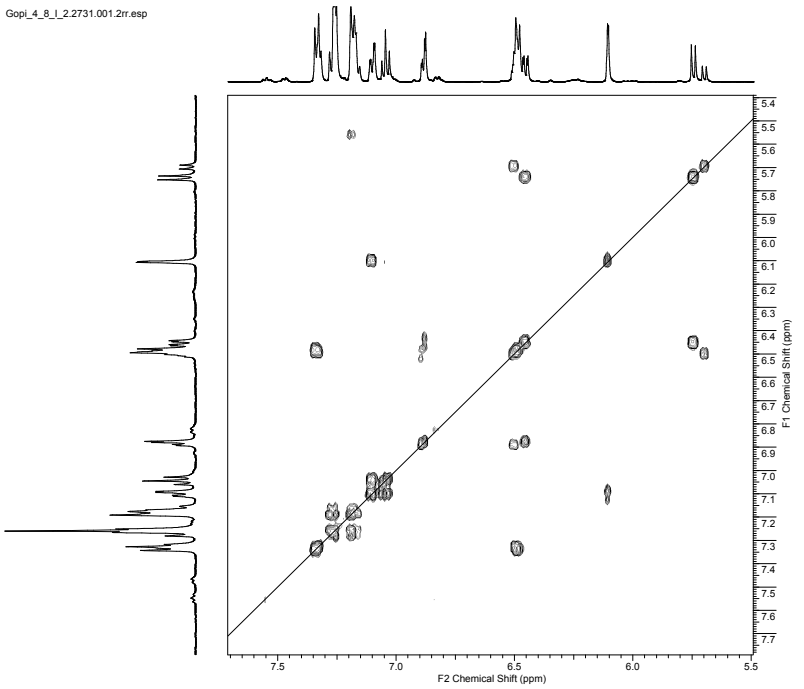

Figure S37. COSY spectrum (500 MHz, $CDCl_3$, 273 K) of (*S*)-**oP^6(*p*-^{t}Bu)**.

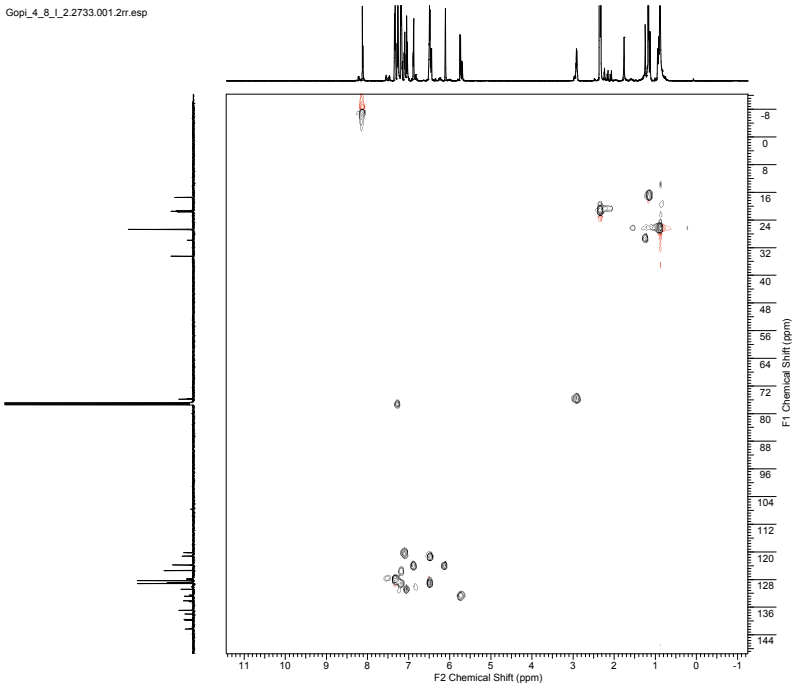

Figure S38. HSQC spectrum (500 MHz, $CDCl_3$, 273 K) of (*S*)-**oP^6(*p*-^{t}Bu)**.

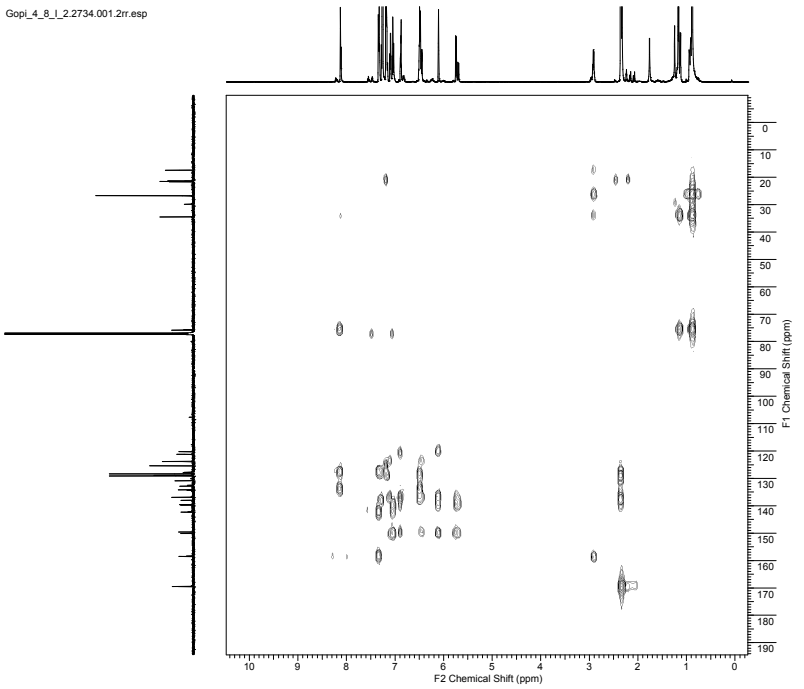

Figure S39. HMBC spectrum (500 MHz, $CDCl_3$, 273 K) of (*S*)-**oP^6(*p*-^{t}Bu)**.

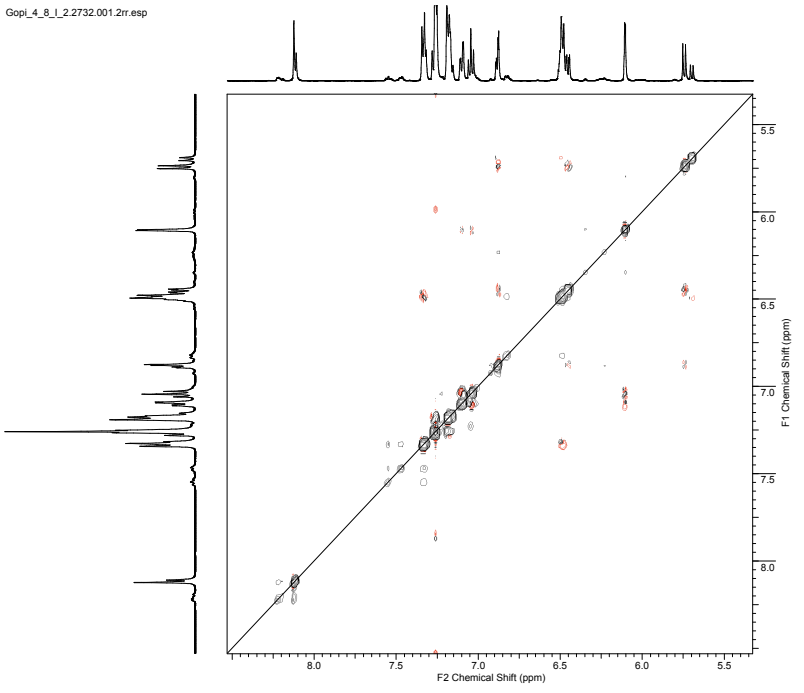

Figure S40. NOESY/EXSY spectrum (500 MHz, $CDCl_3$, 273 K) of (*S*)-**oP^6(*p*-^{t}Bu)**.

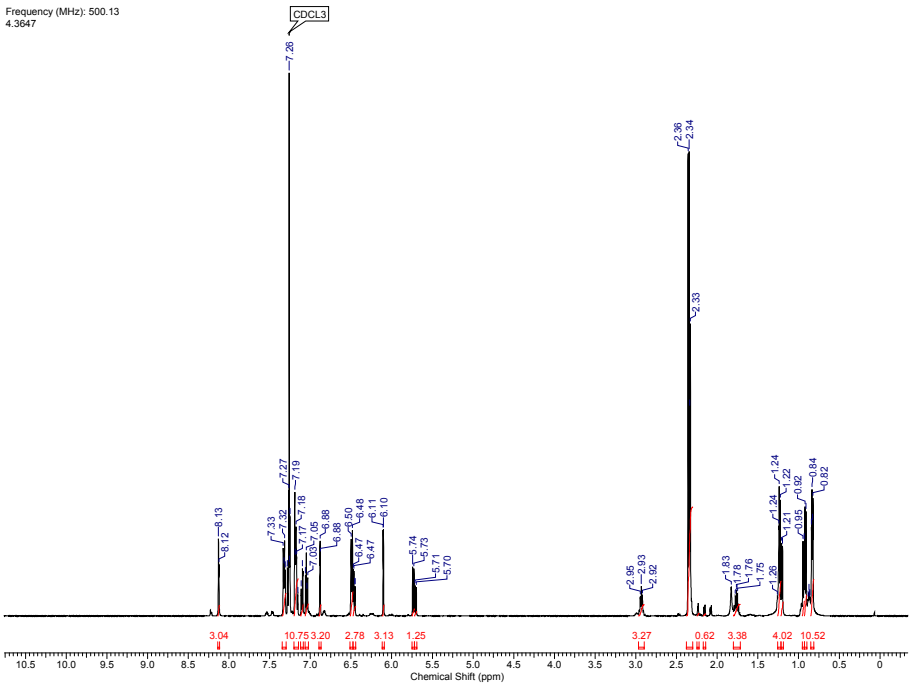

Figure S41. ^{1}H NMR spectrum (500 MHz, $CDCl_3$, 273 K) of (*R*)-**oP^6(*p*-^{i}Pr)**.

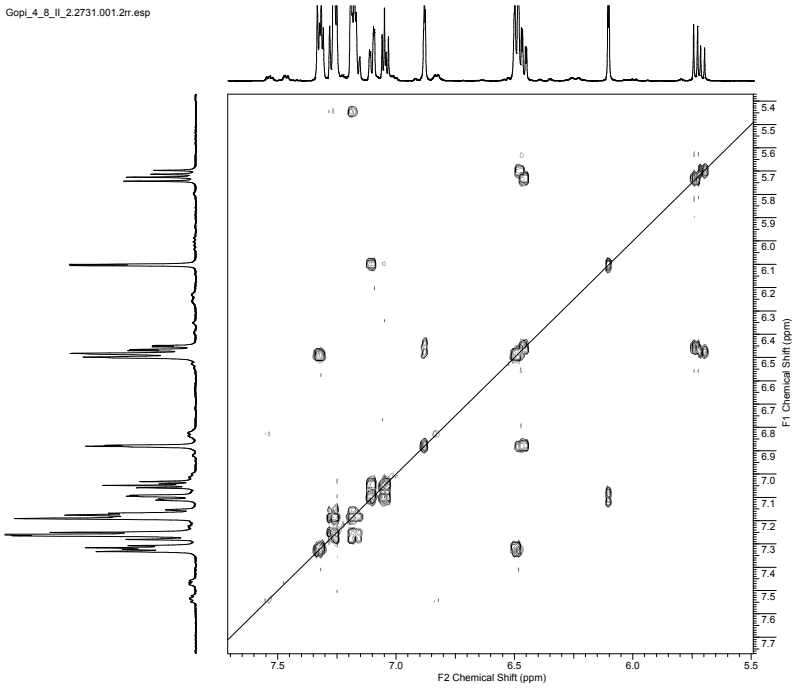

Figure S42. COSY spectrum (500 MHz, $CDCl_3$, 273 K) of (*R*)-**oP^6(*p*-^{i}Pr)**.

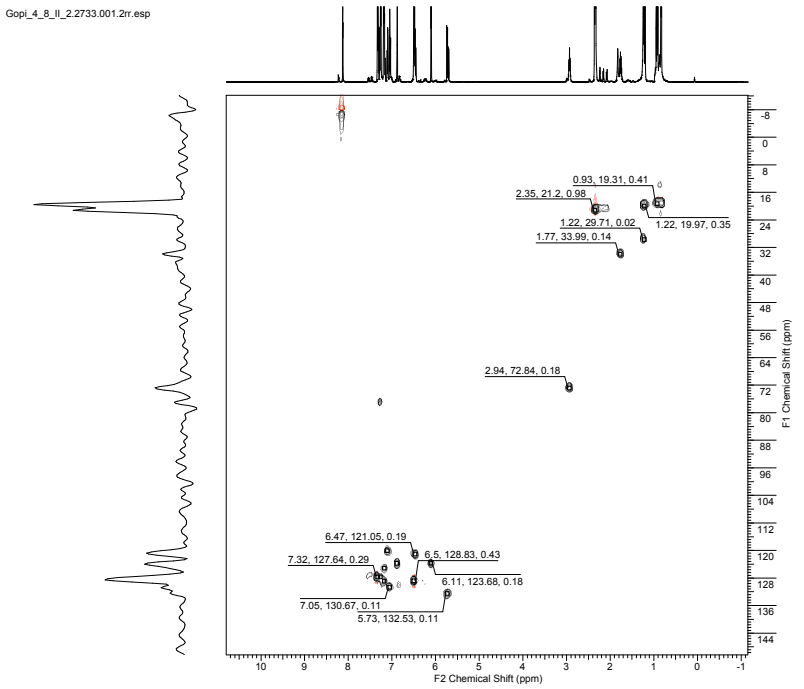

Figure S43. HSQC spectrum (500 MHz, $CDCl_3$, 273 K) of (*R*)-**oP^6(*p*-^{i}Pr)**.

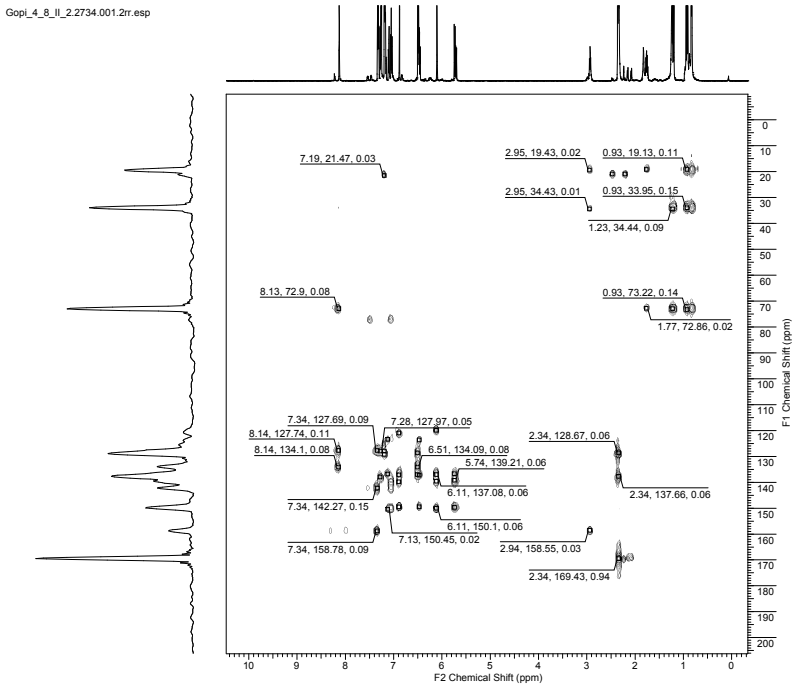

Figure S44. HMBC spectrum (500 MHz, $CDCl_3$, 273 K) of (*R*)-**oP^6(*p*-^{i}Pr)**.

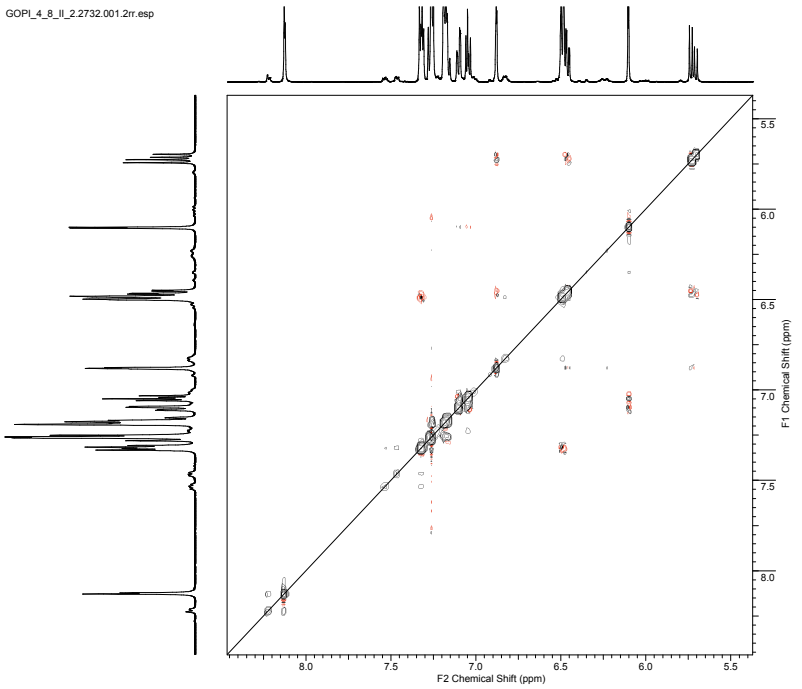

Figure S45. NOESY/EXSY spectrum (500 MHz, $CDCl_3$, 273 K) of (*R*)-**oP^6(*p*-^{i}Pr)**.

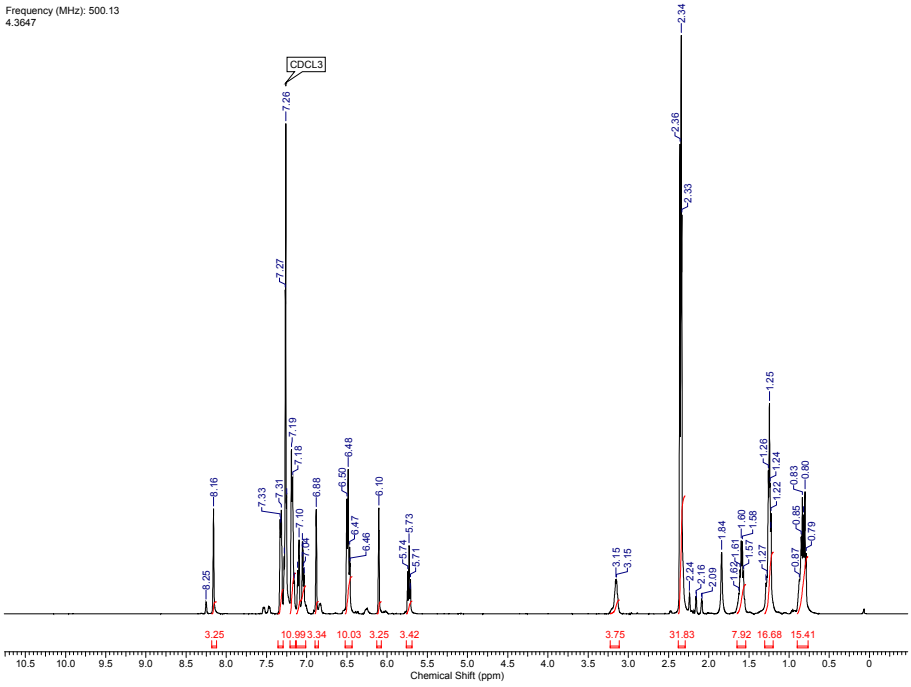

Figure S46. ^{1}H NMR spectrum (500 MHz, $CDCl_3$, 273 K) of (*S*)-**oP^6(*p*-Et)**.

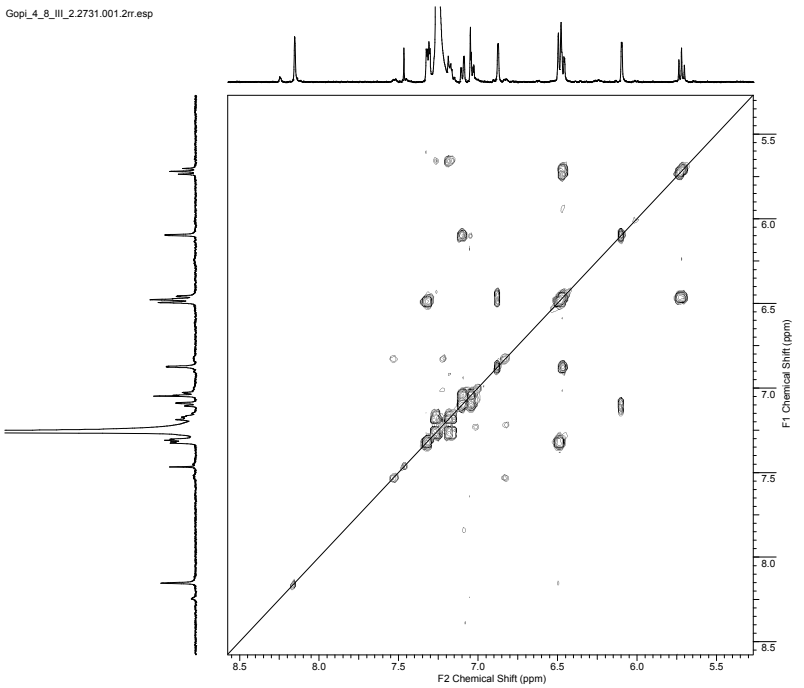

Figure S47. COSY spectrum (500 MHz, $CDCl_3$, 273 K) of (*S*)-**oP^6(*p*-Et)**.

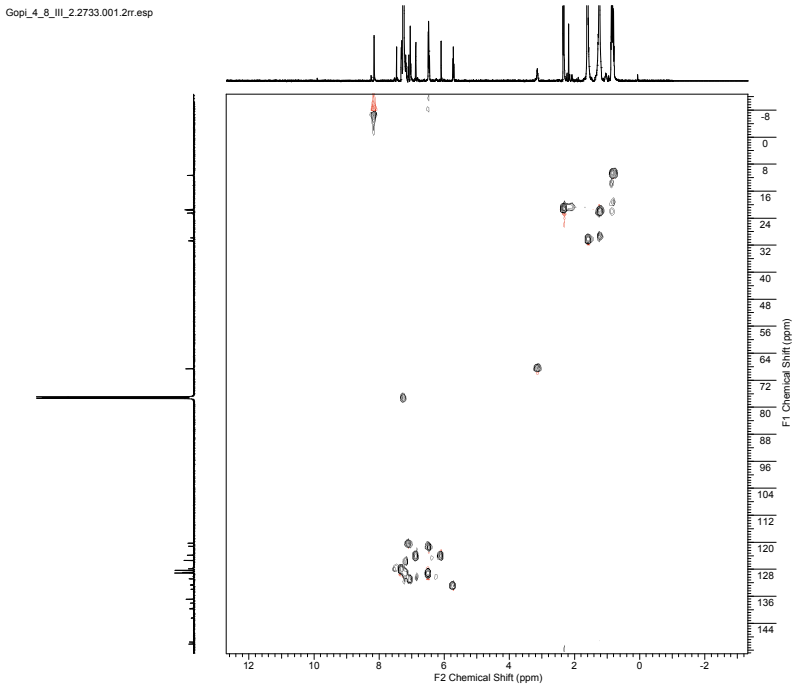

Figure S48. HSQC spectrum (500 MHz, $CDCl_3$, 273 K) of (*S*)-**oP^6(*p*-Et)**.

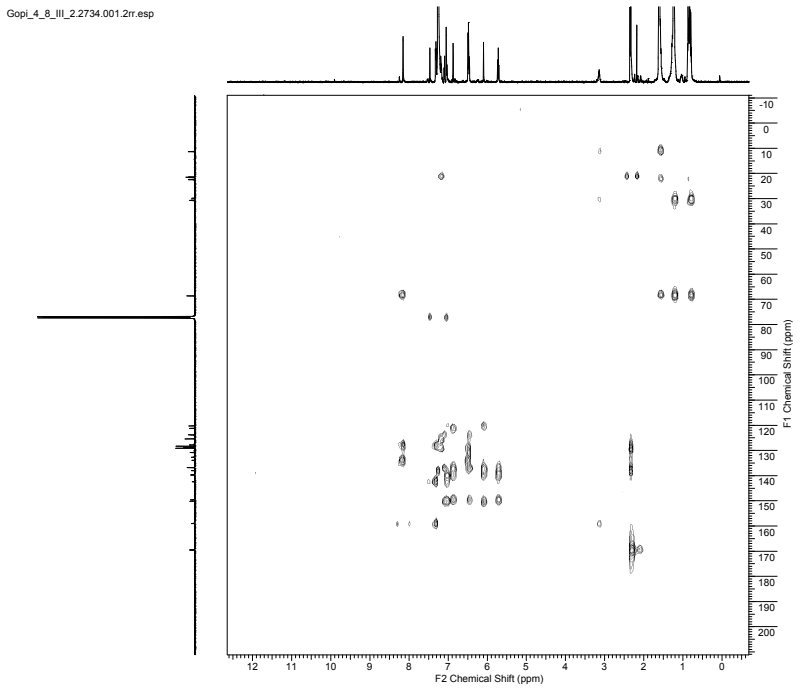

Figure S49. HMBC spectrum (500 MHz, $CDCl_3$, 273 K) of (*S*)-**oP^6(*p*-Et)**.

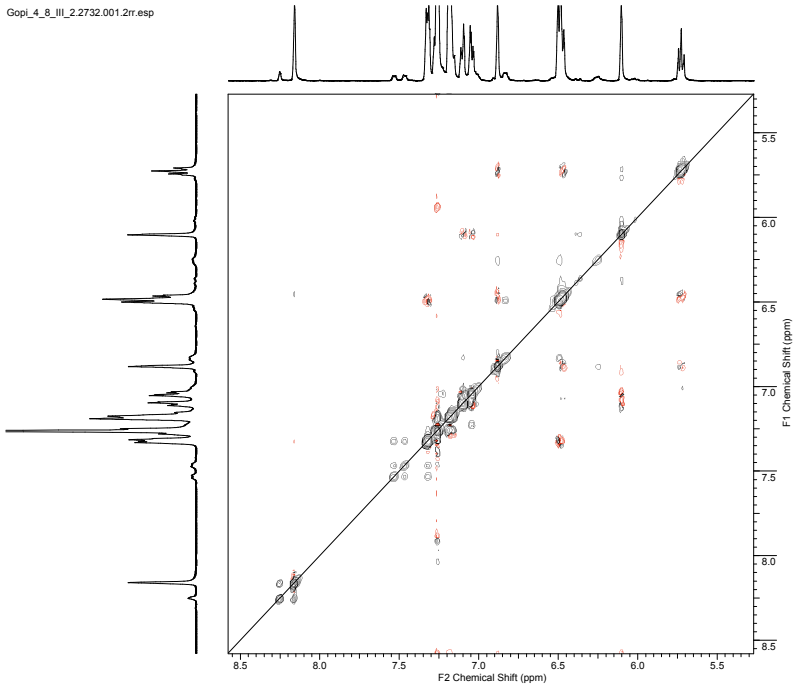

Figure S50. NOESY/EXSY spectrum (500 MHz, $CDCl_3$, 273 K) of (*S*)-**oP^6(*p*-Et)**.

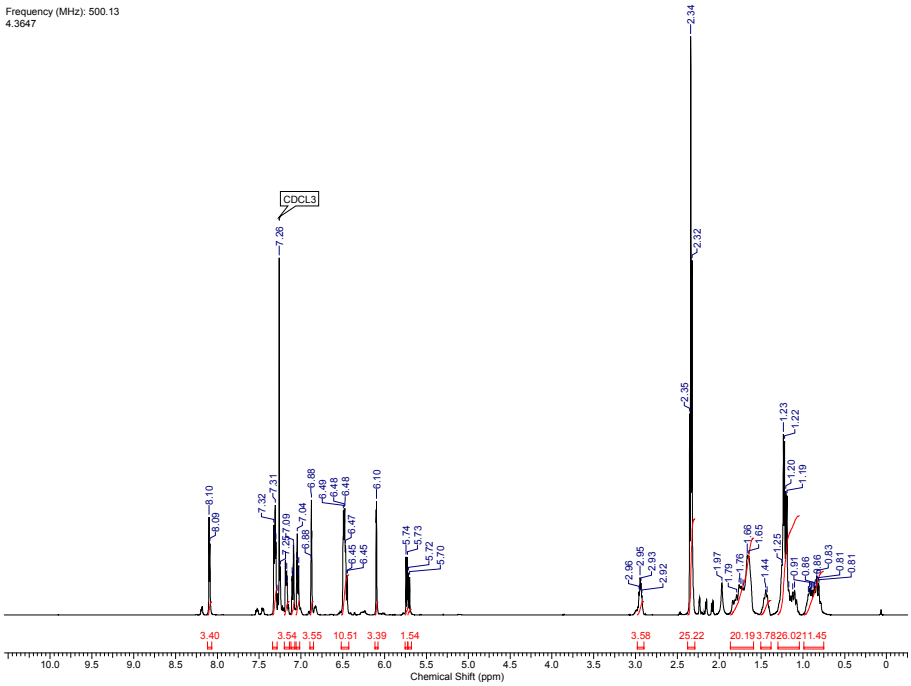

Figure S51. ^{1}H NMR spectrum (500 MHz, $CDCl_3$, 273 K) of (*R*)-**oP^6(*p*-Cy)**.

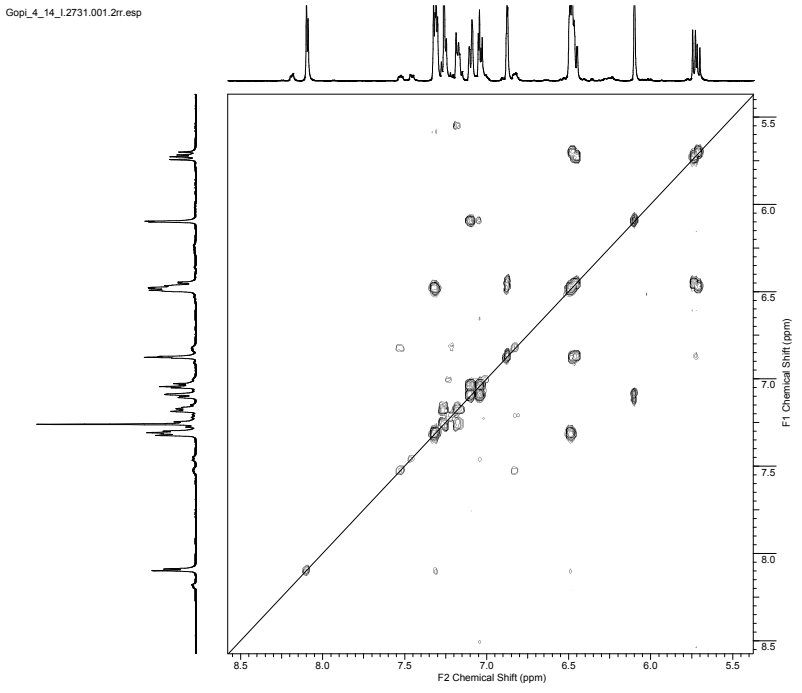

Figure S52. COSY spectrum (500 MHz, $CDCl_3$, 273 K) of (*R*)-**oP^6(*p*-Cy)**.

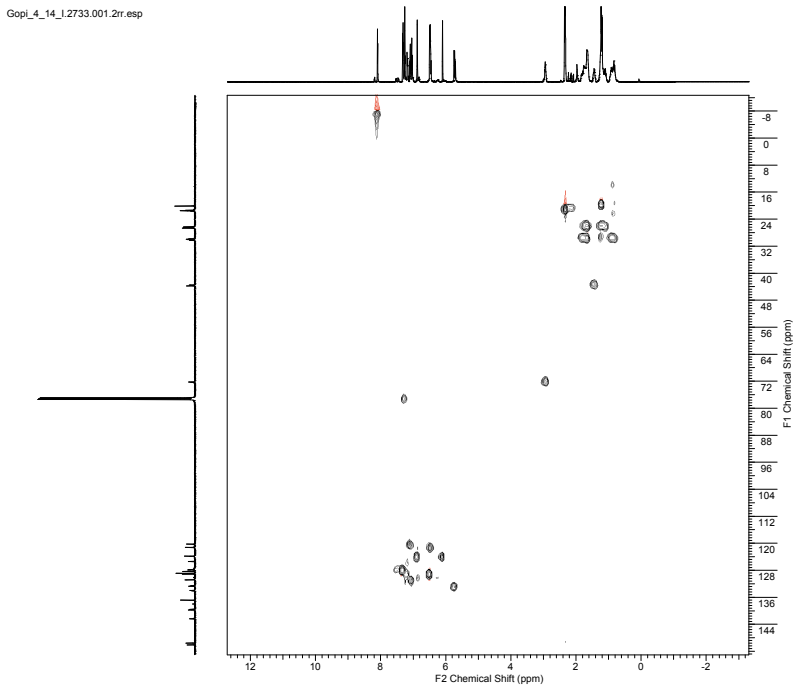

Figure S53. HSQC spectrum (500 MHz, $CDCl_3$, 273 K) of (*R*)-**oP^6(*p*-Cy)**.

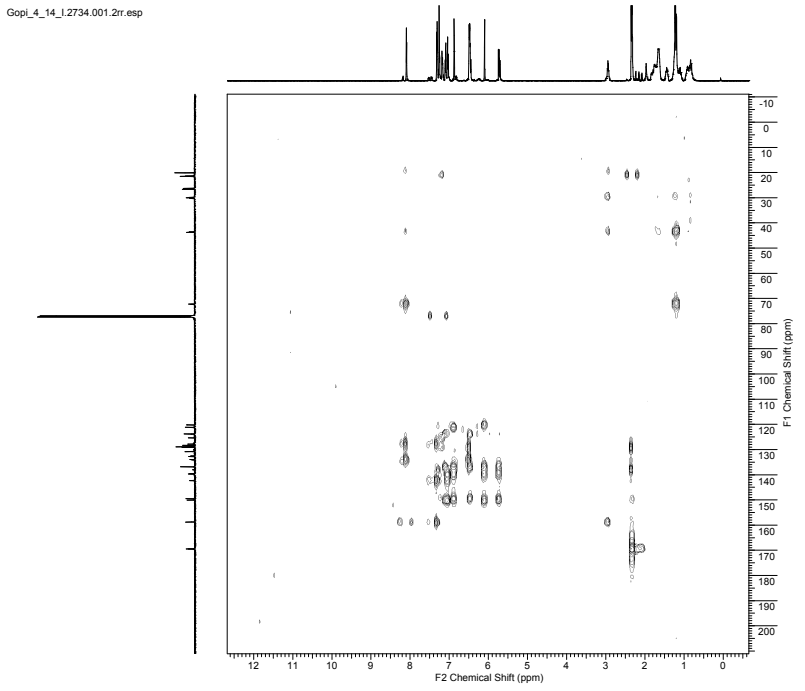

Figure S54. HMBC spectrum (500 MHz, $CDCl_3$, 273 K) of (*R*)-**oP^6(*p*-Cy)**.

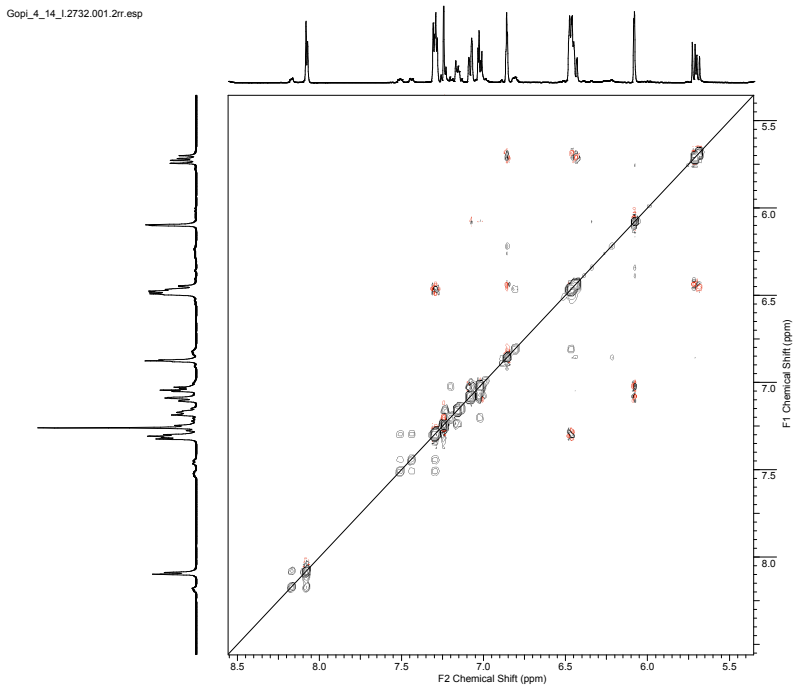

Figure S55. NOESY/EXSY spectrum (500 MHz, $CDCl_3$, 273 K) of (*R*)-**oP^6(*p*-Cy)**.

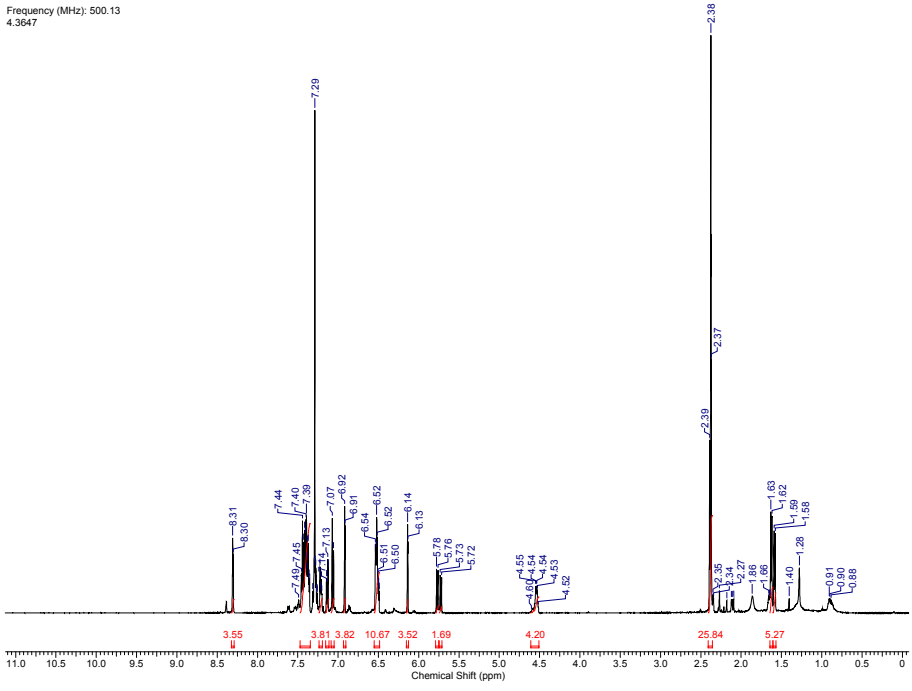

Figure S56. ^{1}H NMR spectrum (500 MHz, $CDCl_3$, 273 K) of (*S*)-**oP^6(*p*-Ph)**.

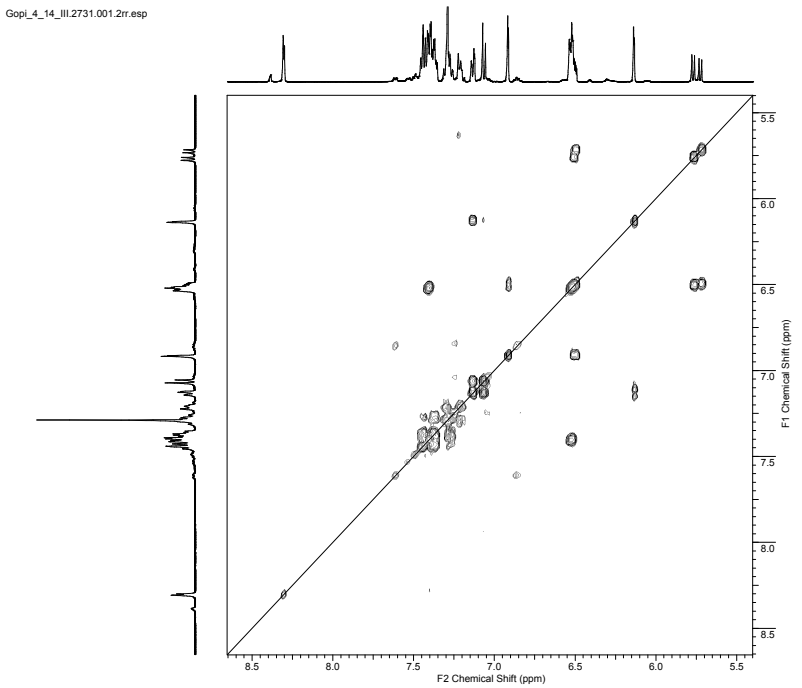

Figure S57. COSY spectrum (500 MHz, $CDCl_3$, 273 K) of (*S*)-**oP^6(*p*-Ph)**.

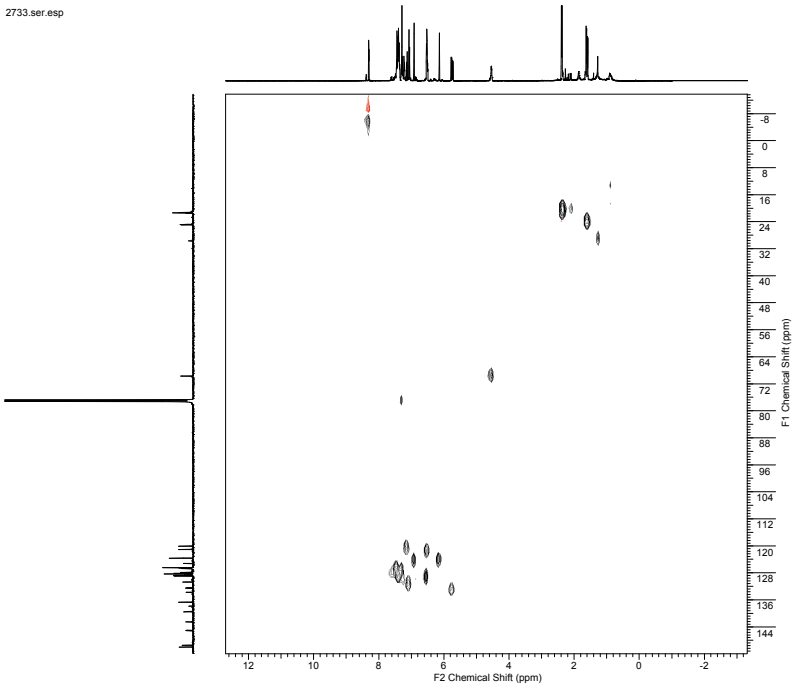

Figure S58. HSQC spectrum (500 MHz, $CDCl_3$, 273 K) of (*S*)-**oP^6(*p*-Ph)**.

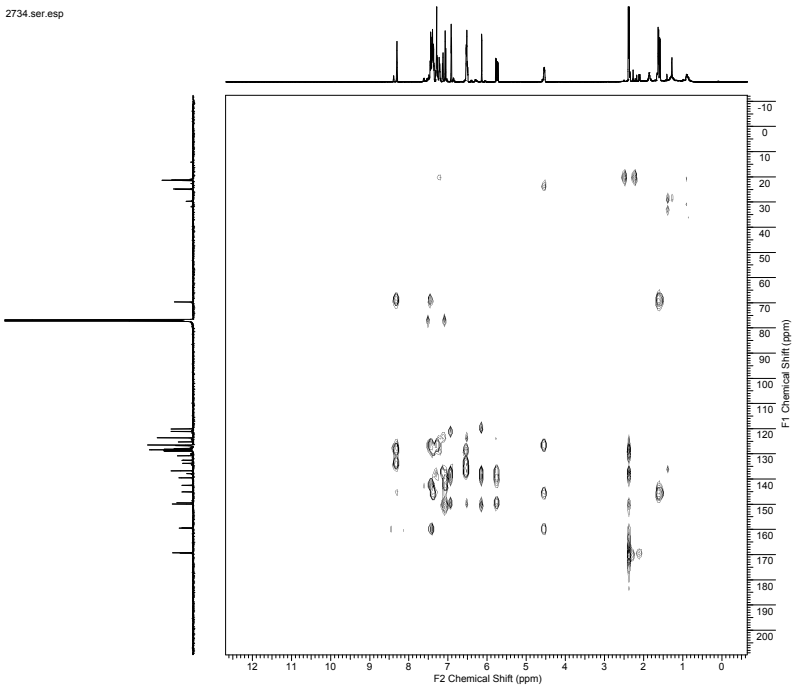

Figure S59. HMBC spectrum (500 MHz, $CDCl_3$, 273 K) of (*S*)-**oP^6(*p*-Ph)**.

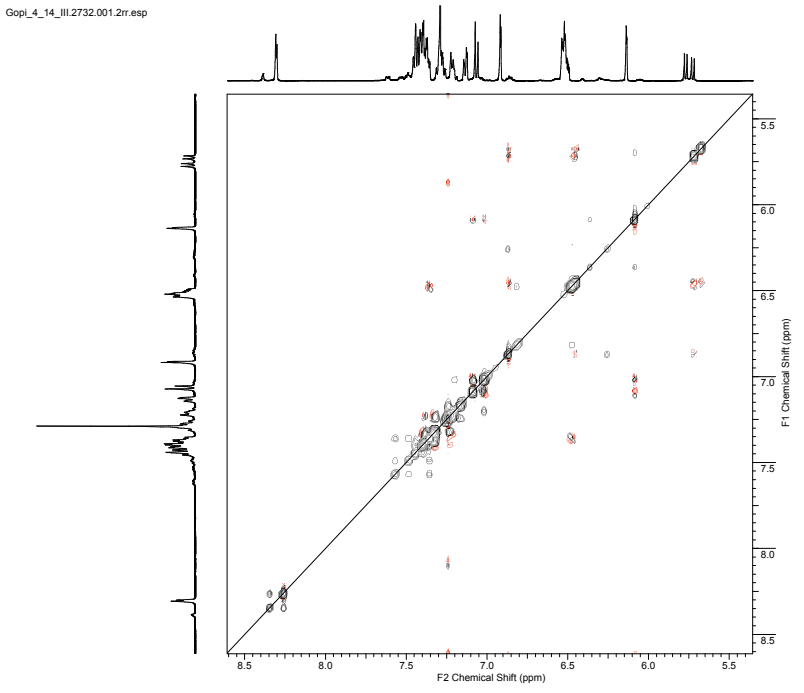

Figure S60. NOESY/EXSY spectrum (500 MHz, $CDCl_3$, 273 K) of (*S*)-**oP^6(*p*-Ph)**.

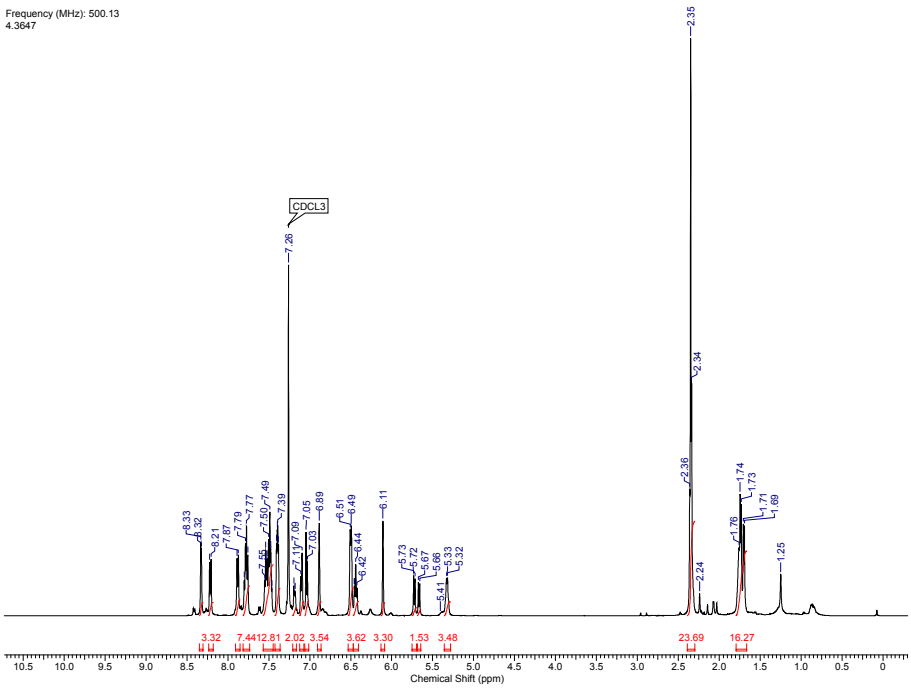

Figure S61. ^{1}H NMR spectrum (500 MHz, $CDCl_3$, 273 K) of (*S*)-**oP^6(*p*-Np)**.

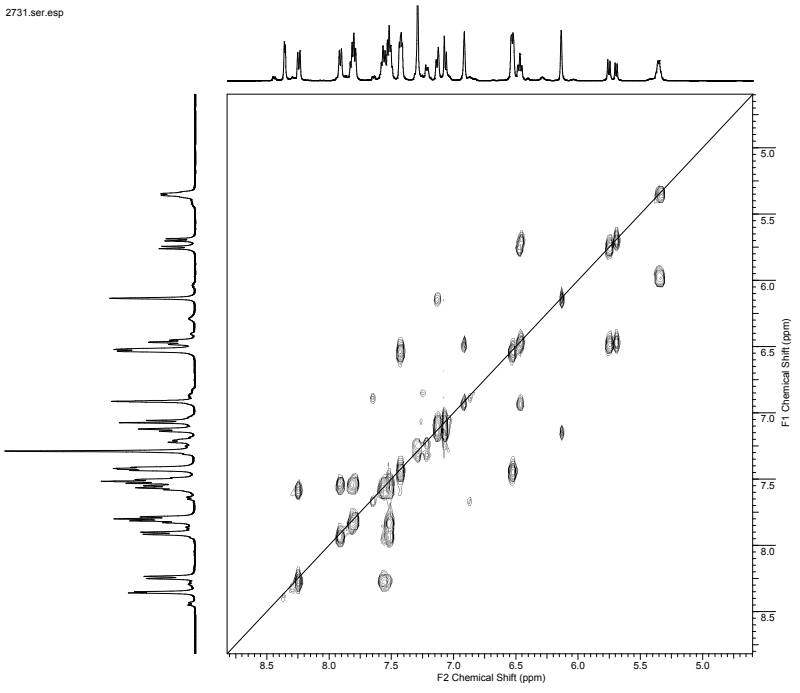

Figure S62. COSY spectrum (500 MHz, $CDCl_3$, 273 K) of (*S*)-**oP^6(*p*-Np)**.

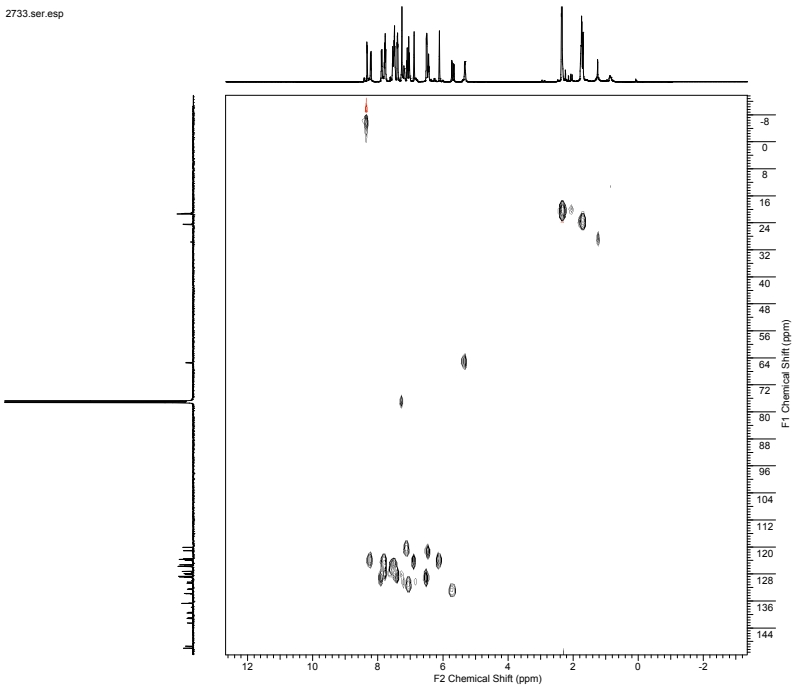

Figure S63. HSQC spectrum (500 MHz, $CDCl_3$, 273 K) of (*S*)-**oP^6(*p*-Np)**.

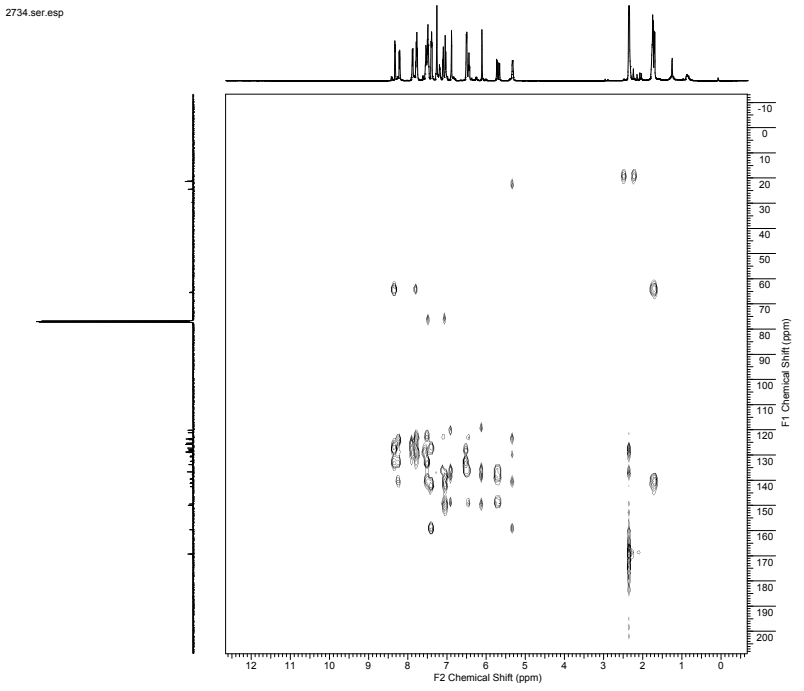

Figure S64. HMBC spectrum (500 MHz, $CDCl_3$, 273 K) of (*S*)-**oP^6(*p*-Np)**.

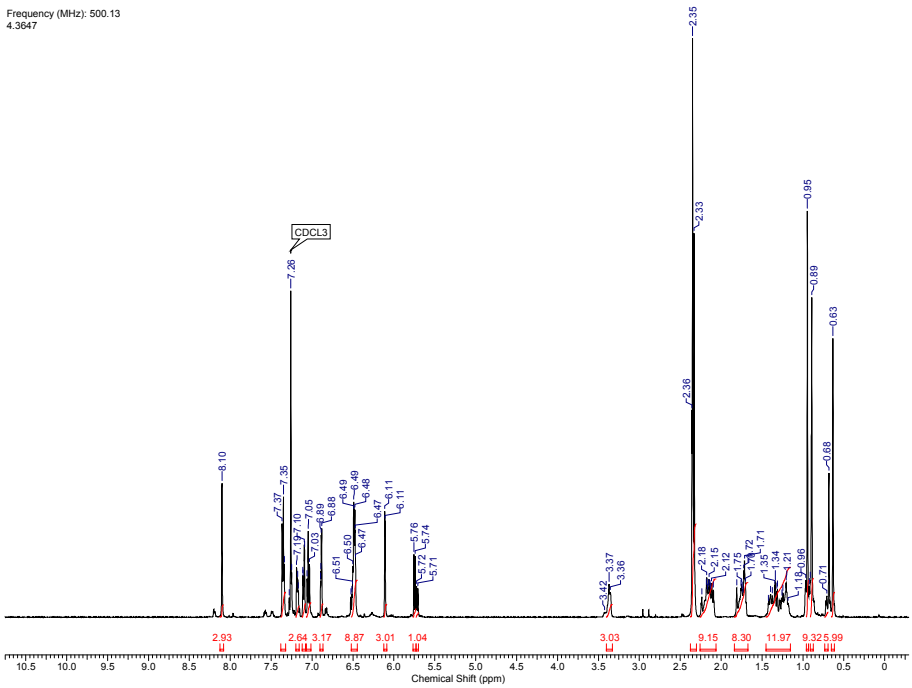

Figure S65. ^{1}H NMR spectrum (500 MHz, $CDCl_3$, 273 K) of (*S*)-**oP^6(*p*-Bo)**.

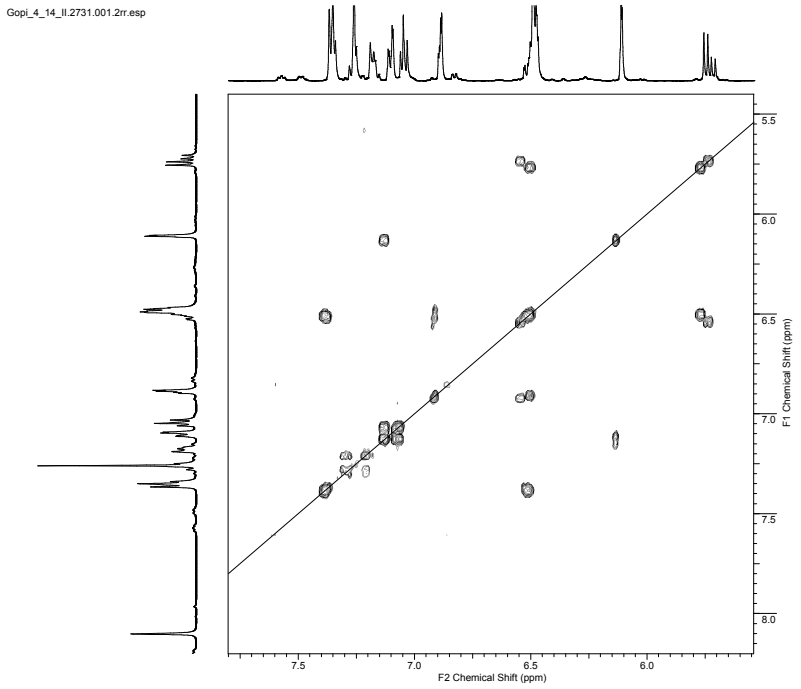

Figure S66. COSY spectrum (500 MHz, $CDCl_3$, 273 K) of (*S*)-**oP^6(*p*-Bo)**.

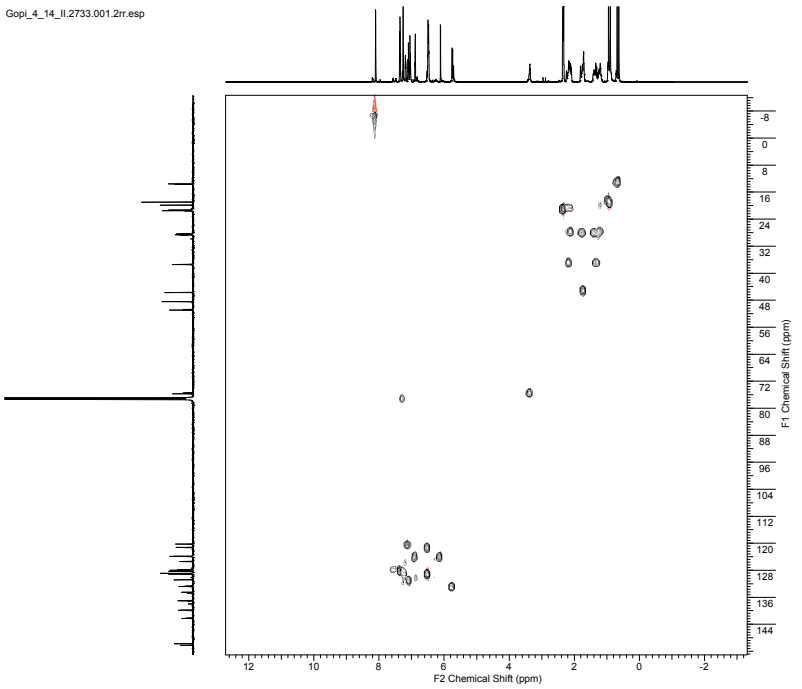

Figure S67. HSQC spectrum (500 MHz, $CDCl_3$, 273 K) of (*S*)-**oP^6(*p*-Bo)**.

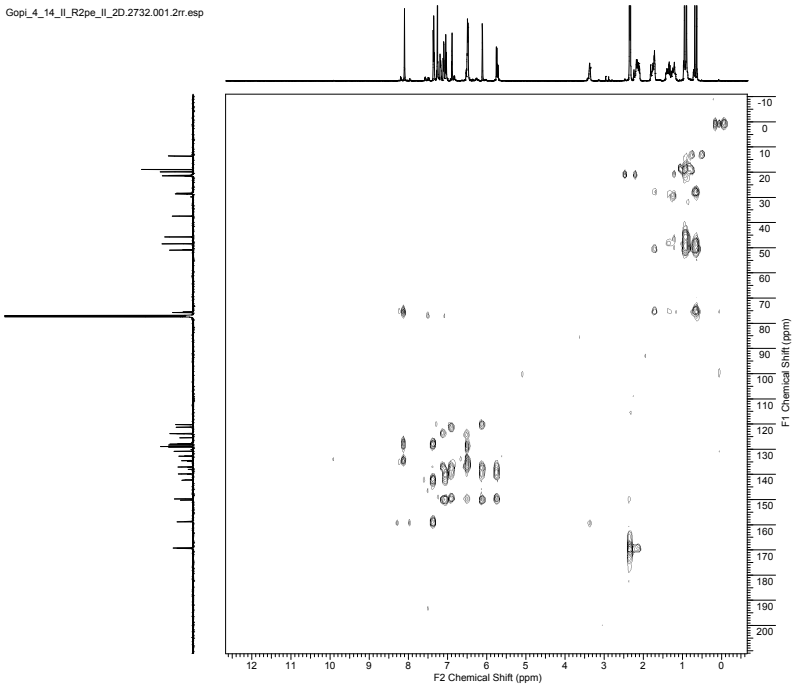

Figure S68. HMBC spectrum (500 MHz, $CDCl_3$, 273 K) of (*S*)-**oP^6(*p*-Bo)**.

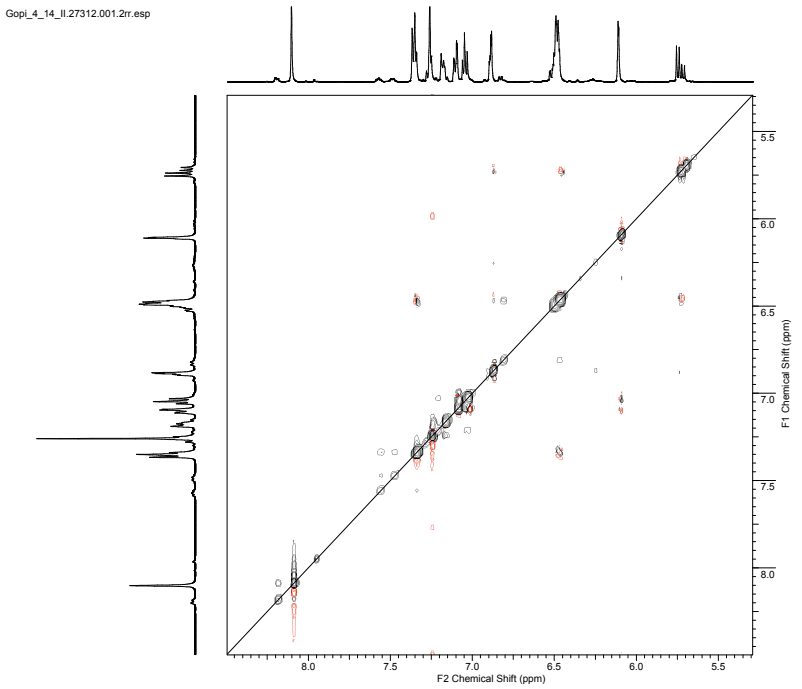

Figure S69. NOESY/EXSY spectrum (500 MHz, $CDCl_3$, 273 K) of (*S*)-**oP^6(*p*-Bo)**.

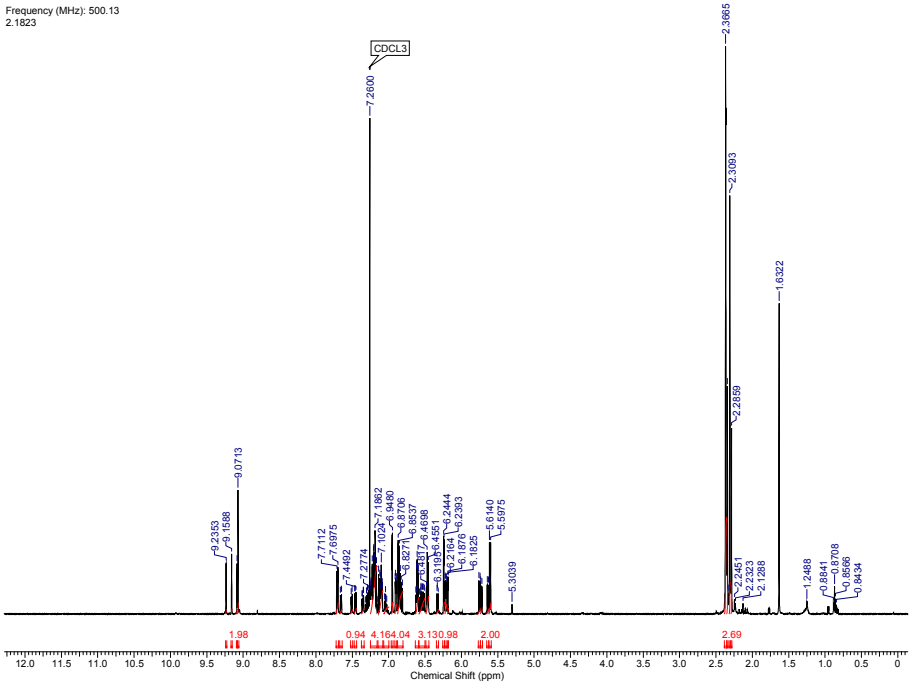

Figure S70. ^{1}H NMR spectrum (500 MHz, $CDCl_3$, 273 K) of **oP^6(*o*-CHO)**.

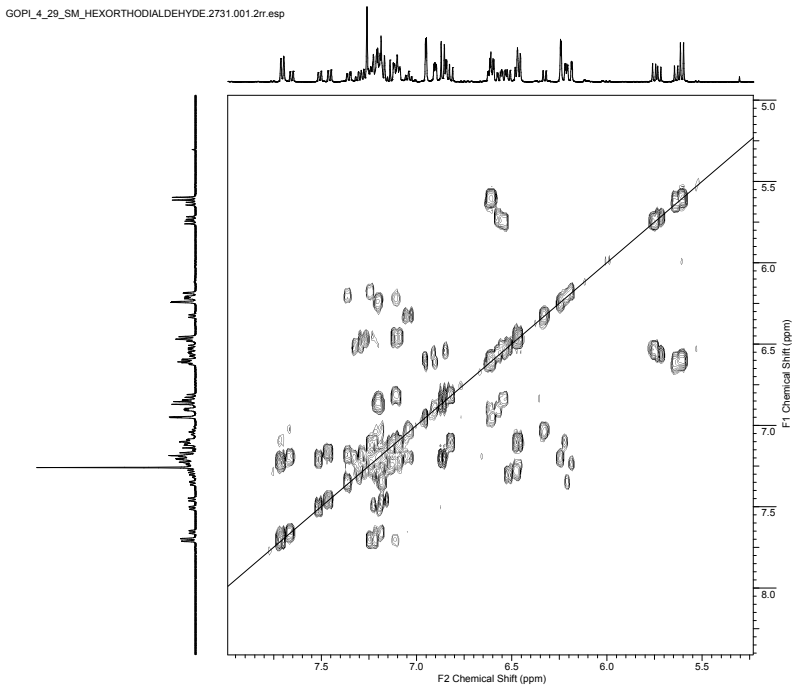

Figure S71. COSY spectrum (500 MHz, $CDCl_3$, 273 K) of **oP^6(*o*-CHO)**.

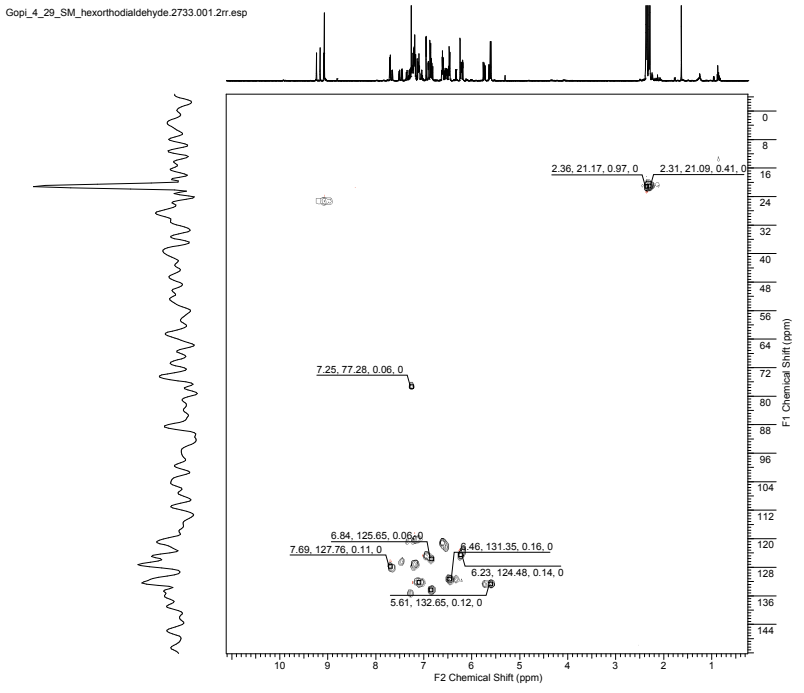

Figure S72. HSQC spectrum (500 MHz, $CDCl_3$, 273 K) of **oP^6(*o*-CHO)**.

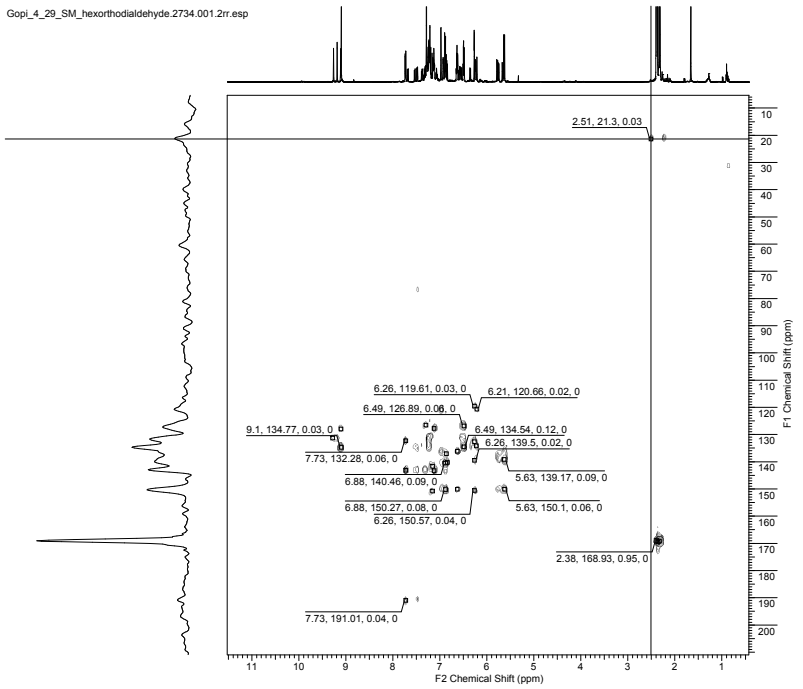

Figure S73. HMBC spectrum (500 MHz, $CDCl_3$, 273 K) of **oP^6(*o*-CHO)**.

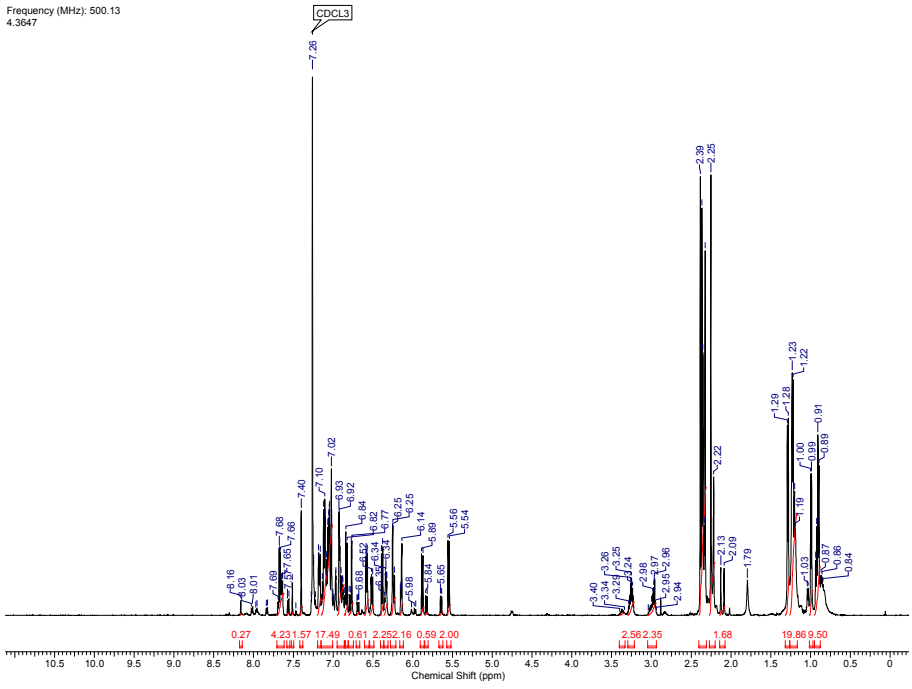

Figure S74. ^{1}H NMR spectrum (500 MHz, $CDCl_3$, 273 K) of **oP^6(*o*-Me)**.

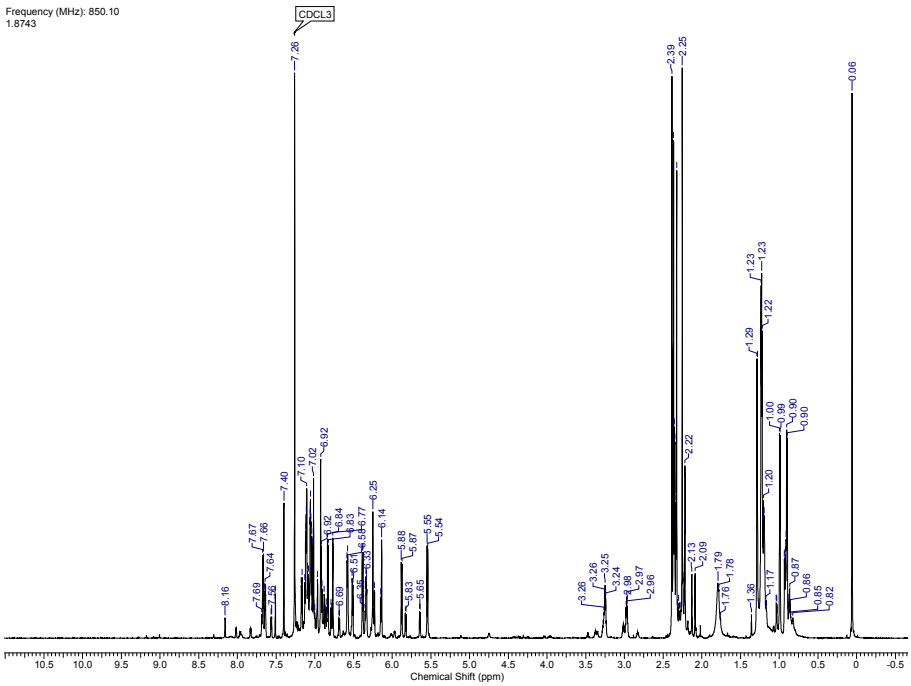

Figure S75. ^{1}H NMR spectrum (850 MHz, $CDCl_3$, 278 K) of **oP^6(*o*-Me)**.

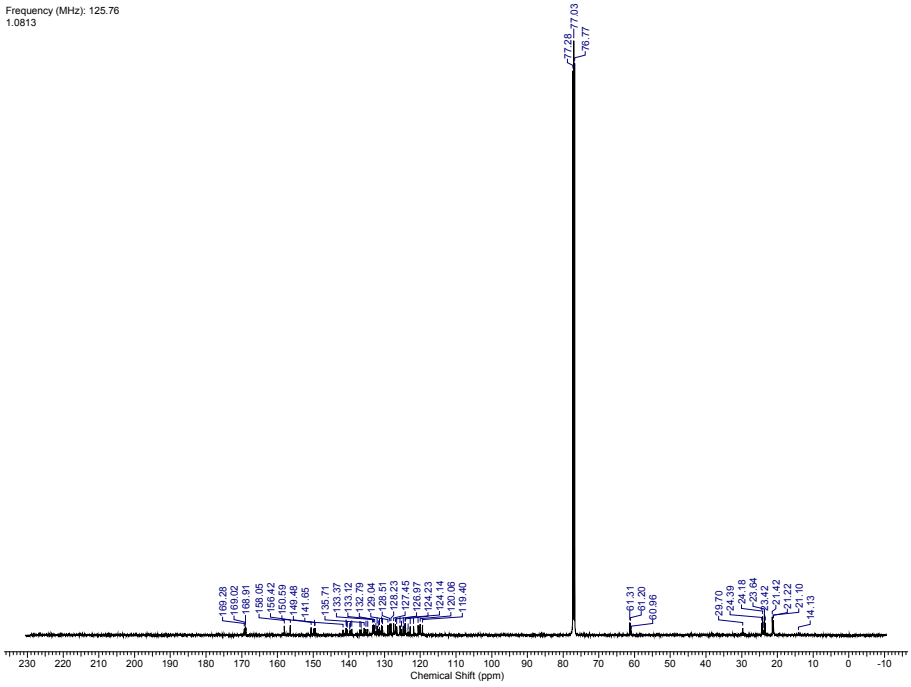

Figure S76. ^{13}C NMR spectrum (125 MHz, $CDCl_3$, 273 K) of **oP^6(*o*-Me)**.

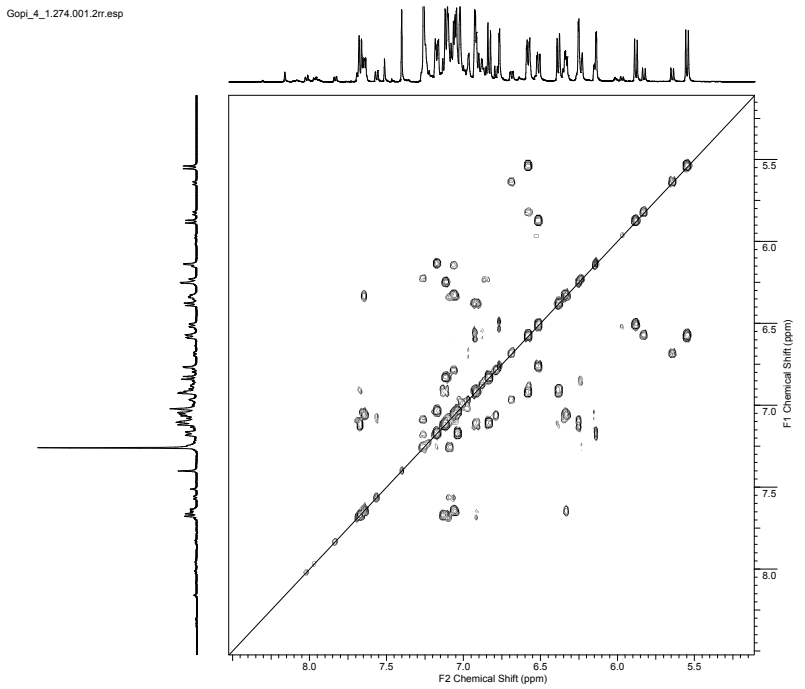

Figure S77. COSY spectrum (500 MHz, $CDCl_3$, 273 K) of **oP^6(*o*-Me)**.

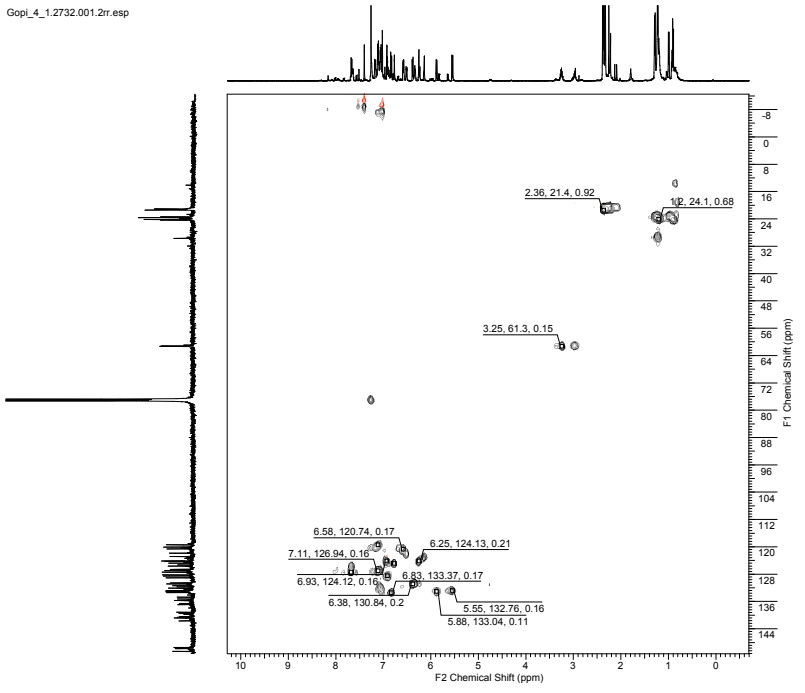

Figure S78. HSQC spectrum (500 MHz, $CDCl_3$, 273 K) of **oP^6(*o*-Me)**.

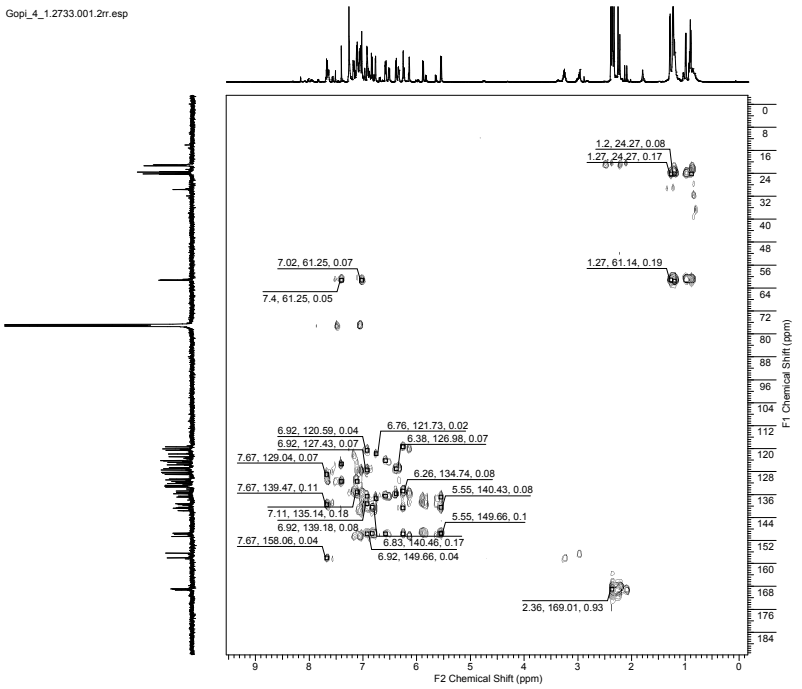

Figure S79. HMBC spectrum (500 MHz, $CDCl_3$, 273 K) of **oP^6(*o*-Me)**.

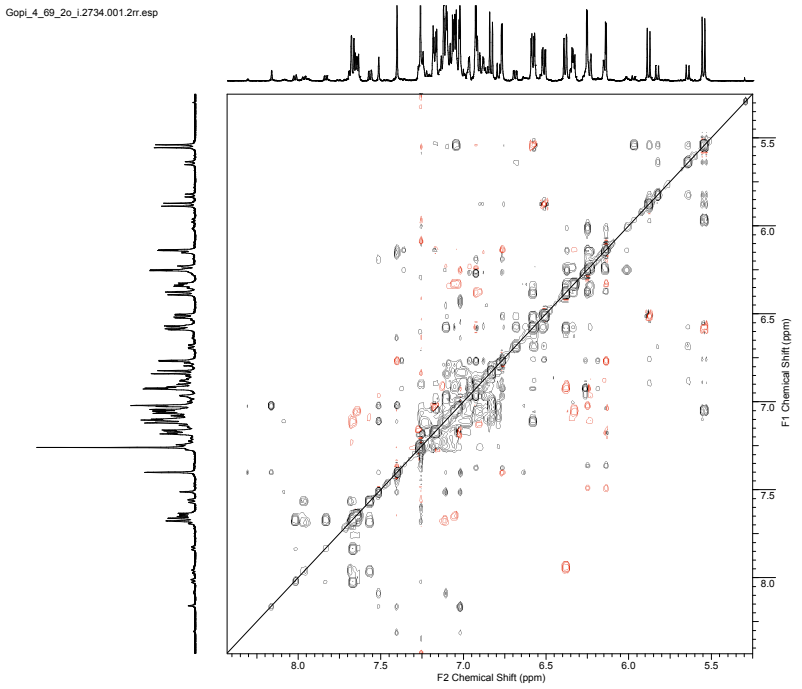

Figure S80. NOESY/EXSY spectrum (500 MHz, $CDCl_3$, 273 K) of **oP^6(*o*-Me)**.

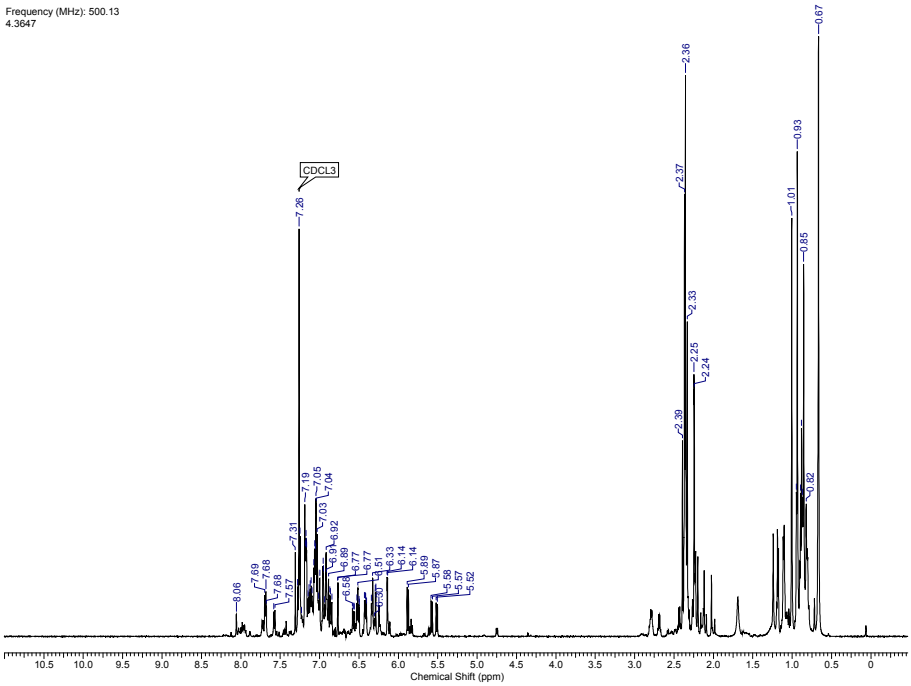

Figure S81. ^{1}H NMR spectrum (500 MHz, $CDCl_3$, 273 K) of (*R*)-**oP^6(*o*-^{t}Bu)**.

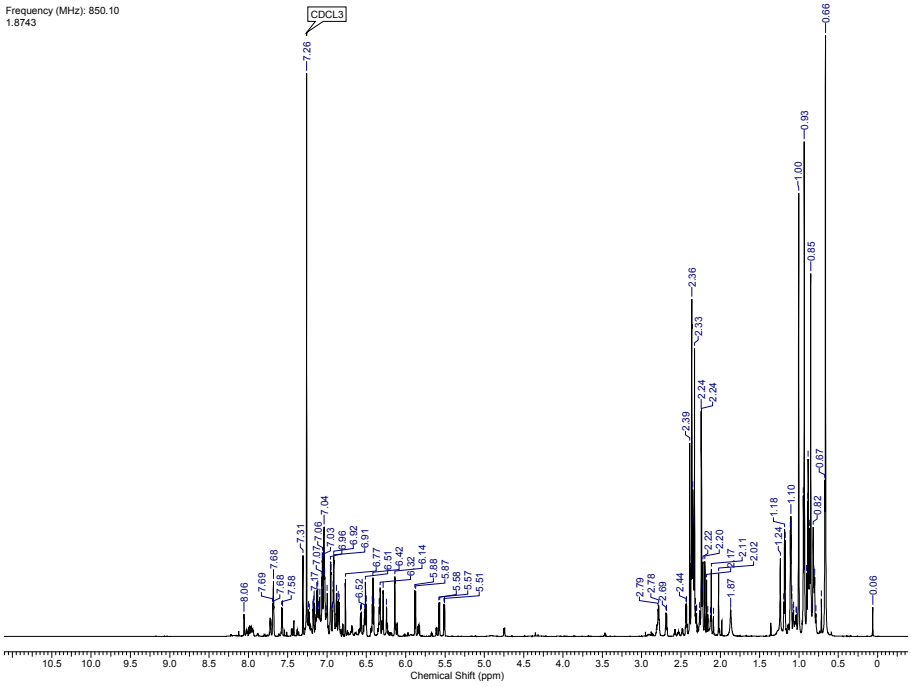

Figure S82. ^{1}H NMR spectrum (850 MHz, $CDCl_3$, 278 K) of (*R*)-**oP^6(*o*-^{t}Bu)**.

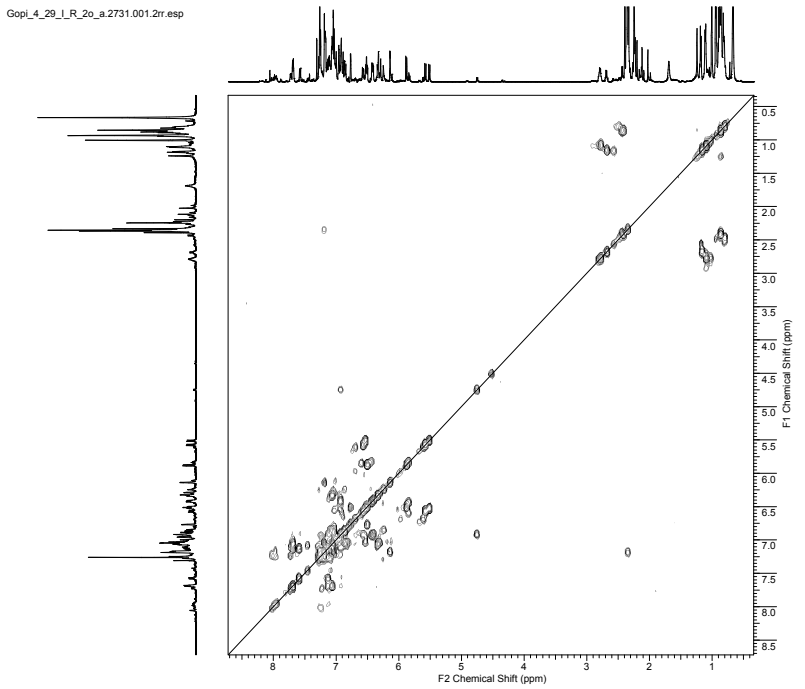

Figure S83. COSY spectrum (500 MHz, $CDCl_3$, 273 K) of (*R*)-**oP^6(*o*-^{t}Bu)**.

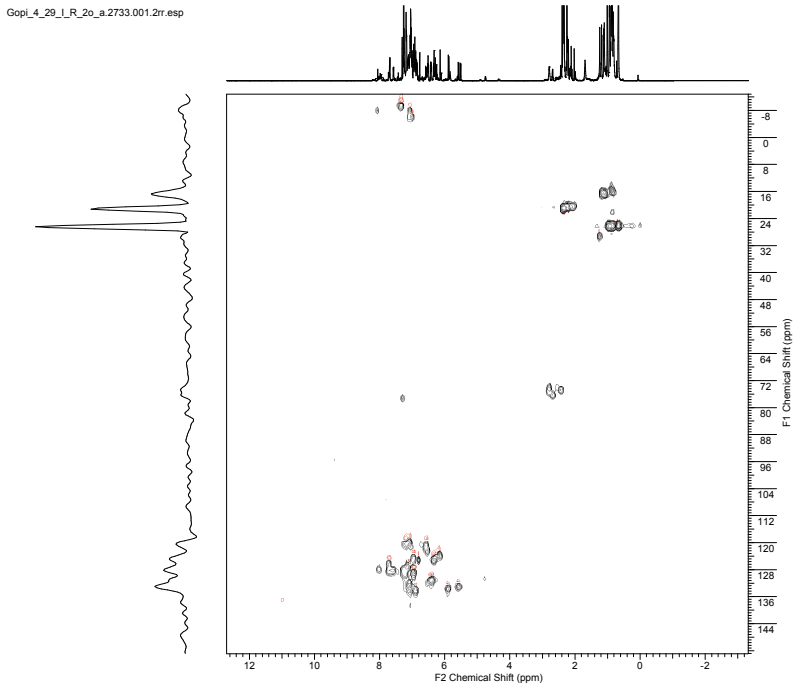

Figure S84. HSQC spectrum (500 MHz, $CDCl_3$, 273 K) of (*R*)-**oP^6(*o*-^{t}Bu)**.

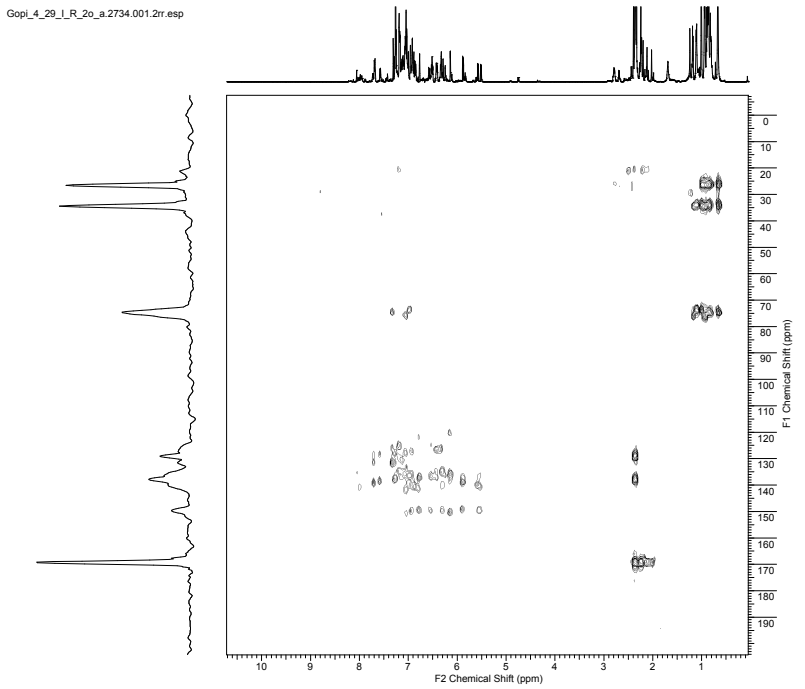

Figure S85. HMBC spectrum (500 MHz, $CDCl_3$, 273 K) of (*R*)-**oP^6(*o*-^{t}Bu)**.

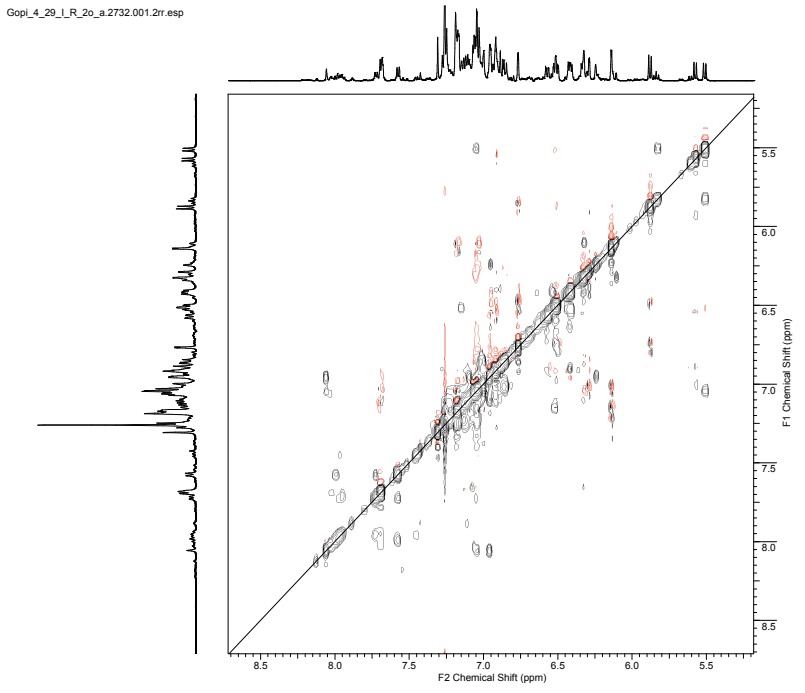

Figure S86. NOESY/EXSY spectrum (500 MHz, $CDCl_3$, 273 K) of (*R*)-**oP^6(*o*-^{t}Bu)**.

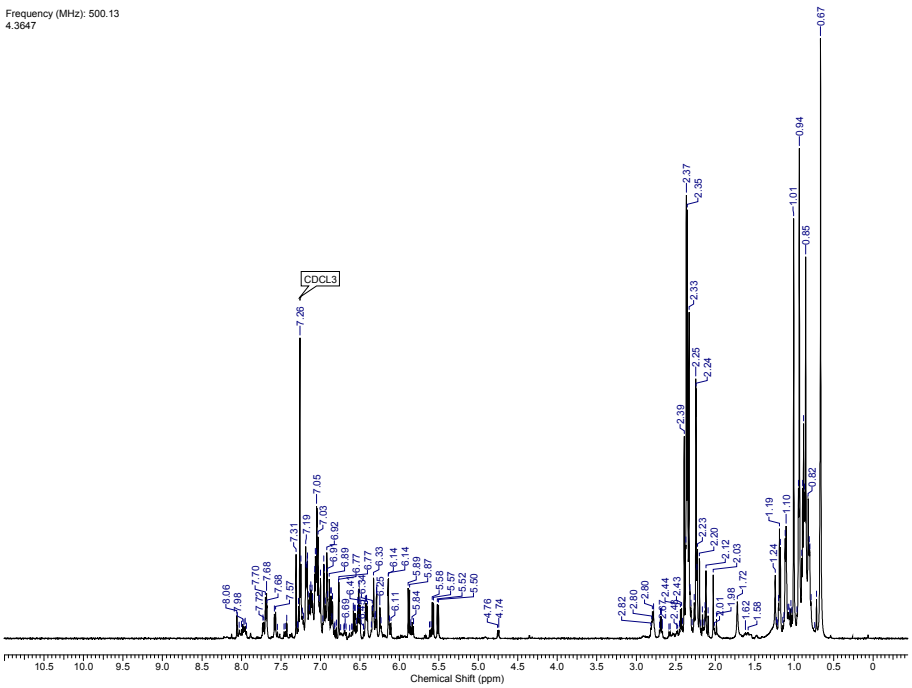

Figure S87. ^{1}H NMR spectrum (500 MHz, $CDCl_3$, 273 K) of (*S*)-**oP^6(*o*-^{t}Bu)**.

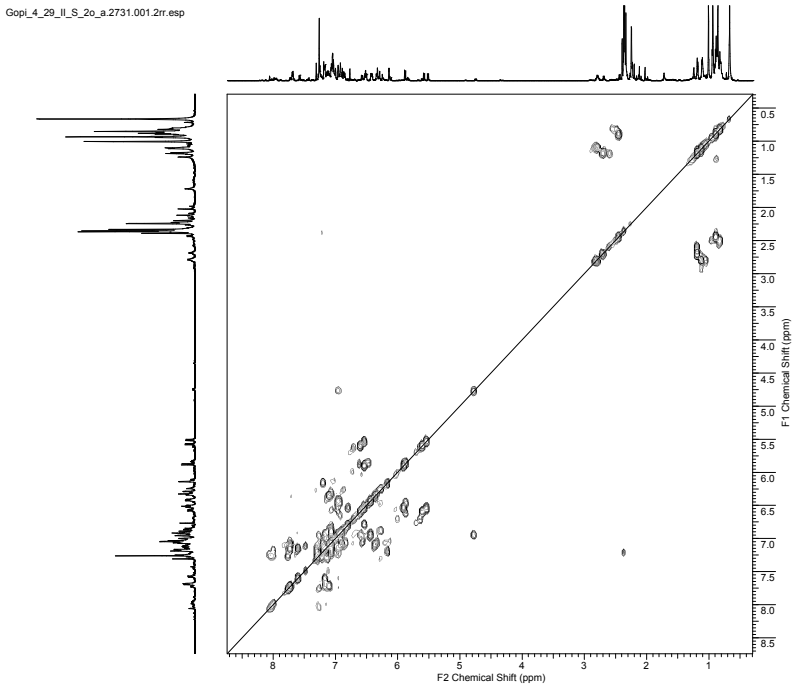

Figure S88. COSY spectrum (500 MHz, $CDCl_3$, 273 K) of (*S*)-**oP^6(*o*-^{t}Bu)**.

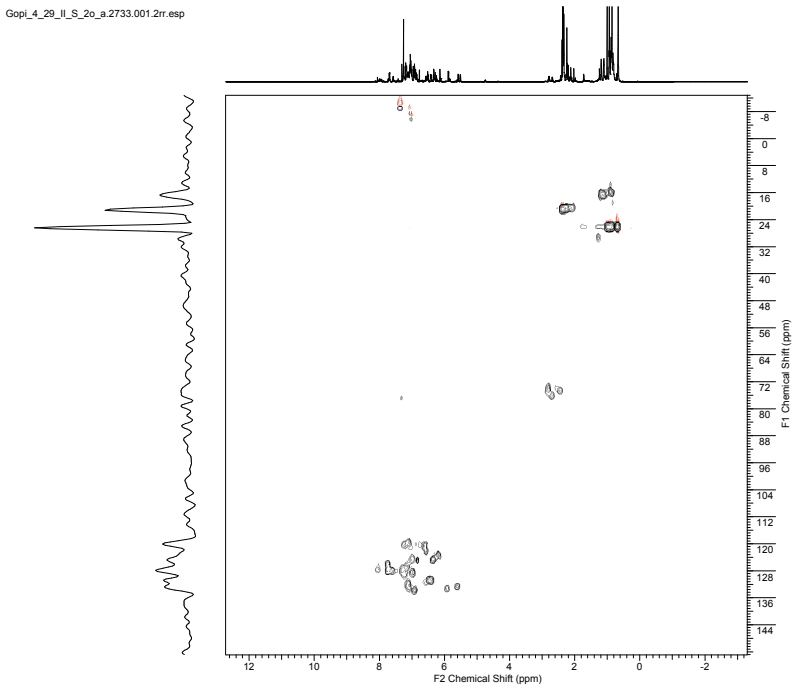

Figure S89. HSQC spectrum (500 MHz, $CDCl_3$, 273 K) of (*S*)-**oP^6(*o*-^{t}Bu)**.

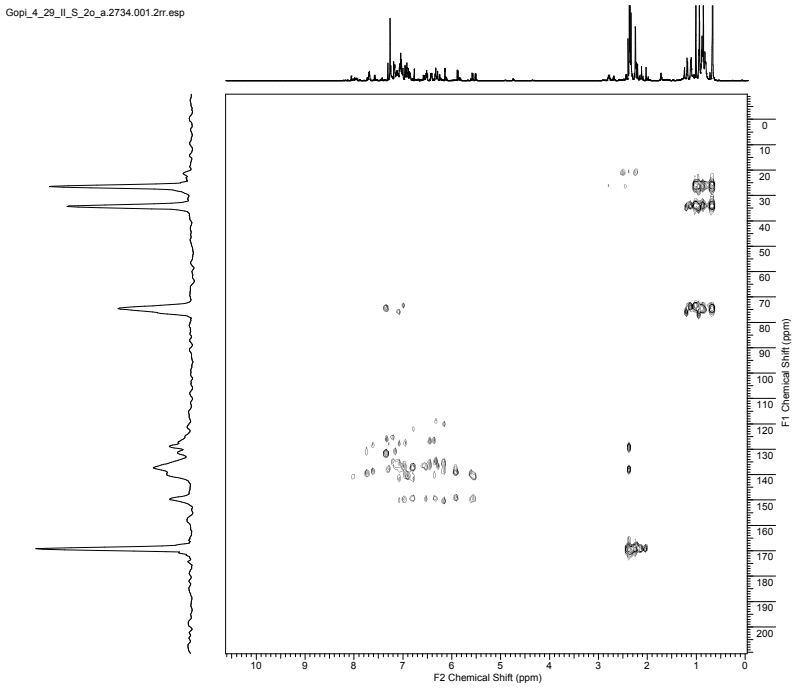

Figure S90. HMBC spectrum (500 MHz, $CDCl_3$, 273 K) of (*S*)-**oP^6(*o*-^{t}Bu)**.

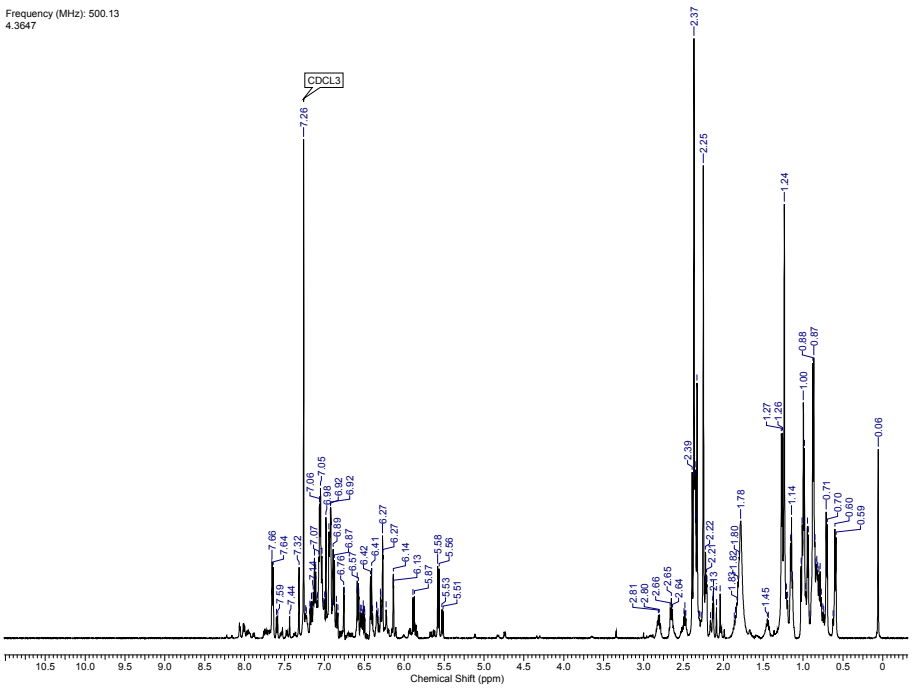

Figure S91. ^{1}H NMR spectrum (500 MHz, $CDCl_3$, 273 K) of (*R*)-**oP^{6}(*o*-^{i}Pr)**.

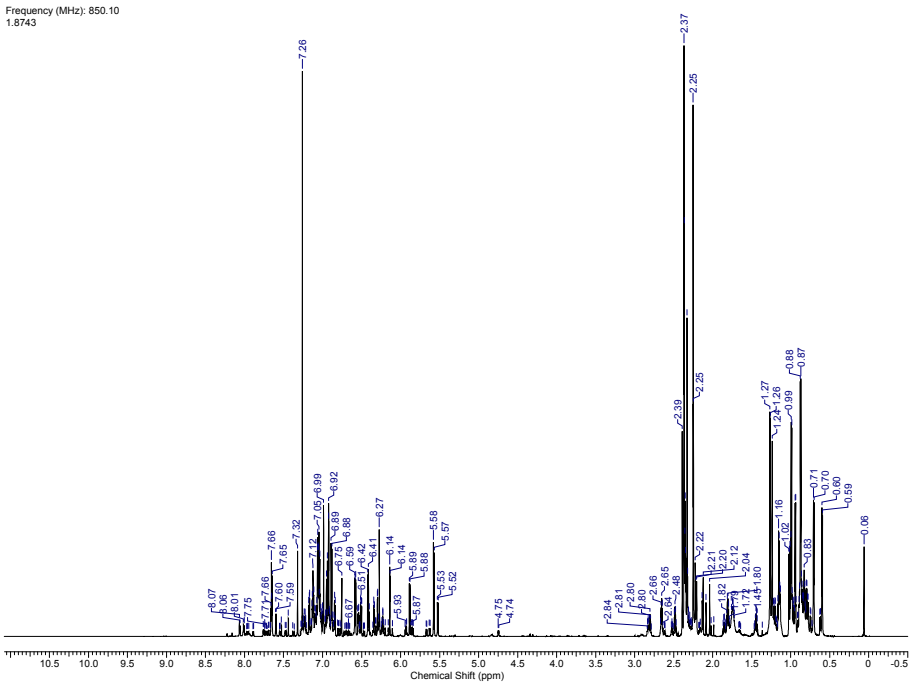

Figure S92. ^{1}H NMR spectrum (850 MHz, $CDCl_3$, 278 K) of (*R*)-**oP^{6}(*o*-^{i}Pr)**.

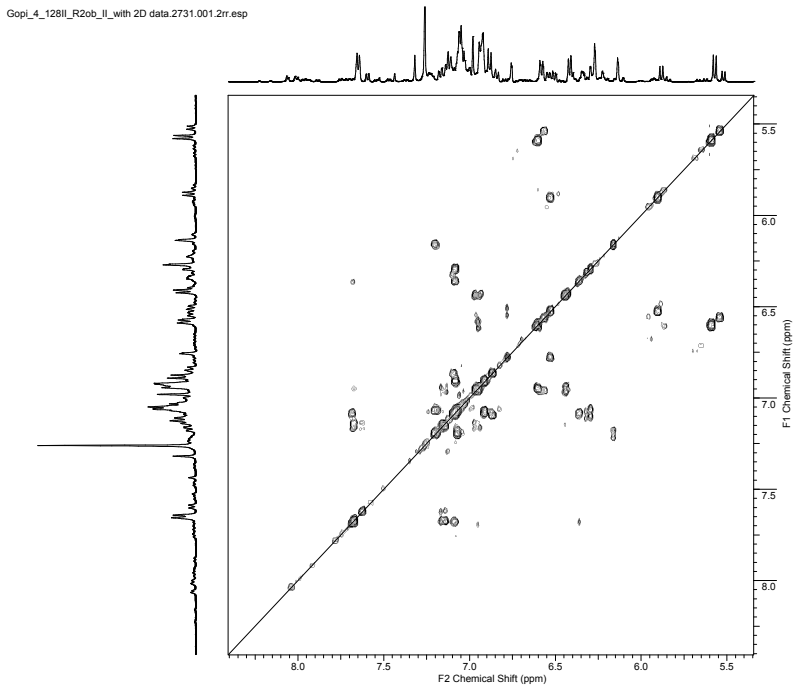

Figure S93. COSY spectrum (500 MHz, $CDCl_3$, 273 K) of (*R*)-**oP^6(*o*-^{i}Pr)**.

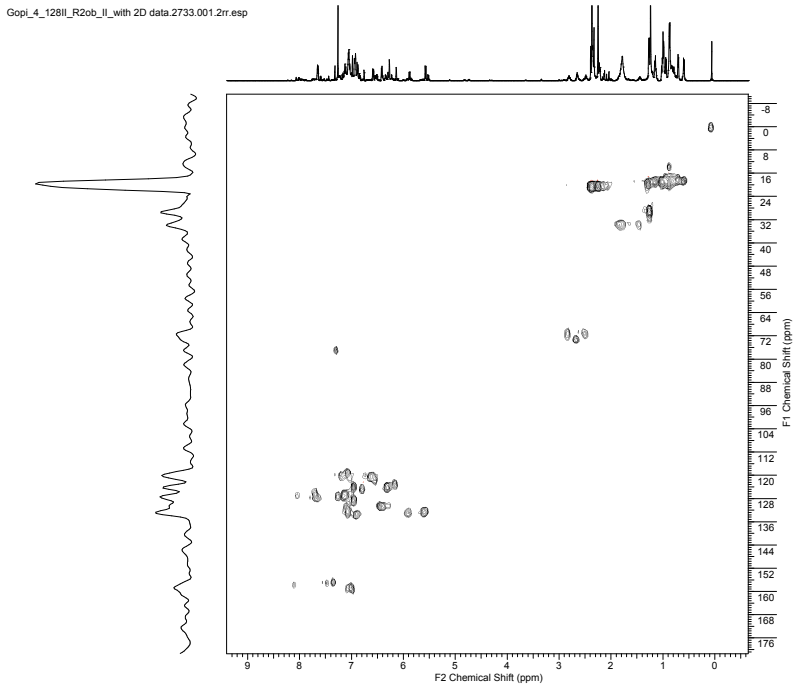

Figure S94. HSQC spectrum (500 MHz, $CDCl_3$, 273 K) of (*R*)-**oP^6(*o*-^{i}Pr)**.

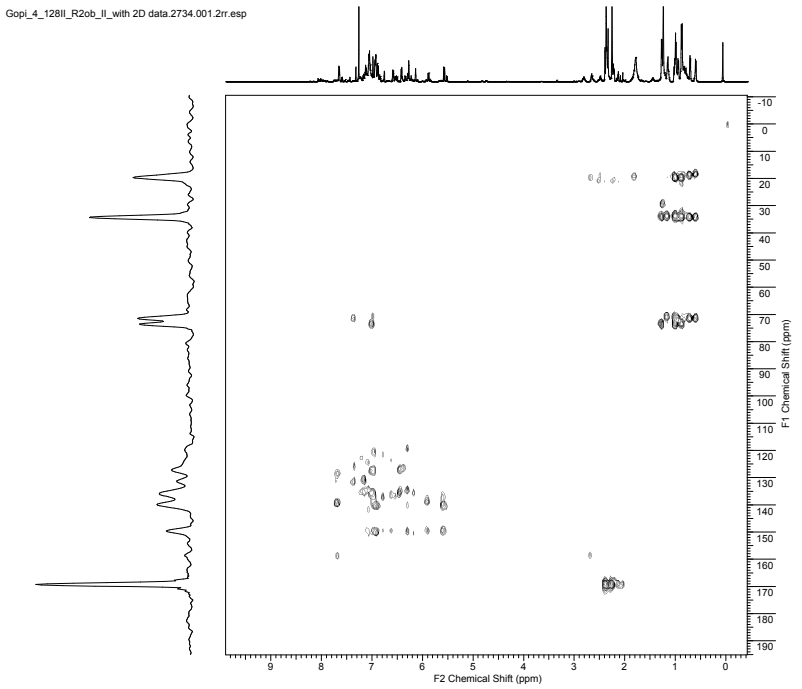

Figure S95. HMBC spectrum (500 MHz, $CDCl_3$, 273 K) of (*R*)-**oP^6(*o*-^{i}Pr)**.

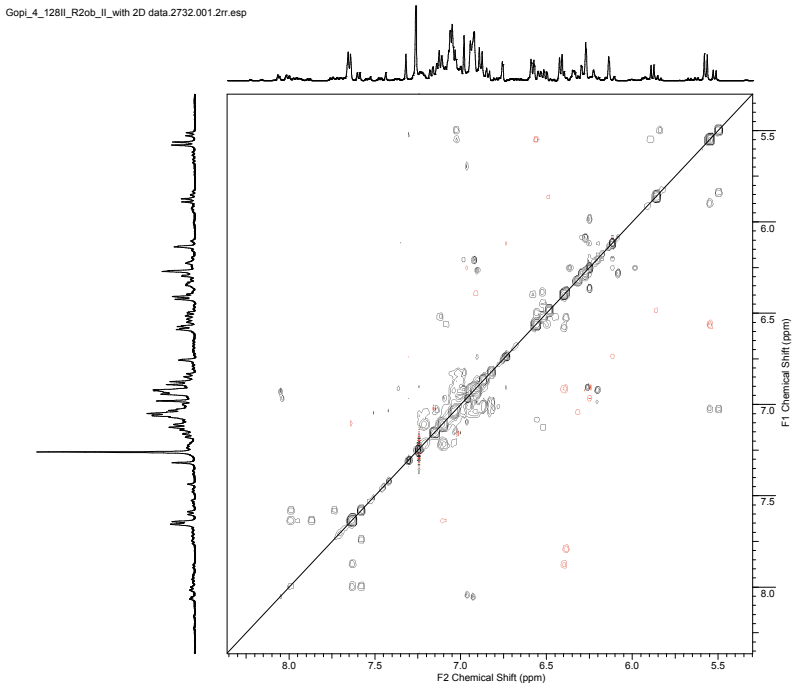

Figure S96. NOESY/EXSY spectrum (500 MHz, $CDCl_3$, 273 K) of (*R*)-**oP^6(*o*-^{i}Pr)**.

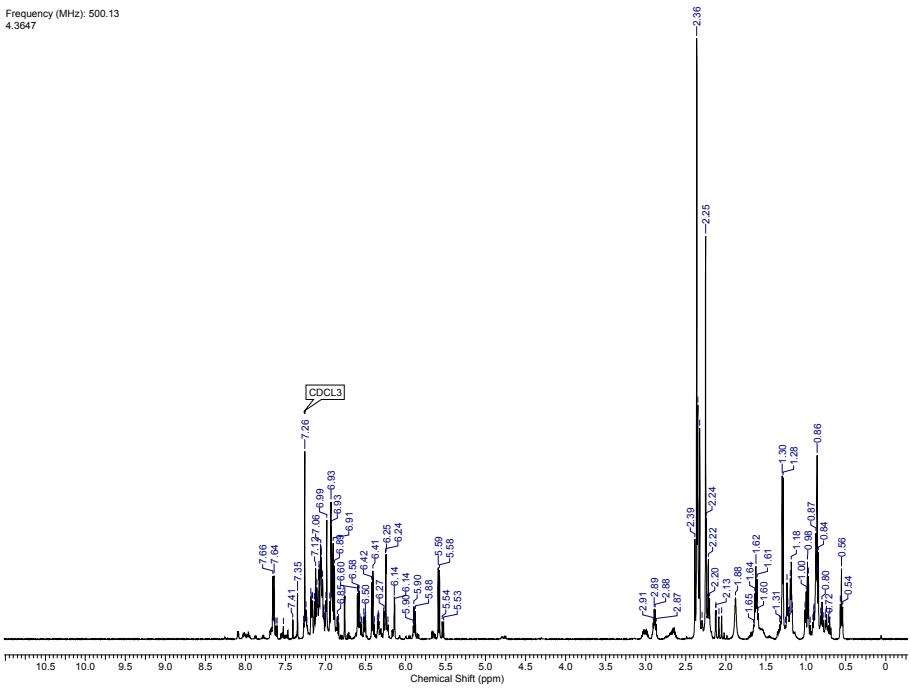

Figure S97. ^{1}H NMR spectrum (500 MHz, $CDCl_3$, 273 K) of (*S*)-**oP^6(*o*-Et)**.

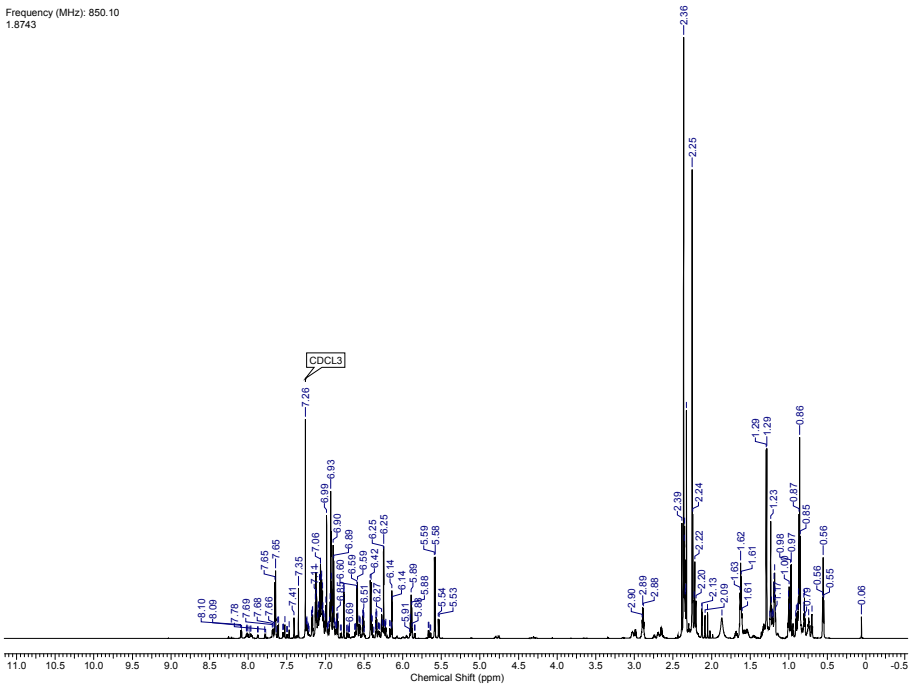

Figure S98. ^{1}H NMR spectrum (850 MHz, $CDCl_3$, 278 K) of (*S*)-**oP^6(*o*-Et)**.

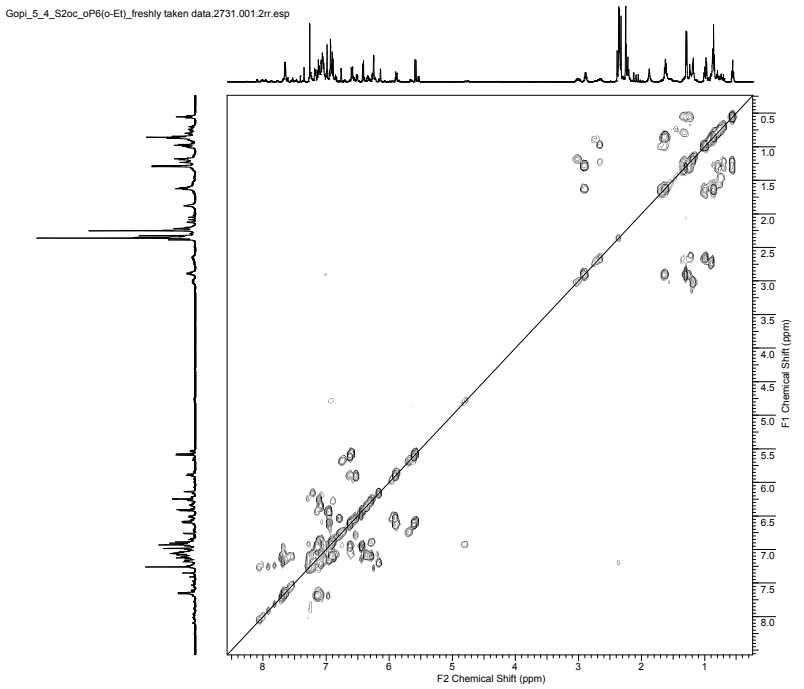

Figure S99. COSY spectrum (500 MHz, $CDCl_3$, 273 K) of (*S*)-**oP^6(*o*-Et)**.

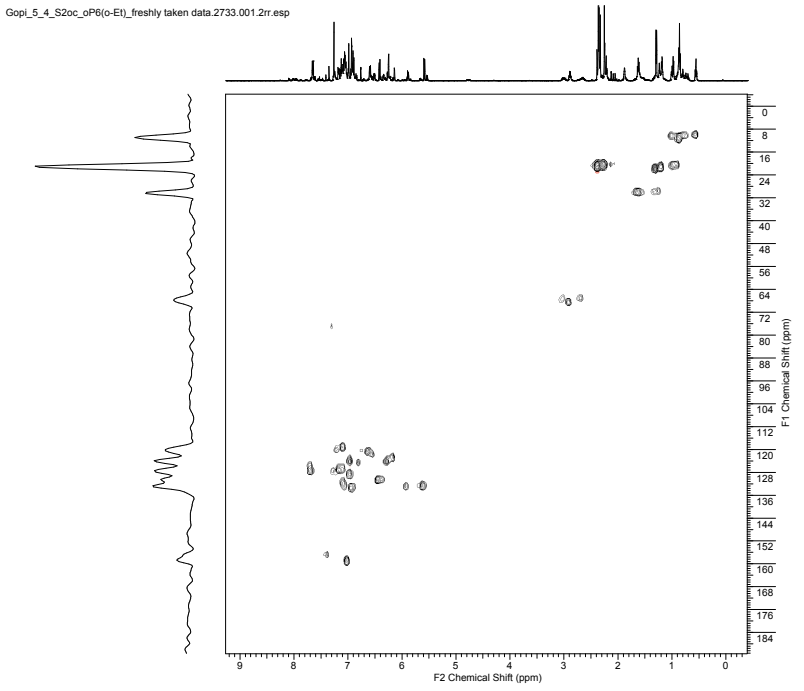

Figure S100. HSQC spectrum (500 MHz, $CDCl_3$, 273 K) of (*S*)-**oP^6(*o*-Et)**.

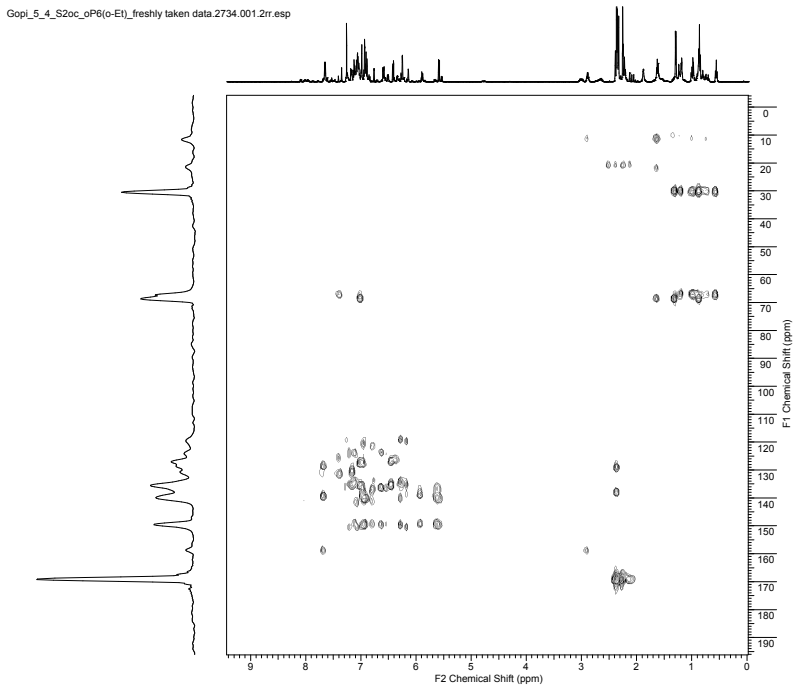

Figure S101. HMBC spectrum (500 MHz, $CDCl_3$, 273 K) of (*S*)-**oP^6(*o*-Et)**.

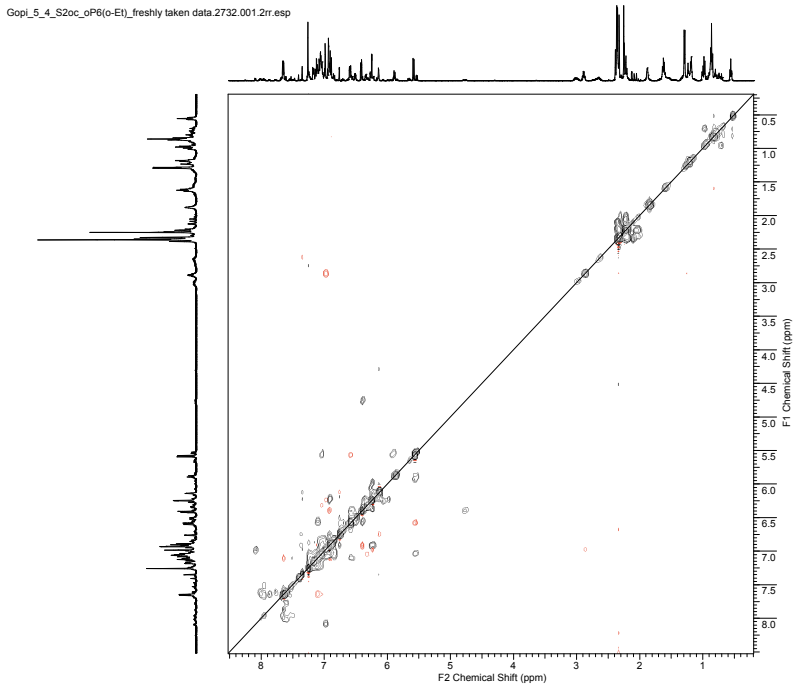

Figure S102. NOESY/EXSY spectrum (500 MHz, $CDCl_3$, 273 K) of (*S*)-**oP^6(*o*-Et)**.

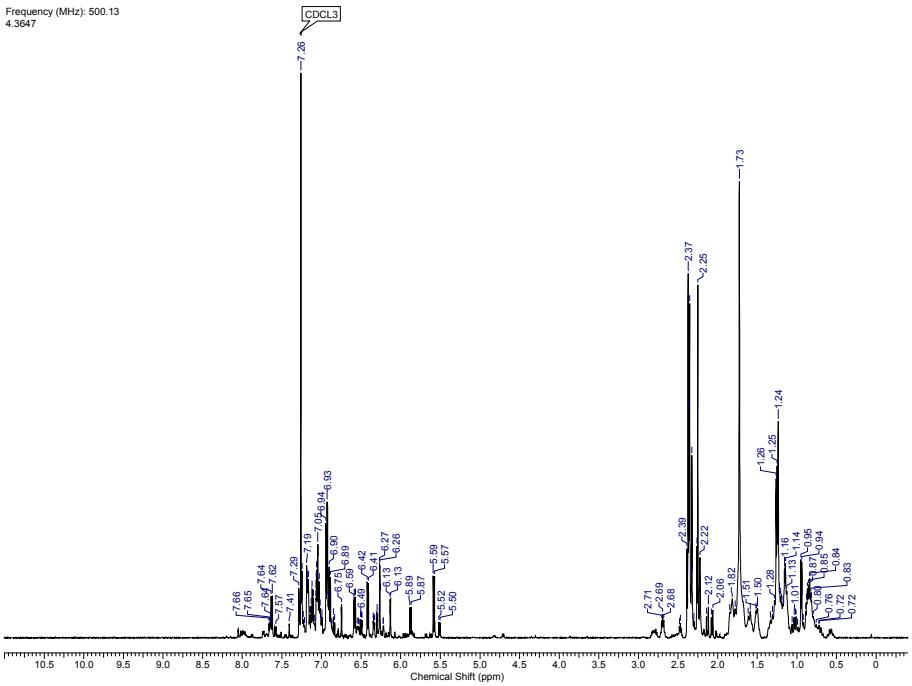

Figure S103. ^{1}H NMR spectrum (500 MHz, $CDCl_3$, 273 K) of (*R*)-**oP^6(*o*-Cy)**.

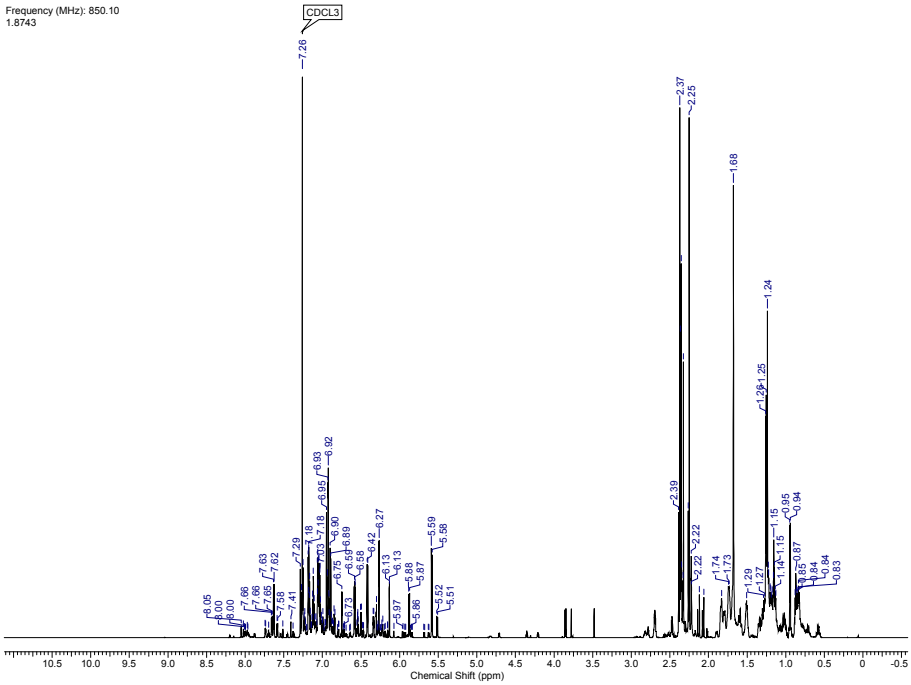

Figure S104. ^{1}H NMR spectrum (850 MHz, $CDCl_3$, 278 K) of (*R*)-**oP^6(*o*-Cy)**.

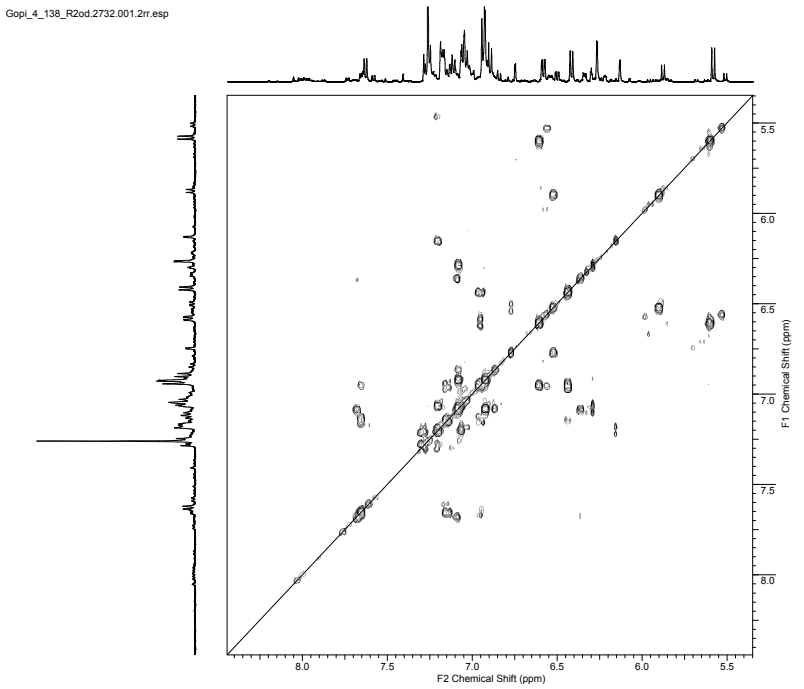

Figure S105. COSY spectrum (500 MHz, $CDCl_3$, 273 K) of (*R*)-**oP^6(*o*-Cy)**.

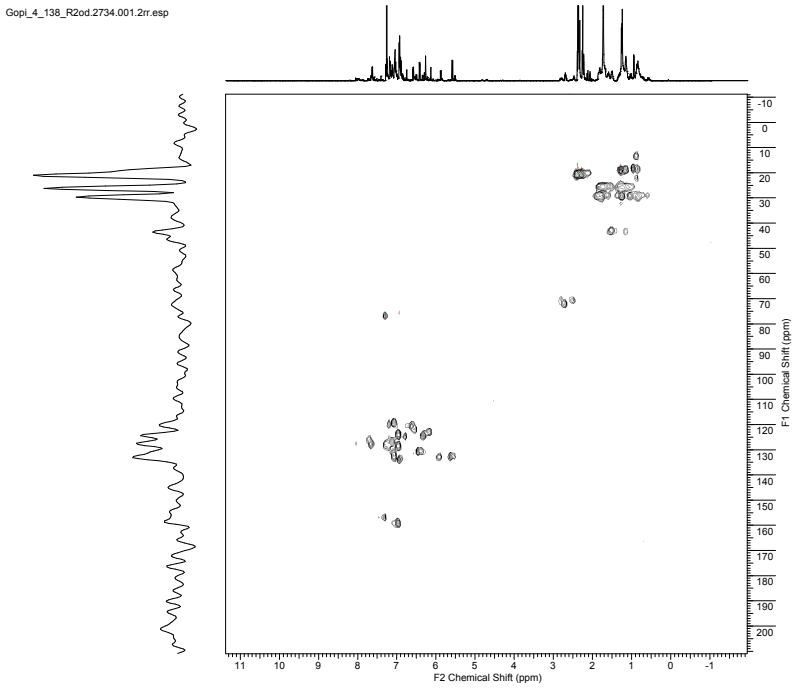

Figure S106. HSQC spectrum (500 MHz, $CDCl_3$, 273 K) of (*R*)-**oP^6(*o*-Cy)**.

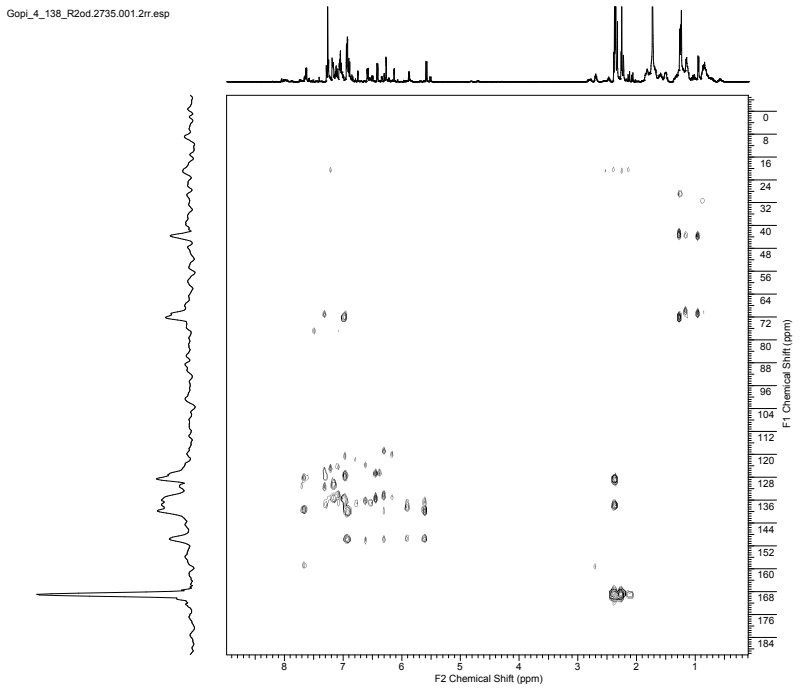

Figure S107. HMBC spectrum (500 MHz, $CDCl_3$, 273 K) of (*R*)-**oP^6(*o*-Cy)**.

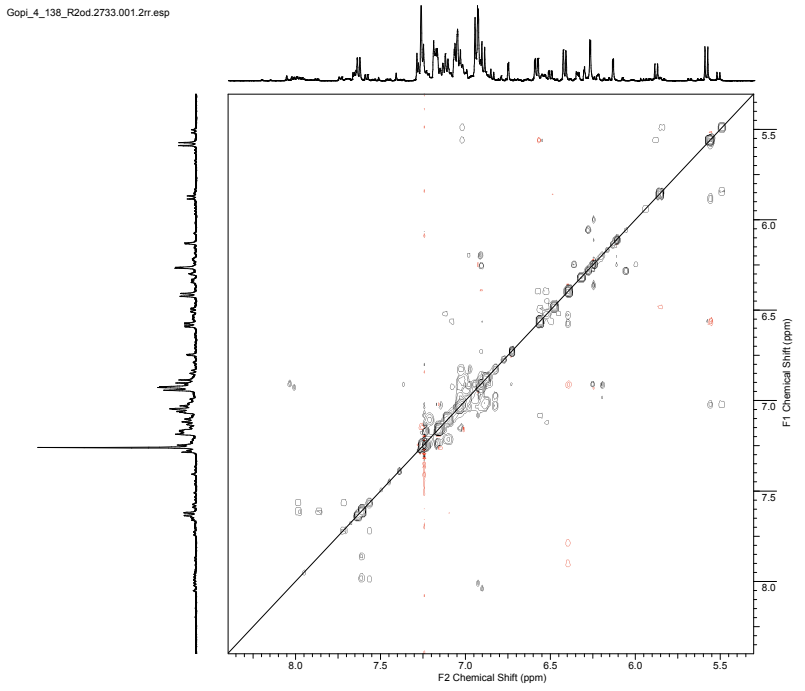

Figure S108. NOESY/EXSY spectrum (500 MHz, $CDCl_3$, 273 K) of (*R*)-**oP^6(*o*-Cy)**.

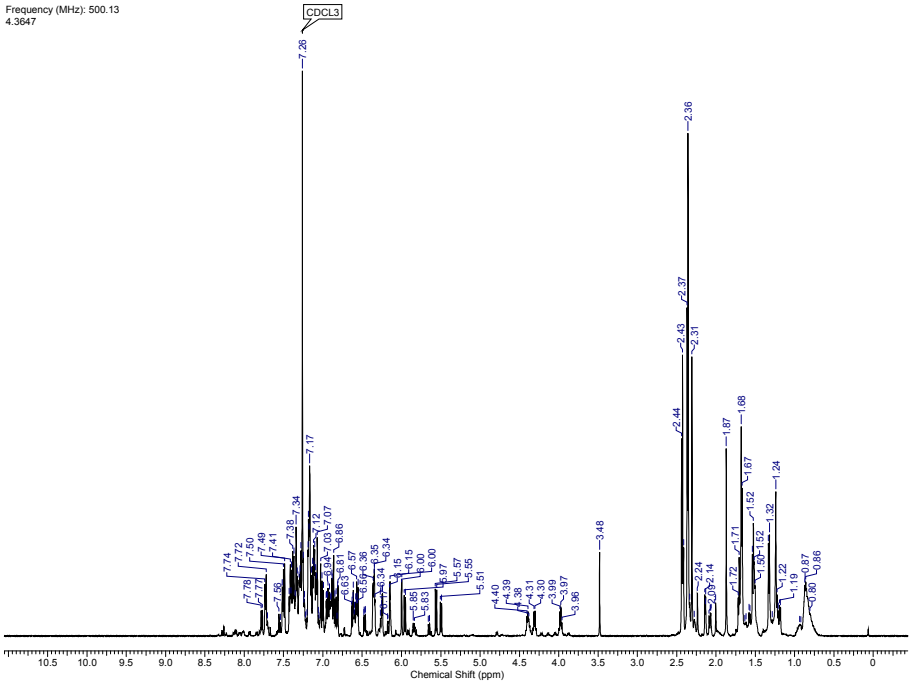

Figure S109. ^{1}H NMR spectrum (500 MHz, $CDCl_3$, 273 K) of (*S*)-**oP^{6}(*o*-Ph)**.

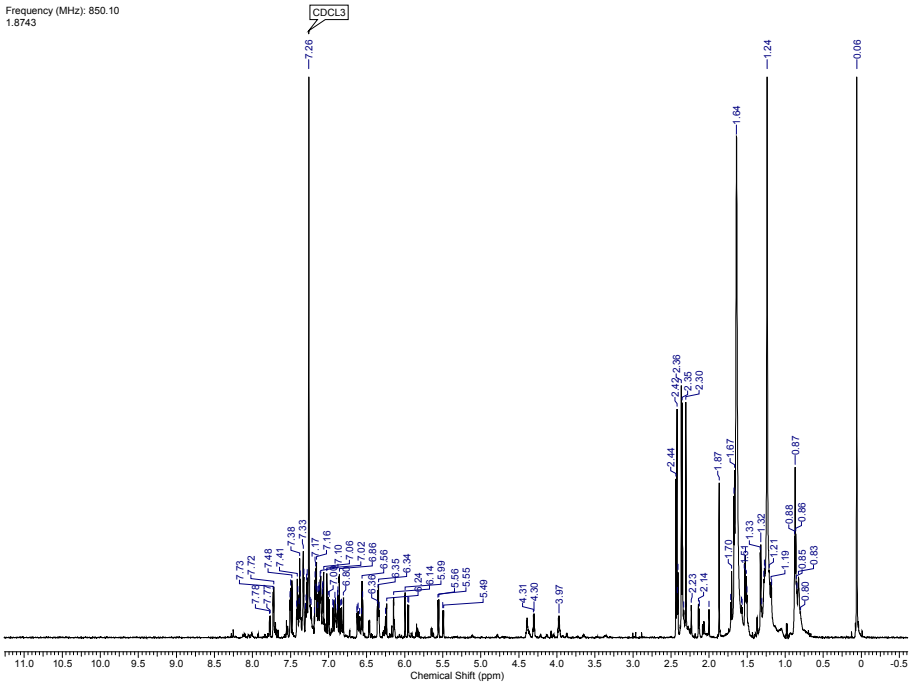

Figure S110. ^{1}H NMR spectrum (850 MHz, $CDCl_3$, 278 K) of (*S*)-**oP^{6}(*o*-Ph)**.

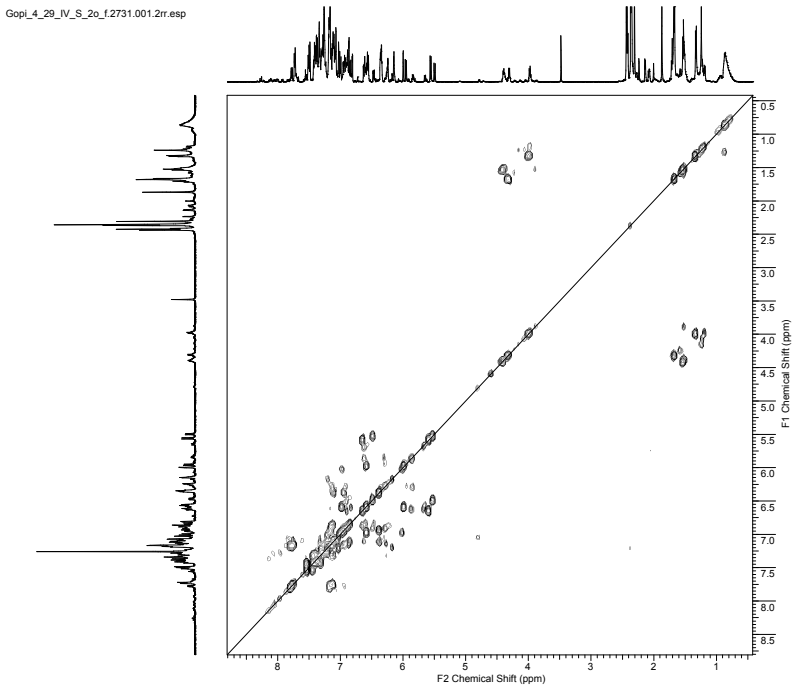

Figure S111. COSY spectrum (500 MHz, $CDCl_3$, 273 K) of (*S*)-**oP^6(*o*-Ph)**.

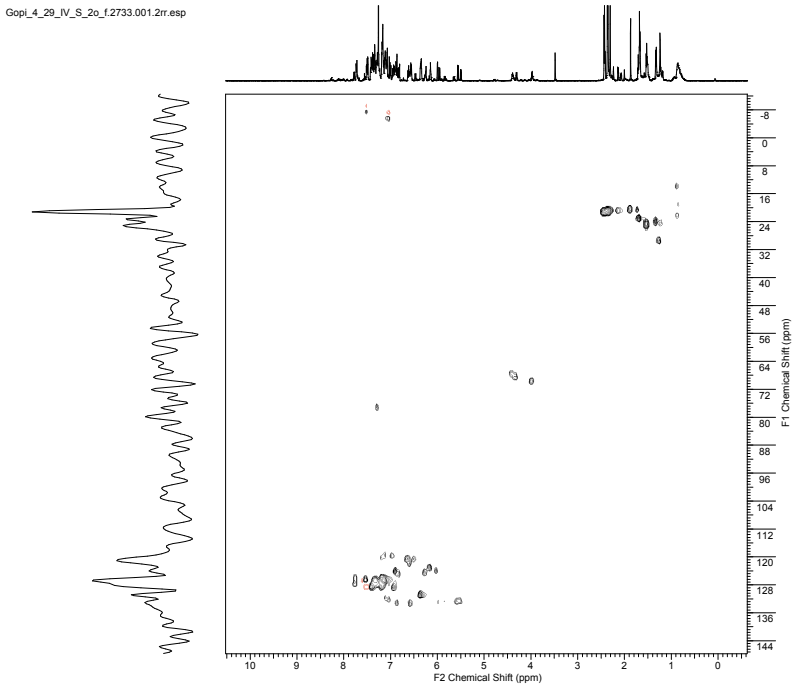

Figure S112. HSQC spectrum (500 MHz, $CDCl_3$, 273 K) of (*S*)-**oP^6(*o*-Ph)**.

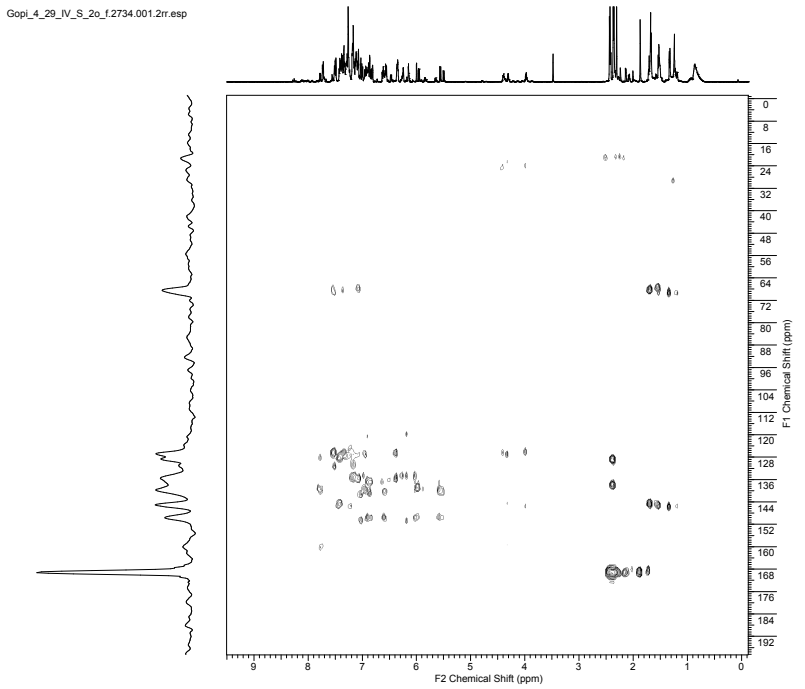

Figure S113. HMBC spectrum (500 MHz, $CDCl_3$, 273 K) of (*S*)-**oP^6(*o*-Ph)**.

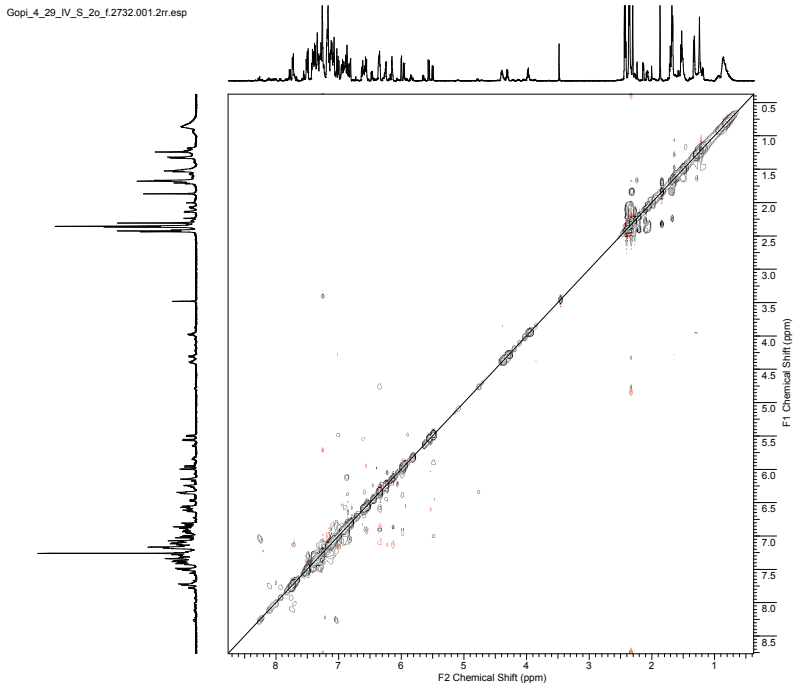

Figure S114. NOESY/EXSY spectrum (500 MHz, $CDCl_3$, 273 K) of (*S*)-**oP^6(*o*-Ph)**.

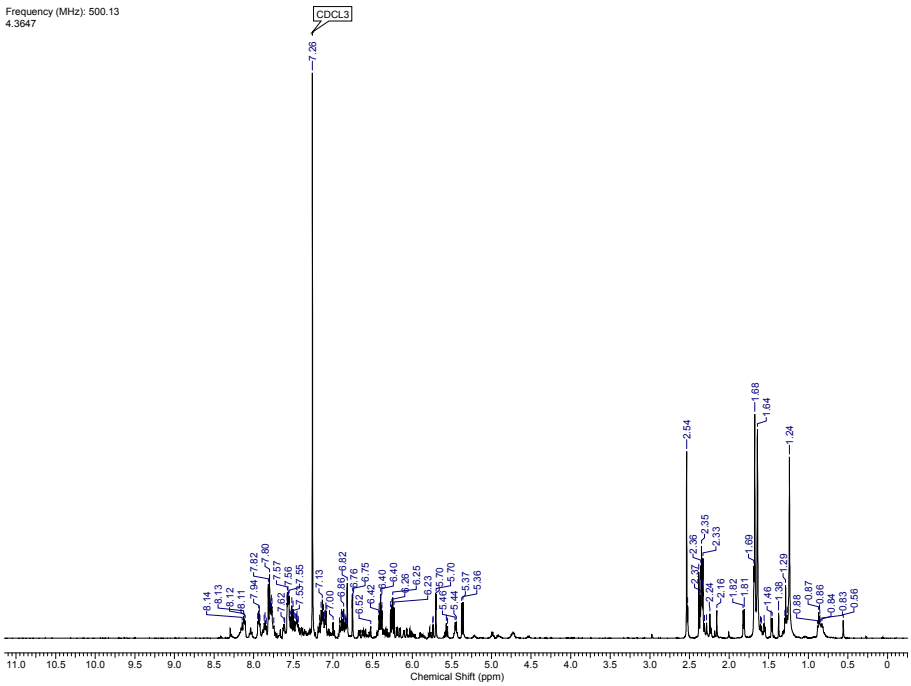

Figure S115. ^{1}H NMR spectrum (500 MHz, $CDCl_3$, 273 K) of (*S*)-**oP^6(*o*-Np)**.

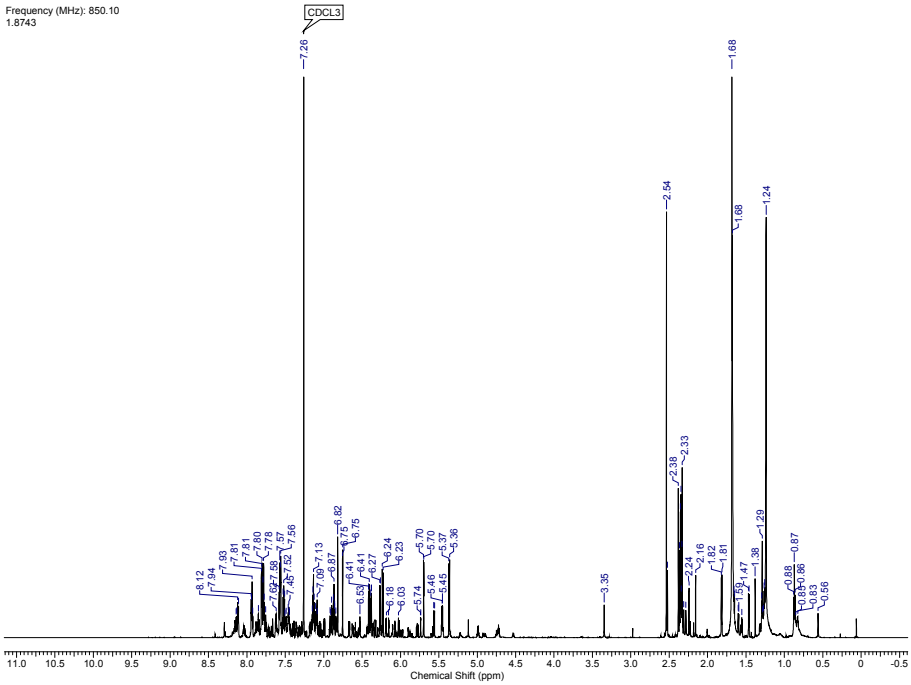

Figure S116. ^{1}H NMR spectrum (850 MHz, $CDCl_3$, 278 K) of (*S*)-**oP^6(*o*-Np)**.

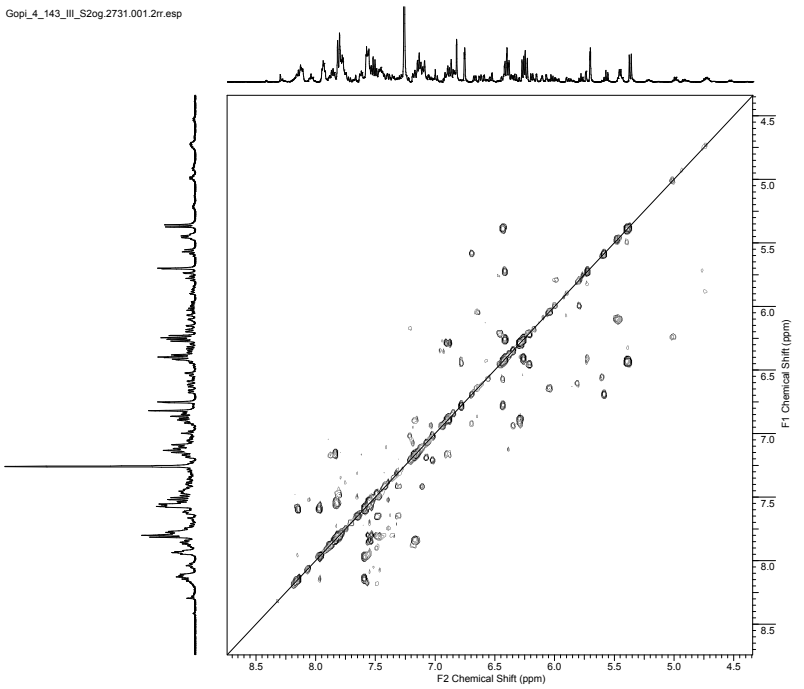

Figure S117. COSY spectrum (500 MHz, $CDCl_3$, 273 K) of (*S*)-**oP^6(*o*-Np)**.

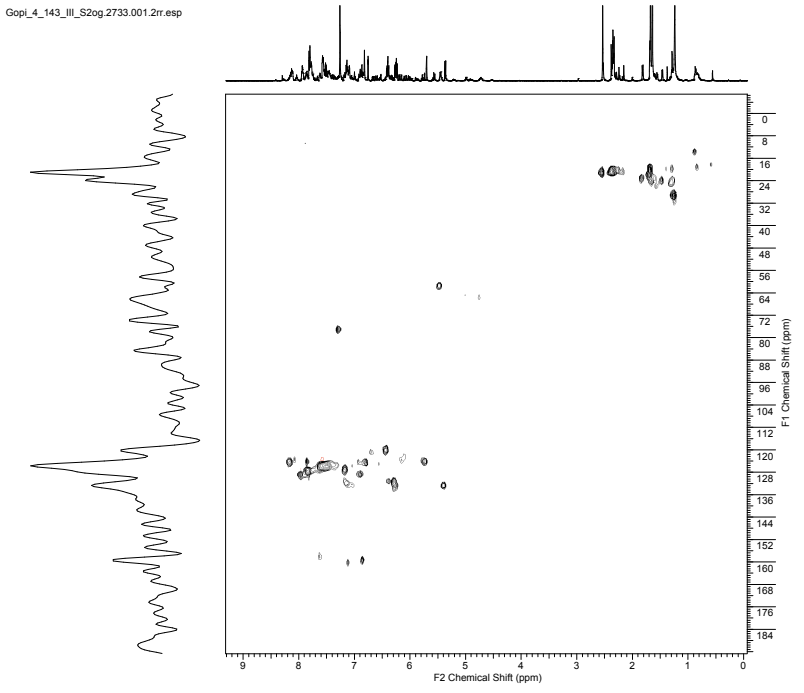

Figure S118. HSQC spectrum (500 MHz, $CDCl_3$, 273 K) of (*S*)-**oP^6(*o*-Np)**.

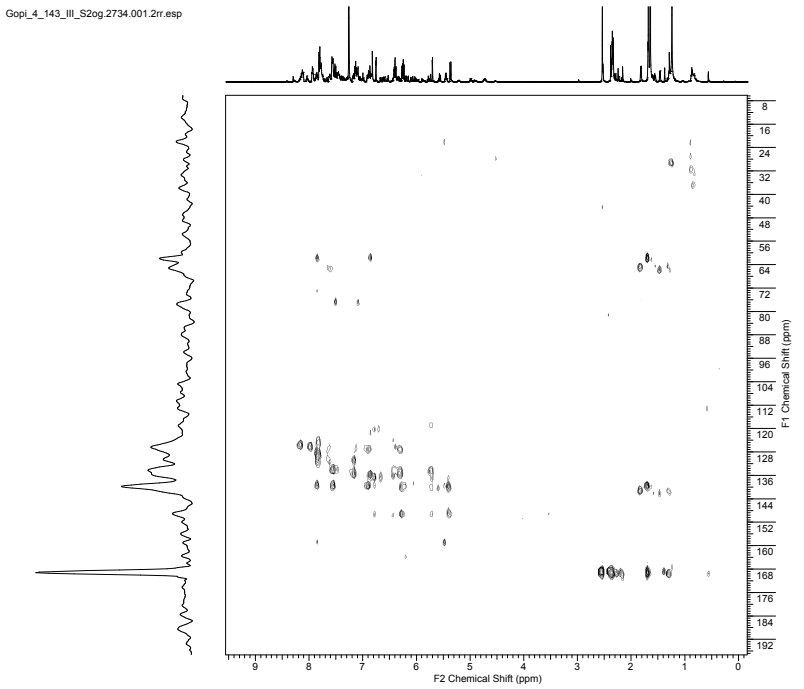

Figure S119. HMBC spectrum (500 MHz, $CDCl_3$, 273 K) of (*S*)-**oP^6(*o*-Np)**.

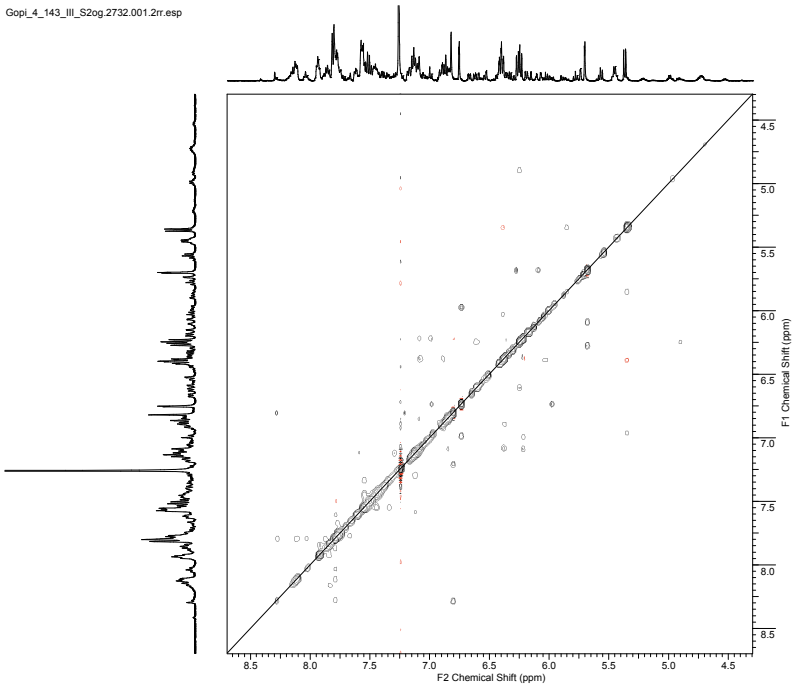

Figure S120. NOESY/EXSY spectrum (500 MHz, $CDCl_3$, 273 K) of (*S*)-**oP^6(*o*-Np)**.

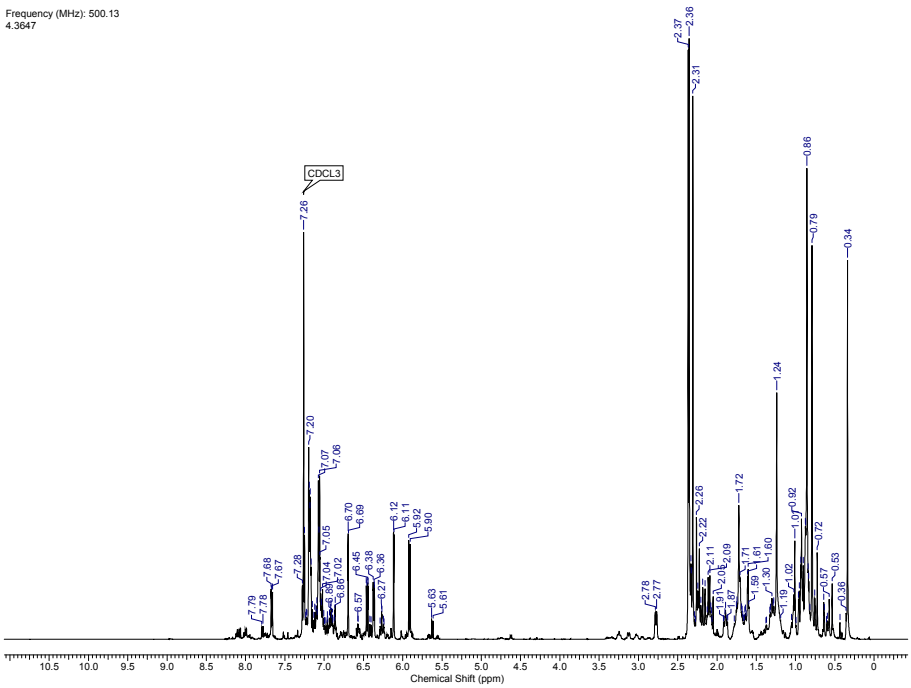

Figure S121. ^{1}H NMR spectrum (500 MHz, $CDCl_3$, 273 K) of (*S*)-**oP^{6}(*o*-Bo)**.

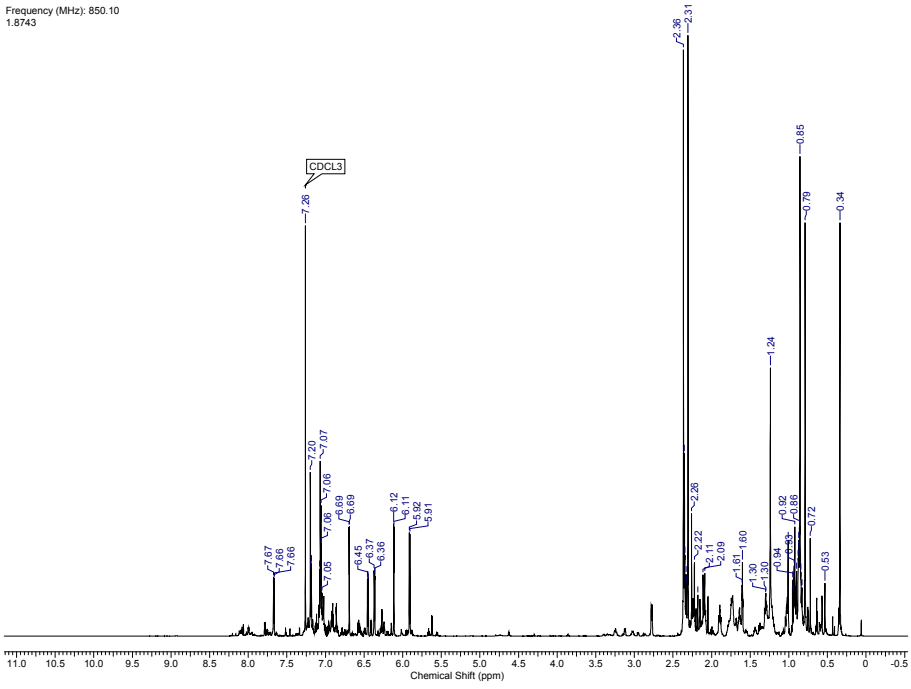

Figure S122. ^{1}H NMR spectrum (850 MHz, $CDCl_3$, 278 K) of (*S*)-**oP^{6}(*o*-Bo)**.

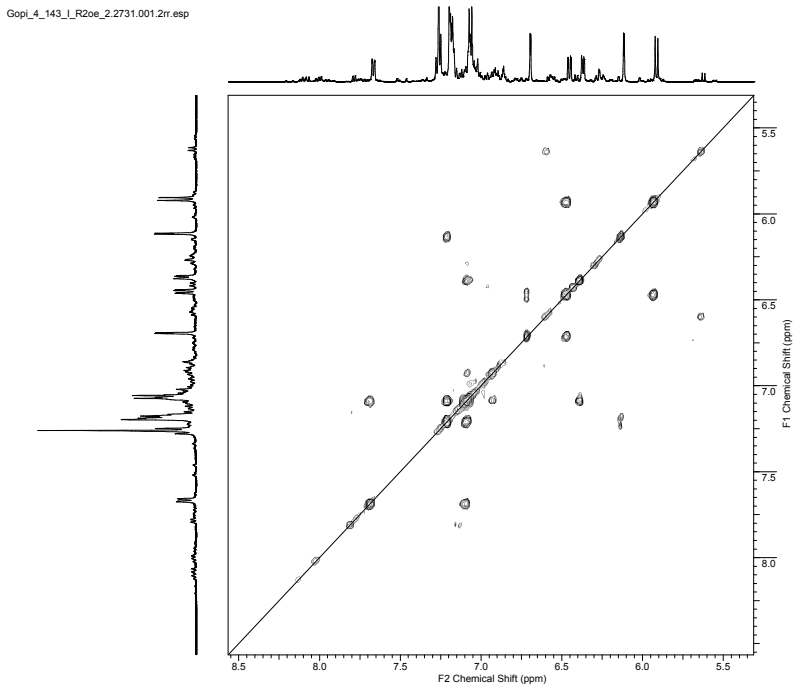

Figure S123. COSY spectrum (500 MHz, $CDCl_3$, 273 K) of (*S*)-**oP^6(*o*-Bo)**.

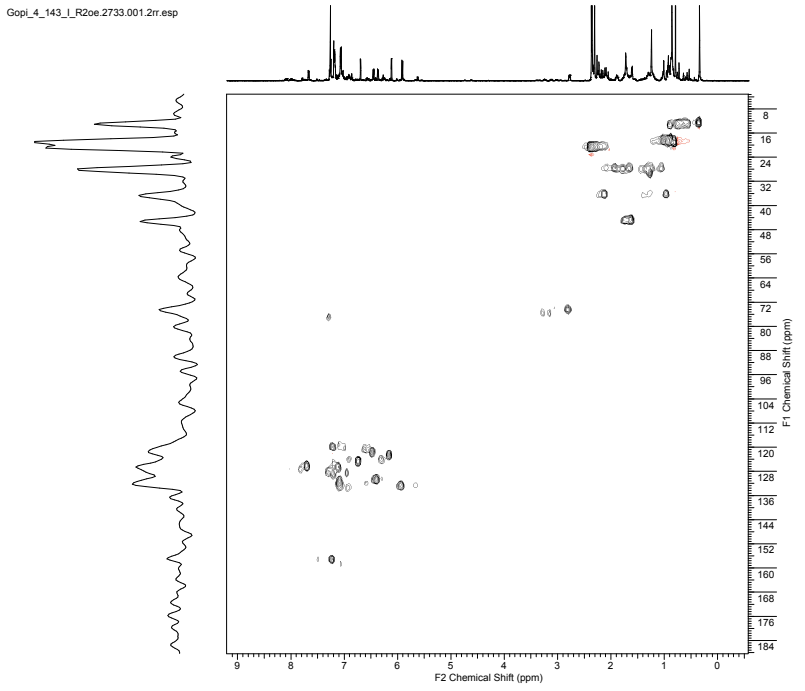

Figure S124. HSQC spectrum (500 MHz, $CDCl_3$, 273 K) of (*S*)-**oP^6(*o*-Bo)**.

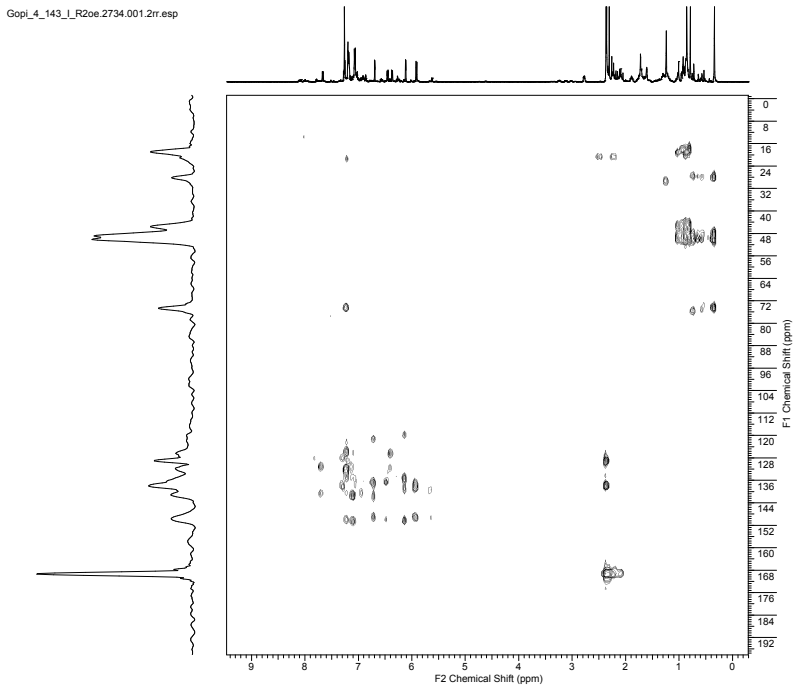

Figure S125. HMBC spectrum (500 MHz, $CDCl_3$, 273 K) of (*S*)-**oP^6(*o*-Bo)**.

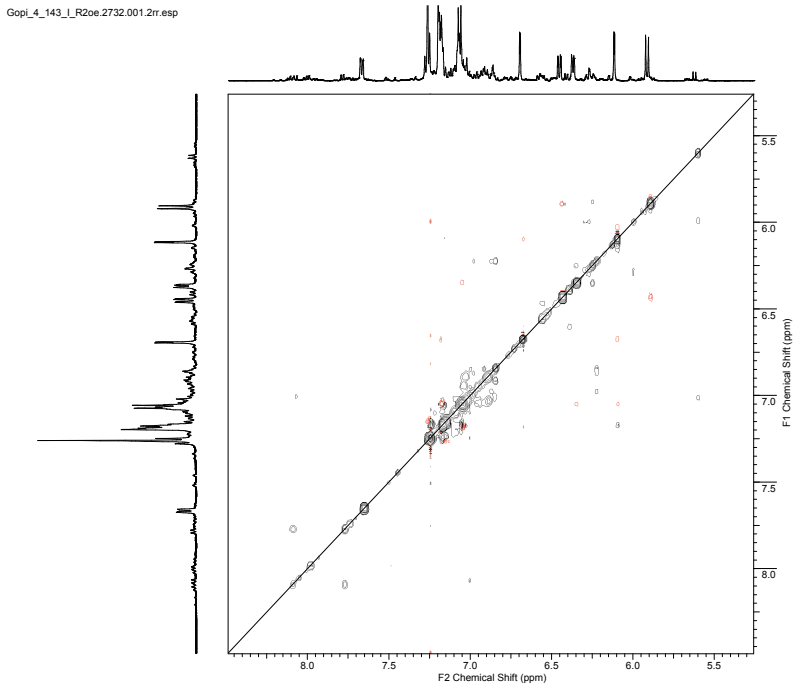

Figure S126. NOESY/EXSY spectrum (500 MHz, $CDCl_3$, 273 K) of (*S*)-**oP^6(*o*-Bo)**.

References

(1) E. Ohta, H. Sato, S. Ando, A. Kosaka, T. Fukushima, D. Hashizume, M. Yamasaki, K. Hasegawa, A. Muraoka, H. Ushiyama, K. Yamashita and T. Aida, *Nat. Chem.*, 2011, **3**, 68–73.

(2) Y. Miyake, M. Wu, M. J. Rahman and M. Iyoda, *Chem. Commun.*, 2005, 411–413.

(3) P. Guiglion and M. A. Zwijnenburg, *Phys. Chem. Chem. Phys.*, 2015, **17**, 17854–17863.

(4) J. W. Ponder, TINKER: Software tools for molecular design, v. 8.2, Washington University School of Medicine, Saint Louis, MO, 2017.

(5) J. J. P. Stewart, *J. Mol. Model.*, 2013, **19**, 1–32.

(6) S. Grimme, *J. Comput. Chem.*, 2006, **27**, 1787–1799.

(7) Y. Guan, M. L. Jones, A. E. Miller and S. E. Wheeler, *Phys. Chem. Chem. Phys.*, 2017, **19**, 18186–18193.

(8) S. E. Wheeler and J. W. G. Bloom, *J. Phys. Chem. A*, 2014, **118**, 6133–6147.

(9) S. M. Mathew, J. T. Engle, C. J. Ziegler and C. S. Hartley, *J. Am. Chem. Soc.*, 2013, **135**, 6714–6722.

(10) N. Campbell and A. H. Scott, *J. Chem. Soc. C*, 1966, 1050–1052.

(11) M. J. Frisch, G. W. Trucks, H. B. Schlegel, G. E. Scuseria, M. A. Robb, J. R. Cheeseman, G. Scalmani, V. Barone, B. Mennucci, G. A. Petersson, H. Nakatsuji, M. Caricato, X. Li, H. P. Hratchian, A. F. Izmaylov, J. Bloino, G. Zheng, J. L. Sonnenberg, M. Hada, M. Ehara, K. Toyota, R. Fukuda, J. Hasegawa, M. Ishida, T. Nakajima, Y. Honda, O. Kitao, H. Nakai, T. Vreven, J. A. Montgomery, Jr, J. E. Peralta, F. Ogliaro, M. Bearpark, J. J. Heyd, E. Brothers, K. N. Kudin, V. N. Staroverov, T. Keith, R. Kobayashi, J. Normand, K. Raghavachari, A. Rendell, J. C. Burant, S. S. Iyengar, J. Tomasi, M. Cossi, N. Rega, J. M. Millam, M. Klene, J. E. Knox, J. B. Cross, V. Bakken, C. Adamo, J. Jaramillo, R. Gomperts, R. E. Stratmann, O. Yazyev, A. J. Austin, R. Cammi, C. Pomelli, J. W. Ochterski, R. L. Martin, K. Morokuma, V. G. Zakrzewski, G. A. Voth, P. Salvador, J. J. Dannenberg, S. Dapprich, A. D. Daniels, O. Farkas, J. B. Foresman, J. V. Ortiz, J. Cioslowski and D. J. Fox, *Gaussian 09, Rev. B.01*, Gaussian, Inc., Wallingford, CT, 2010.

(12) J. J. P. Stewart, MOPAC2016, Stewart Computational Chemistry, Colorado Springs, CO, 2016.